POLITECNICO DI MILANO

Scuola di Ingegneria dei Processi Industriali

Corso di Laurea Specialistica in Ingegneria Nucleare

THERMODYNAMIC CHACTERIZATION OF SALT COMPONENTS FOR MOLTEN SALT REACTOR FUEL

Elisa Capelli

Matr. 745225

Relatore: Lelio Luzzi

Co-relatore: Ondřej Beneš

Anno accademico 2010/2011

"Some things have to be believed to be seen."

R.Hodgson

Contents

List of Figures

List of Tables

Acronyms

AGR	Advanced Gas-cooled Reactor
AHTR	Advanced High Temperature Reactor
ARE	Aircraft Reactor Experiment
BWR	Boiling Water Reactor
CANDU	CANadian Deuterium Uranium reactor
CALPHAD	CALculation PHase Diagram
DSC	Differential Scanning Calorimeter
GFR	Gas-cooled Fast Reactor
GIF	Generation IV International Forum
ITU	Institute for Transuranium Elements
JRC	Joint Research Centre
LFR	Lead-cooled Fast Reactor
LWR	Light Water Reactor
MOSART	MOlten Salt Advanced Recycler and Transmuter
MSBR	Molten Salt Breeder Reactor
MSFR	Molten Salt Fast Reactor
MSR	Molten Salt Reactor
MSRE	Molten Salt Reactor Experiment
MS-FR	Molten Salt cooled Fast Reactor
NGNP	Next Generation Nuclear Plant
NHI	Nuclear Hydrogen Initiative

ORNL	Oak Ridge National Laboratory
PWR	Pressurized Water Reactor
SCWR	SuperCritical Water Reactor
SFR	Sodium-cooled Fast Reactor
TMSR	Thorium Molten Salt Reactor
VHTR	Very High Temperature Reactor
VVER	Vodo-Vodyanoy Energeticheskiy Reaktor

Abstract

The Molten Salt Reactor (MSR) is one of the six nuclear reactor concepts considered in the Generation IV initiative. In the MSR concept, the fissile material is dissolved in a molten salt mixture, which serves as both fuel and coolant. The main task of this work was to study thermodynamic properties of molten salts systems, in order to determine the safety limit for the molten salt fuel. The investigations were carried out entirely on fluoride salts, which are currently the most relevant salts considered as potential fuel for MSR. In the present work, two techniques - Differential Scanning Calorimetry (DSC) and drop calorimetry - were employed to measure the thermodynamic properties (heat capacity, phase diagram equilibrium points, fusion enthalpy and mixing enthalpy) of some fluoride systems. A challenging task was the measurement of the mixing enthalpy of binary systems, which required the development of a new method compatible with the used DSC technique. In order to verify the possibility to measure the mixing enthalpy using this calorimeter, the well-known LiF-KF system was adopted as reference and studied. Based on the good results obtained, the technique was applied for the LiF-ThF_4 system, important for Molten Salt Fast Reactor (MSFR), and its enthalpy of mixing has never been measured before. Moreover, the phase diagram equilibrium points were measured for both systems using the same technique, confirming the existence of $LiThF_5$ phase. The Li_3ThF_7 compound was synthesized and its fusion enthalpy was determined. All the experimental data collected were used to assess the phase diagrams, using the CALPHAD method.

Experimental determination of heat capacity were carried out using drop calorimeter on the following fluoride systems: CsF in the solid phase, $(Li_{0.5}Rb_{0.5})F$ in the liquid phase and ThF_4 in the solid phase. While the data on ThF_4 are not yet finalized and only preliminary results are shown in this thesis, the study of the other two systems has been concluded. The study of LiF-RbF liquid solution confirmed a trend of the excess heat capacity behaviour in the LiF-AlkF (Alk=Na,K,Rb,Cs) system.

Abstract

Il reattore a sali fusi (*MSR-Molten Salt Reactor*) è uno dei sei concetti di reattori che costituiscono la Generazione IV. In questo reattore, il materiale fissile è disciolto in una miscela di sali fusi che svolge la duplice funzione di combustibile e fluido termovettore. L'obiettivo principale di questo lavoro di tesi è stato lo studio delle proprietà termodinamiche dei sistemi di sali fusi, utile a stabilire i limiti di sicurezza delle miscele. Le misure sono state svolte sulla classe dei fluoruri, i cui sali sono i principali candidati come combustibile per il reattore a sali fusi. Le proprietà termodinamiche (calore specifico, punti del diagramma di fase, entalpia di fusione ed entalpia di miscelamento) sono state misurate utilizzando la calorimetria differenziale a scansione e la calorimetria a caduta. Un compito importante è stato la misura dell'entalpia di miscelamento dei sistemi binari, che ha richiesto lo sviluppo di un nuovo metodo di misura compatibile con il calorimetro a scansione differenziale. Per confermare la possibilità di misurare l'entalpia di miscelamento con questo metodo, è stato scelto come riferimento il sistema LiF-KF, ben noto in letteratura. Grazie ai buoni risultati ottenuti, il metodo è stato applicato al sistema LiF-ThF_4, fondamentale per il reattore veloce a sali fusi (*MSFR-Molten Salt Fast Reactor*), ed è stata misurata l'entalpia di miscelamento per la prima volta. Inoltre, sono stati misurati i punti del diagramma di fase, confermando l'esistenza della fase $LiThF_5$, ed è stato sintetizzato il composto Li_3ThF_7, misurandone l'entalpia di fusione. Tutti i dati sperimentali ottenuti sono stati combinati per la modellazione del diagramma di fase, utilizzando l'approccio CALPHAD.

Utilizzando il calorimetro a caduta, sono state eseguite misure di calore specifico su tre sistemi di fluoruri: CsF e ThF_4 in fase solida e $(Li_{0.5}Rb_{0.5})F$ in fase liquida. Mentre i risultati sul ThF_4 sono preliminari, lo studio degli altri due sistemi è da ritenersi concluso. L'analisi del sistema LiF-RbF ha confermato una tendenza del calore specifico in eccesso nel sistema LiF-AlkF (Alk=Na,K,Rb,Cs).

Estratto in italiano

Introduzione

A fronte di una domanda energetica in continua crescita, prevalentemente soddisfatta dall´utilizzo di combustibili fossili, e di una necessitá di ridurre le emissioni di anidride carbonica, l´energia nucleare potrebbe svolgere un ruolo significativo per uno sviluppo futuro "sostenibile". Affinché questo sia possibile appare necessario migliorare l´opinione pubblica nei confronti della sicurezza e dell´affidabilità delle centrali nucleari, offrendo una tecnologia più innovativa. Sei nuove tipologie di reattori sono state identificate come le piú promettenti per la nuova generazione (*Generation IV*), basandosi su quattro obiettivi principali: miglioramento della sicurezza e affidabilità, riduzione della possibilitá di proliferazione nucleare, miglioramento della sostenibilità e diminuzione dei costi di costruzione e di esercizio di tali impianti. Tutte queste tecnologie, ognuna in misura diversa, necessitano di ulteriori ricerche e sviluppi per dimostrarne la fattibilità e ottimizzarne i progetti.

Il reattore a sali fusi (*MSR - Molten Salt Reactor*) è uno dei concetti selezionati ed è basato su un´idea sviluppata negli anni ´60 presso ORNL (*Oak Ridge National Laboratory*). La caratteristica principale è l´utilizzo di una miscela liquida di sali fusi avente la duplice funzione di combustibile e termovettore. La scelta della composizione del fluido è cruciale in quanto esso deve rispondere a una serie di requisiti sulle proprietá neutroniche, chimiche, termiche e di trasporto, nonché essere vantaggioso dal punto di vista economico. La classe di composti che meglio si adatta ai requisiti citati è quella dei fluoruri, già studiata in passato.

Questo lavoro di tesi, la cui parte sperimentale è stata svolta durante un tirocinio di nove mesi presso ITU (*Institute for Transuranium Elements*, Karlsruhe, Germania), si

colloca nell´ambito della ricerca in campo termodinamico sulle potenziali miscele di sali fusi, utilizzate come combustibile. Tuttavia, le applicazioni dei sali fusi non si limitano a questa funzione ma si estendono sia in campo nucleare che convenzionale, ad esempio come fluido termovettore. La caratterizzazione termodinamica dei composti puri e dei sistemi multi-componente è necessaria a stabilire la composizione ottimale per la miscela e i limiti di sicurezza. Fondamentale per giudicare le prestazioni dei potenziali candidati è la determinazione di proprietá quali punto di fusione, capacità termica, tensione di vapore, densità, viscosità, conduttività termica e capacità di solubilizzare attinidi. Per descrivere il comportamento di una miscela multi-componente è fondamentale conoscere le proprietà dei composti puri che la compongono. La combinazione di queste proprietà è in grado di caratterizzare una soluzione ideale, mentre è necessario aggiungere ulteriori dati per descrivere la soluzione reale. Uno dei risultati finali piú importanti è la costruzione del diagramma di fase che si compone di una parte sperimentale e di una fase di modellazione.

Per quanto riguarda la parte sperimentale, i dati sono stati raccolti utilizzando due diverse tipologie di calorimetri: il calorimetro a caduta (*Drop Calorimeter*), per la determinazione del calore specifico, e il calorimetro differenziale a scansione (*DSC - Differential Scanning Calorimeter*), per la determinazione dei punti di equilibrio del diagramma di fase e dell´entalpia di miscelamento. La determinazione del calore specifico è stata eseguita su tre sali appartenenti alla classe dei fluoruri e interessanti per le loro applicazioni: CsF in fase solida, $Li_{0,5}Rb_{0,5}F$ in fase liquida e ThF_4 in fase solida. Per quanto riguarda invece la calorimetria differenziale a scansione, questa tecnica é stata utilizzata per la prima volta per misurare l´entalpia di miscelamento dei sistemi. Trattandosi di una tecnica mai utilizzata a tale scopo, l´applicabilità del metodo è stata verificata su un sistema con comportamento noto (LiF-KF) e i risultati ottenuti sono stati soddisfacenti. È stato quindi possibile misurare l´entalpia di miscelamento per il sistema LiF-ThF_4, che è uno dei sali di riferimento per il reattore veloce a sali fusi (*MSFR - Molten Salt Fast Reactor*) e su cui non esistevano dati sperimentali al riguardo. Durante lo studio di entrambi i sistemi, sono stati misurati i punti di equilibrio del diagramma di fase che hanno fornito ulteriori dati utili alla fase di modellazione.

I dati sperimentali raccolti sui sistemi binari, LiF-KF e LiF-ThF_4, sono stati utilizzati

come base per la modellazione dei diagrammi di fase. A tale scopo è stato utilizzato il software FactSage, che sfrutta l'approccio CALPHAD per l'ottimizzazione dei diagrammi di fase. In generale, tale approccio consiste nella determinazione dell'energia di Gibbs per ognuna delle fasi del sistema considerato, ovvero di un opportuno modello che le descriva, da cui è possibile calcolare il diagramma di fase e numerose altre grandezze termodinamiche del sistema. Il processo di ottimizzazione consiste nel trovare il miglior compromesso tra le funzioni calcolate e i risultati sperimentali, variando i parametri del modello. Maggiore è il numero di dati sperimentali disponibili, minore è il numero di gradi di libertà del modello.

Descrizione parte sperimentale

Lo studio delle proprietà dei fluoruri comporta l´adozione di precauzioni durante il trattamento dei campioni legate alle caratteristiche degli stessi. Un primo aspetto è la tendenza ad assorbire molecole di acqua e in alcuni casi a ossidarsi facilmente. Per questo motivo, la preparazione e il trattamento dei campioni deve avvenire completamente in ambiente asciutto e i composti puri vengono sottoposti a un riscaldamento, prima dell´utilizzo, per allontanare l´umidità residua. Nel caso dei composti che mostrano la tendenza ad ossidarsi, ad esempio ThF_4 e UF_4, la purificazione è più complessa e consiste in una conversione degli ossidi in fluoruri, utilizzando bifluoruro d´ammonio (NH_4HF_2). La reazione chimica che avviene durante la purificazione è la seguente:

$$ThO_2 + 4NH_4HF_2 \longrightarrow ThF_4 + 4NH_4F + 2H_2O \tag{1}$$

E' importante osservare che l´adeguata purezza del composto ThF_4, recentemente raggiunta, è stata un fattore chiave per la buona riuscita delle misure.

La seconda caratteristica da tenere in considerazione lavorando con i fluoruri alle alte temperature è la produzione di vapori corrosivi. Tra i materiali danneggiati da questi vapori, particolare importanza è assunta dal platino che costituisce i filamenti delle termocoppie utilizzate negli strumenti. La corrosione è tale da rendere i rivelatori inutilizzabili dopo soli pochi cicli termici e può essere evitata incapsulando il campione all´interno di

appositi crogioli.

Il calorimetro a scansione differenziale

Il principio di base di questa tecnica consiste nel misurare la differenza di temperatura, e quindi il flusso termico, tra un crogiolo in cui è contenuto il campione e un crogiolo di riferimento. Entrambi i crogioli vengono riscaldati o raffreddati in maniera controllata, mantenendoli alla stessa temperatura. Durante una trasformazione di fase, la differenza di temperatura aumenta dato che il crogiolo di riferimento continua a riscaldarsi, mentre il riscaldamento del campione è ritardato dalla trasformazione in corso. Questo comporta la presenza di un flusso termico che viene registrato dallo strumento come un picco, contenente le informazioni relative all´evento termico. Il punto di inizio del picco corrisponde alla temperatura a cui avviene la trasformazione, mentre la sua area è proporzionale al calore scambiato durante la trasformazione. Per ricavare queste informazioni dal segnale elettrico, lo strumento deve essere calibrato, sia in temperatura, sia in energia. La calibrazione in temperatura viene eseguita utilizzando diversi materiali standard con punti di fusione distribuiti nell'intervallo di temperatura richiesto e sottoposti allo stesso ciclo termico dei campioni. Lo scarto tra la temperatura reale e misurata viene registrato in funzione della velocitá di riscaldamento e della temperatura stessa. Per quanto riguarda la calibrazione in energia, un nuovo metodo è stato utilizzato inserendo un material standard (Ag) all´interno del crogiolo di riferimento. In questo modo è possibile calibrare lo strumento durante ogni misura e migliorare l´accuratezza nella determinazione dell´energia.

Calorimetro a caduta

Il calorimetro a caduta è uno strumento che consente di misurare l´incremento di entalpia tra due diverse temperature. Il campione, mantenuto a temperatura ambiente, viene fatto cadere all´interno del calorimetro, preriscaldato alla temperatura desiderata, mentre il flusso termico viene misurato. La caduta viene registrata dallo strumento come un picco di area proporzionale all´incremento di entalpia nel campione tra la temperatura ambiente e la temperatura pre-impostata. Numerosi esperimenti sullo stesso campione vengono eseguiti cambiando la temperatura del calorimetro, in modo da ottenere una descrizione

del salto entalpico in funzione della temperatura. A questo punto il calore specifico del campione viene calcolato come derivata della funzione interpolante la serie di dati. Anche questo strumento necessita delle calibrazioni in temperatura e in energia, che sono state eseguite in maniera analoga a quelle già discusse per lo strumento precedente.

Risultati sperimentali

Il lavoro sperimentale svolto riguarda diversi sistemi, ognuno avente un´applicazione diversa nell´ambito dei reattori a sali fusi e piú in generale nella ricerca di base in campo termodinamico. In Tabella 1 sono riportate le misure effettuate durante questo lavoro di tesi. I principali risultati ottenuti sono descritti di seguito separatamente per ogni sistema.

LiF-KF

Il sistema binario LiF-KF è un sistema molto ben descritto in letteratura e una discreta quantitá di dati sperimentali è disponibile, sia per quanto riguarda il diagramma di fase che l´entalpia di miscelamento. Per questo motivo, questo sistema è stato scelto per confermare la possibilità di misurare l´entalpia di miscelamento utilizzando il calorimetro a scansione differenziale.

La tecnica introdotta per la misura dell´entalpia di miscelamento è schematizzata in Figura 1. I due composti puri, LiF e KF, vengono compressi in pastiglie, in modo da essere più compatti, e inseriti nel crogiolo. Il composto con il minor punto di fusione è posto nella parte inferiore e le due pastiglie sono tenute separate da un sottile strato di nichel. Durante la fase di misura il crogiolo viene riscaldato in maniera controllata fino ad una temperatura superiore a entrambi i punti di fusione. Quando il composto sul fondo del crogiolo fonde, lo strato di nichel cade all´interno del crogiolo trasportando anche la seconda pastiglia che inizia a solubilizzarsi. Se questo evento è sufficientemente veloce, lo strumento registra un singolo evento termico contenente tre informazioni: la fusione del primo composto LiF, la fusione del secondo composto KF e il miscelamento dei due composti. L´entalpia di miscelamento viene quindi calcolata partendo dall´area totale del picco e sottraendo i contributi dovuti alla fusione dei due composti puri. Dato

Tabella 1: Misure sperimentali effettuate in questo lavoro di tesi.

Sistema	**Dati sperimentali raccolti**	**Numero di misure**	**Commento**
LiF	Temperatura di fusione, entalpia di fusione	19	*Calibrazione in energia DSC*
NaCl	Temperatura di fusione, entalpia di fusione	13	*Calibrazione in energia DSC*
KF	Temperatura di fusione, entalpia di fusione	23	*Calibrazione in energia DSC*
LiF-KF	Punti di equilibrio	36	*9 composizioni, misurate ognuna 4 volte*
	Entalpia di miscelamento	9	*Misurate a T=1121 K*
ThF_4	Temperatura di fusione, entalpia di fusione	20	*Conferma della purezza del composto*
	Incremento di entalpia	109	*Determinazione del calore specifico fase solida*
LiF-ThF_4	Entalpia di miscelamento	7	*Misurate a T=1121 K e T=1383 K*
	Punti di equilibrio	124	*31 composizioni, misurate ognuna 4 volte*
Li_3ThF_7	Temperatura di fusione, entalpia di fusione.	3	*Conferma della purezza del composto e misura entalpia di fusione*
CsF	Temperatura di fusione, entalpia di fusione	12	*Conferma della purezza del composto*
	Incremento di entalpia	120	*Determinazione del calore specifico fase solida*
$Li_{0,5}Rb_{0,5}F$	Temperatura di fusione, entalpia di fusione	3	*Conferma della purezza del composto*
	Incremento di entalpia	69	*Determinazione del calore specifico fase liquida*

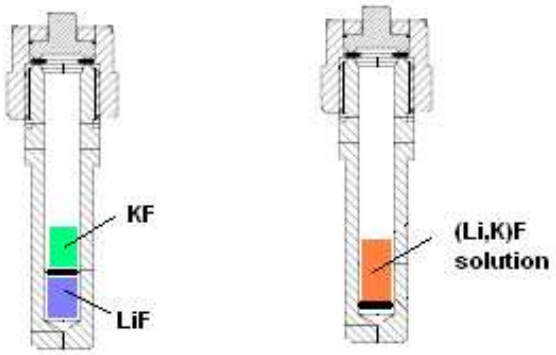

Figura 1: Schema della tecnica utilizzata per misurare l´entalpia di miscelamento. Le due pastiglie sono separate da uno strato di nichel ed entrano in contatto solo dopo la fusione del composto sul fondo, formando la soluzione finale.

che il calorimetro differenziale a scansione non misura direttamente questa grandezza, l´errore sui dati risulta maggiore rispetto ai corrispondenti dati di letteratura. Tuttavia i punti ottenuti sono in grado di descrivere correttamente l´andamento dell´entalpia di miscelamento e rientrano nel corretto ordine di grandezza, come mostrato nel grafico superiore in Figura 2. Ogni esperimento consiste in quattro cicli termici di riscaldamento e raffreddamento a cui ogni campione viene sottoposto. Il primo riscaldamento è utilizzato per ricavare l´entalpia di miscelamento, mentre i successivi forniscono informazioni sugli equilibri di fase, misurati anch´essi in questo lavoro.

Entalpia di miscelamento, punti di equilibrio del diagramma di fase e nuovi dati sul calore specifico della soluzione, misurati recentemente in ITU, sono stati utilizzati per la costruzione del diagramma di fase. L´energia di Gibbs del sistema LiF-KF è stata descritta utilizzando un semplice modello polinomiale con la seguente forma generale:

$$\triangle G_{excess} = \sum_{n,m} X^n_{LiF} \cdot X^m_{KF} \cdot [A^{n,m} + B^{n,m} \cdot T + C^{n,m} \cdot T \cdot ln(T)] \qquad (2)$$

in cui X^n_{LiF} e X^m_{KF} sono le frazioni molari dei due composti puri e $A^{n,m}$, $B^{n,m}$, $C^{n,m}$ sono parametri da ottimizzare durante la modellazione. Questi parametri sono stati selezionati sulla base dei dati sperimentali disponibili di entalpia di miscelamento e calore specifico, allo scopo di ottenere il miglior accordo possibile con gli equilibri di fase misurati. Il

risultato finale è mostrato nel grafico inferiore in Figura 2. L´introduzione dei nuovi dati nel modello non ha cambiato la forma generale del diagramma di fase ma è stato utile a migliorarne la descrizione, fondamentale ai fini dell´estrapolazione per sistemi di ordine superiore.

LiF-ThF_4

I progetti piú recenti sui reattori a sali fusi comprendono anche reattori veloci, ad esempio il (MSFR - *Molten Salt Fast Reactor*), in cui la miscela di sali fusi puó avere una composizione diversa. Uno dei sali di riferimento per questo concetto è il sistema LiF-ThF_4, oggetto di questo lavoro. I dati sperimentali trovati in letteratura sono relativi agli equilibri di fase mentre non sono stati trovati dati che descrivano la soluzione liquida. Come conseguenza, il modello sviluppato mostra diversi gradi di libertá e necessita di nuovi dati sperimentali a conferma. Lo scopo dello studio è stato la misura sperimentale dell´entalpia di miscelamento e di ulteriori dati sulle transizioni di fase. Inoltre, è stato sintetizzato il composto intermedio Li_3ThF_7 ed è stata misurata la sua entalpia di fusione.

La determinazione dell´entalpia di miscelamento per questo sistema ha comportato sforzi maggiori rispetto al sistema precedente. Infatti, i punti di fusione dei due composti puri sono molto piú distanti (T=1121 K per LiF e T=1383 K per ThF_4) e il processo risente della velocitá di solubilizzazione del ThF_4. In alcuni casi lo spettro ottenuto mostrava la presenza di due o tre picchi, segno di un incompleto miscelamento, e i dati non sono stati considerati. A causa di questa difficoltá, il numero di punti misurati è limitato ma essi sono comunque sufficienti a indicare l'ordine di grandezza della funzione. Il risultato ottenuto, riportato nel grafico superiore in Figura 3, mostra una chiara differenza tra l´entalpia di miscelamento misurata e quella calcolata dal modello precedente del diagramma di fase, suggerendo la necessitá di una nuova ottimizzazione. Allo scopo sono stati utilizzati anche i nuovi punti del diagramma di fase misurati anch'essi in questo lavoro di tesi.

Basandosi sull´evidenza sperimentale, un diverso composto intermedio ($LiThF_5$ invece di Li_6ThF_7) è stato considerato durante la fase di modellazione in modo da fornire una migliore interpretazione i dati. Le proprietá termodinamiche dei composti intermedi, non note, sono state ottimizzate durante la fase di modellazione insieme ai parametri

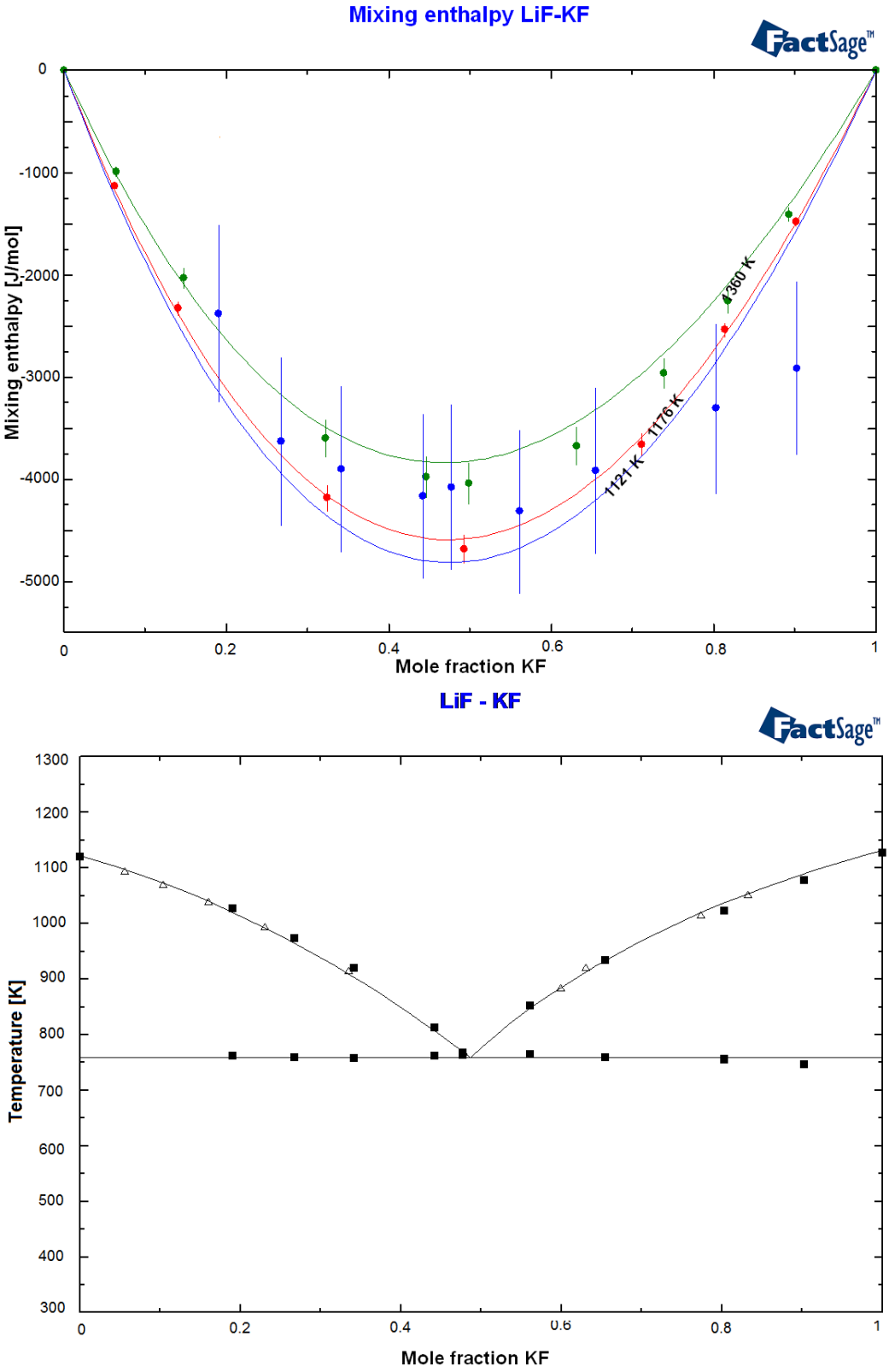

Figura 2: Sistema LiF-KF. Grafico superiore: Confronto tra l´entalpia di miscelamento misurata a T=1121 K (●) e i dati di letteratura a T=1176 K (●) e T=1360 K (●). Le curve mostrate sono calcolate dal modello ottimizzato in questo lavoro. Grafico inferiore: Confronto tra il diagramma di fase ottimizzato in questo lavoro e i dati sperimentali misurati (■) e da letteratura (△).

dell´energia di Gibbs. Il risultato finale è mostrato nel grafico inferiore in Figura 3 ed è in grado di fornire una descrizione migliore dei dati sperimentali rispetto al precedente.

Infine, come parte dello studio sul sistema LiF-ThF_4, è stato sintetizzato il composto intermedio Li_3ThF_7 utile per indagini sperimentali future. Questo composto fonde in maniera congruente a T=831 K ed è il composto che offre le maggiori potenzialità come combustibile per il reattore a sali fusi. Il sale è stato preparato miscelando stechiometricamente i due composti puri e la purezza finale del composto è stata controllata con due tecniche diverse. Il calorimetro differenziale a scansione e l´analisi a raggi X hanno entrambi confermato la purezza del campione. L´entalpia di fusione di questo composto è stata misurata e confrontata con i dati di letteratura, fornendo un buon accordo. Al contrario, il valore sperimentale si discosta significativamente dal valore calcolato basandosi sul modello. Questo problema potrebbe essere risolto variando due diversi parametri del modello, il calore specifico della soluzione o del composto intermedio, ma non è facile stabilire come le due funzioni debbano essere cambiate. Dato che nuove misure sono previste nell´imminente futuro in ITU su entrambe le grandezze, si è preferito non apportare nessuna modifica.

CsF

Lo studio delle proprietá termodinamiche del CsF sono importanti dal punto di vista delle applicazioni nel campo dei reattori a sali fusi, anche se non rientra nella composizione iniziale del combustibile. Infatti, questo sale è uno dei composti stabili del prodotto di fissione Cs, che si forma durante il funzionamento del reattore, e puó influenzare il comportamento finale della miscela di sali. I dati sperimentali sul calore specifico del CsF in fase solida vanno a completare un studio piú generale volto a determinare il calore specifico di questo composto da 5 K a 1400 K.

Le misure sono state effettuate utilizzando pastiglie di CsF, con una massa media di circa 70-80 mg, incapsulate in crogioli di nichel. I campioni sono stati poi misurati utilizzando il calorimetro a caduta in un intervallo di temperatura da 400 K a 960 K. I dati relativi all´incremento di entalpia misurati sono stati poi, in prima approssimazione, interpolati linearmente fornendo un calore specifico molto simile ai dati di letteratura.

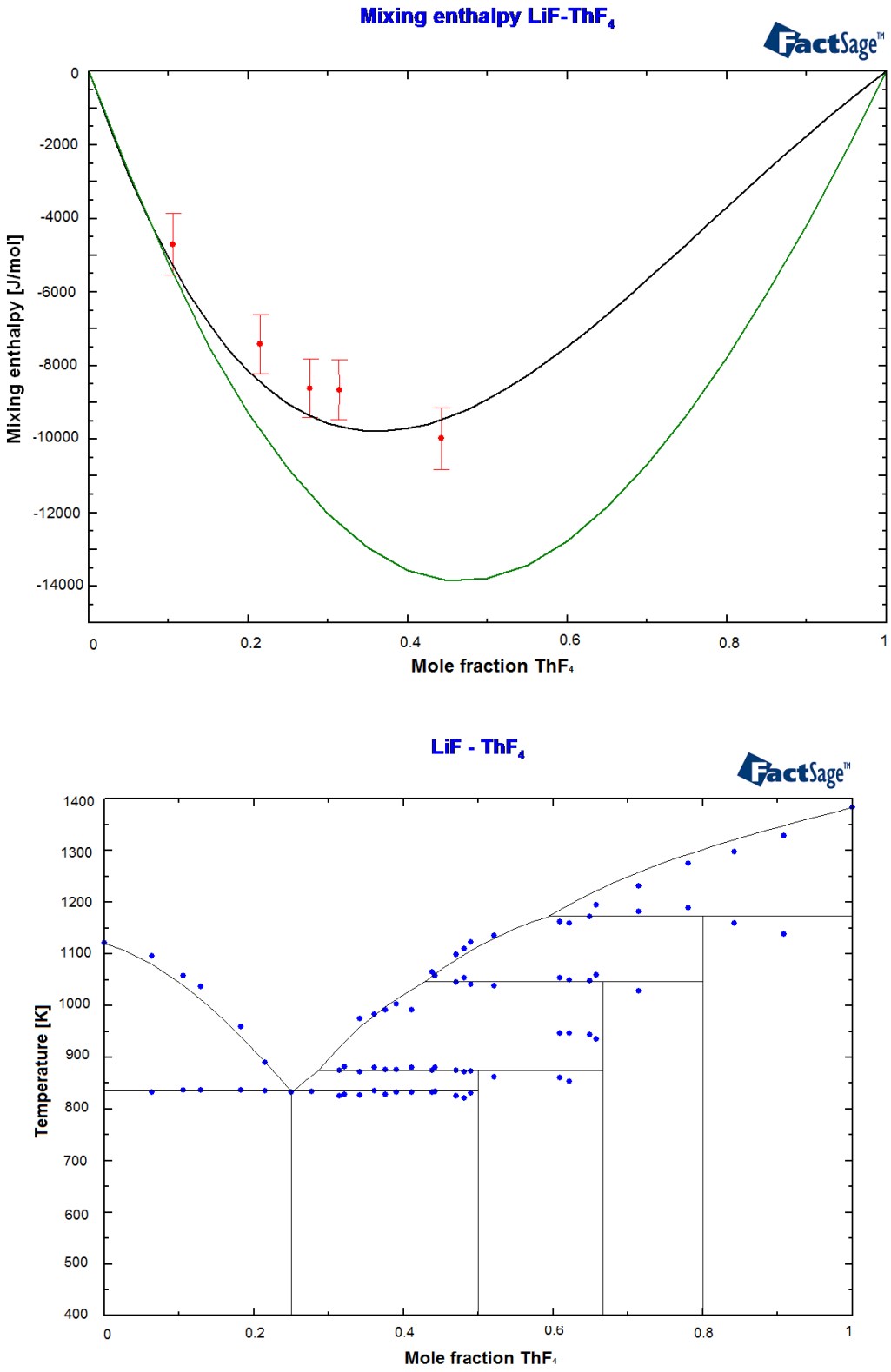

Figura 3: Sistema LiF-ThF_4. Grafico superiore: Entalpia di miscelamento calcolata a T=1121 K rispettivamente dal modello ottimizzato in questo studio (linea nera) e dal modello precedente (linea verde). I dati sperimentali sono riportati in rosso. Grafico inferiore: Diagramma di fase ottimizzato del sistema LiF-ThF_4 e dati sperimentali misurati.

Tuttavia, questa assunzione porta a una valore costante del calore specifico, che risulta troppo alto a temperatura ambiente se confrontato con l´evidenza sperimentale. Risulta quindi necessario tenere in considerazione i dati sperimentali sul calore specifico a basse temperature, misurati recentemente con un calorimetro adiabatico. Una nuova interpolazione è stata quindi eseguita utilizzando una funzione polinomiale di ordine maggiore e con la seguente forma generale:

$$C_p^0(T) = A + B \cdot T + C \cdot T^{-2} \tag{3}$$

I coefficienti ottenuti sono stati:

$$A = 24,291 \pm 7,646 \;\; J \cdot mol^{-1} \cdot K^{-1} \tag{4}$$

$$B = 6,4607 \cdot 10^{-2} \pm 1,6683 \cdot 10^{-2} \;\; J \cdot mol^{-1} \cdot K^{-2}$$

$$C = 589981 \pm 242592 \;\; J \cdot mol^{-1} \cdot K$$

Per quanto riguarda la fase liquida, i dati sono stati raccolti da 1030 K a 1385 K e interpolati linearmente. Il calore specifico risultante è:

$$C_P = 70,56 \pm 5,5 \;\; J \cdot mol^{-1} \cdot K^{-1}$$

in perfetto accordo con i dati in letteratura. Infine, utilizzando le equazioni dell´entalpia in fase liquida e solida, è stato calcolato il calore di fusione del composto come differenza di entalpia alla temperatura di fusione. Il valore ottenuto è stato poi confrontato con il dato di letteratura e con il dato ottenuto dalla misura tramite calorimetro differenziale a scansione. I tre valori sono risultati pressoché coincidenti indicando quindi un buon accordo tra le due tecniche utilizzate.

$\mathbf{ThF_4}$

Il ThF_4 è uno dei composti piú rilevanti per le sue applicazioni nel campo dei reattori a sali fusi ma, nonostante ció, i dati termodinamici disponibili sono molto carenti. Non

esistono dati sperimentali pubblicati sul calore specifico a temperature superiori a 298 K né sul calore di fusione. Gli unici dati disponibili sono basati su un lavoro preliminare di Dworkin e sono stati successivamente utilizzati per ricavare un´equazione approssimata. Appare evidente la necessitá di misurare dati sperimentali sul ThF_4 in grado di confermare o ridefinire le proprietá termodinamiche attualmente assunte. L´obiettivo di questo studio è stato quindi la determinazione del calore specifico in fase liquida e solida e dell´entalpia di fusione. Tuttavia a causa di vincoli temporali e difficoltá dovute alla resistenza dei crogioli ad alte temperature, è stata misurata solo la fase solida. I campioni sono stati misurati in un vasto intervallo di temperatura (da 320 K a 1290 K) e i dati sono stati interpolati linearmente. Il risultato ottenuto per il calore specifico è pari a :

$$C_{p,sol} = 173,02\, J \cdot K^{-1} \cdot mol^{-1}. \tag{5}$$

che devia significativamente dall´equazione stimata in letteratura. A conferma dei risultati ottenuti, ulteriori analisi che giustifichino la purezza del campione sono in corso presso ITU. Tuttavia è improbabile che la sola presenza di impuritá possa spiegare una tale deviazione del calore specifico, data la precisione con cui è stato misurato il punto di fusione.

LiF-RbF

Come precedentemente accennato, la classe dei fluoruri è di importanza centrale per la tecnologia dei sali fusi. Nell´ottica di uno studio sistematico dei composti binari e ternari di interesse, il calore specifico della soluzione è stato studiato per la serie di sistemi LiF-MF (M= Na, K, Cs). Dai risultati ottenuti è stata osservata un significativa deviazione del calore specifico rispetto al valore ideale e una possibile correlazione tra questa deviazione e la differenza tra i raggi dei cationi nel sistema. Per confermare questa ipotesi e completare la descrizione del generico sistema tra LiF e il generico fluoruro alcalino, è stato studiato il sistema LiF-RbF. Dato che la massima deviazione dall´idealitá nei precedenti sistemi è stata riscontrata a composizioni 1:1, il primo composto studiato è stato $Li_{0,5}Rb_{0,5}F$. Il calore specifico della soluzione è stato determinato nell´intervallo di temperatura tra 930

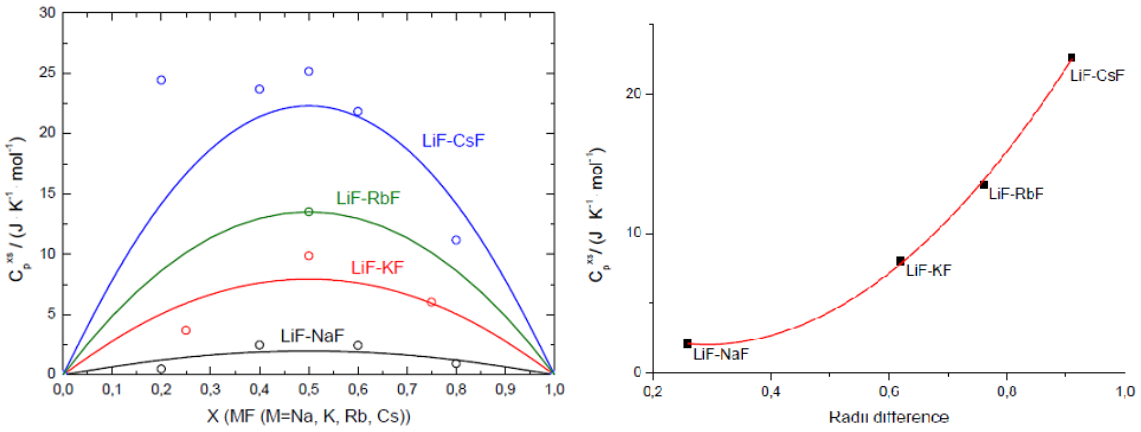

(A) (B)

Figura 4: (A) Confronto tra il calore specifico della soluzione nella serie di sistemi LiF-MF (M=Na, K, Rb, Cs). (B) Rappresentazione della correlazione tra il calore specifico della soluzione e la differenza di raggio atomico tra i cationi.

K e 1290 K ed è risultato pari a:

$$C_P = 81,11 \ \ J \cdot mol^{-1} \cdot K^{-1}. \tag{6}$$

Questo valore è stato poi confrontato con il calore specifico ideale della soluzione e l´eccesso ottenuto è stato graficato insieme ai dati ottenuti precedentemente. Come mostrato in Figura 4, il risultato è perfettamente concorde con le previsioni, confermando la correlazione ipotizzata.

Conclusioni

In questo lavoro di tesi sono state studiate le proprietá termodinamiche di diversi sistemi di fluoruri. Utilizzando due diverse tecniche calorimetriche, è stato possibile ottenere diverse tipologie di dati sperimentali utili alla caratterizzazione: entalpia di miscelamento, equilibri di fase e calore specifico. Il calorimetro differenziale a scansione, normalmente utilizzato per la determinazione degli equilibri di fase, è stato utilizzato per la prima volta per misurare l´entalpia di miscelamento. La tecnica utilizzata è stata verificata su un sistema noto (LiF-KF), ottenendo risultati soddisfacenti. Nonostante i dati sperimentali mostrano un'incertezza significativa, la tecnica si è rivelata adatta a descrivere l'andamento dell'entalpia di miscelamento. Un'applicazione importante di questa tec-

nica è stata la determinazione dell'entalpia di miscelamento del sistema LiF-ThF_4, mai misurata in passato. Questa proprietà, combinata ai nuovi dati sugli equilibri di fase, è stata utilizzata per la modellazione del diagramma di fase. Il risultato ottenuto è stato un miglioramento del diagramma di fase rispetto al modello precedente, in grado di interpretare meglio i dati sperimentali. Ulteriori perfezionamenti possono essere ancora apportati misurando, ad esempio, le proprietà termodinamiche dei composti intermedi e le proprietà della soluzione non ancora note. A tal proposito è stato sintetizzato il composto Li_3ThF_7, che è disponibile per esperimenti futuri. Inoltre, l'entalpia di fusione di questo composto è stata misurata fornendo risultati simili alla letteratura.

Utilizzando il calorimetro a caduta, sono state effettuate misure riguardanti il calore specifico dei composti su tre sistemi di fluoruri:

- Lo studio del calore specifico della fase solida del CsF ha contribuito alla completa caratterizzazione di questa proprietá da 5 K a 1400 K.
- La fase liquida del composto $Li_{0,5}Rb_{0,5}F$ è stata misurata per completare la descrizione sistematica del sistema LiF-MF (M=Na, K, Rb, Cs), ottenendo un risultato molto simile alle previsioni.
- E' stato iniziato uno studio sulle proprietá del ThF_4, ottenendo un primo risultato sul calore specifico in fase solida. Il calore specifico misurato è molto maggiore rispetto quello stimato in letteratura e ulteriori studi sono in corso in ITU per confermare la purezza del composto.

Concludendo, in questo lavoro di tesi sono stati studiati cinque sistemi interessanti per le loro applicazioni nel campo dei reattori nucleari a sali fusi. Una nuova tecnica è stata sviluppata per la misura dell'entalpia di miscelamento e sono stati ottenuti nuovi dati sperimentali. La determinazione delle proprietà dei sistemi di fluoruri, come il calore specifico e il diagramma di fase, saranno basilari per il progetto futuro del reattore a sali fusi.

Introduction

In the framework of an increasing energy demand in the future, climate change and decreasing fossil resource availability, the nuclear energy could have an important role in the future energy supplies. In order to make it possible, it is necessary to enhance the public confidence in the nuclear power, specially in these times after the Fukushima´s event. Improving the safety and the reliability will be a key factor to achieve this purpose, which is the main aim of the new generation of reactors called Generation IV. Six reactor concepts were selected by the Generation IV International Forum (GIF) as the most promising technologies based on four main goals: safety and reliability, proliferation resistance, sustainability and economics.

The Molten Salt Reactor (MSR), which is the subject of this work, is one of the six reactor concepts selected and it is based on a molten salt mixture in which the fissile material is dissolved and serves both as fuel and coolant. Fundamental research and developments in different fields are needed to assess the reactor parameters and to establish the feasibility and performance of such system. In order to determine the safety limits for the molten salt fuel, basic research on thermodynamic properties of fluoride salts is necessary and includes experimental determination of heat capacity and phase equilibrium points, which are presented in this work and are used to extend and improve the thermodynamic database of these systems.

This thesis describes the work performed during a traineeship at the Institute for Transuranium Elements (ITU) in Karlsruhe, Germany. The work, carried out in the Materials Research Unit, mostly deals with the investigation of the physico-chemical properties of nuclear materials. The main task of the thesis was the thermodynamic characterization of the salt component for nuclear application in MSR. Experimental data were collected

for five interesting systems and in two cases they were used for the optimization of the phase diagram, using CALPHAD method. Moreover, a new technique for the enthalpy of mixing determination was employed and tested.

The thesis is organized in five chapters. In Chapter 1, an overview on nuclear energy and Generation IV reactors is presented. The six reactors concepts selected for further developments are mentioned and shortly described. The emphasis is placed on the Molten Salt Reactor, which is introduced with a description of the system, the main advantages that it offers, the proposed fuel concepts and its history.

Thermodynamics of the molten salts is the subject of Chapter 2, where the relevant properties of the salts studied in this work are introduced. The chapter is divided into two parts dedicated to the description of pure compounds and binary systems, respectively.

Chapter 3 presents the experimental method used in this work. The first part describes the handling of the fluoride salts, the adopted purification process and the two encapsulation techniques developed to measure high temperature properties of fluoride salts. Drop calorimetry and differential scanning calorimetry, which are the two techniques employed, are then explained as well. Furthermore, the temperature calibrations and the new energy calibration performed for the instruments are discussed.

Chapter 4 is the main part of the work and is dedicated to the experimental results obtained in this study. The work was carried out on several systems, which are described separately throughout the chapter. Experimental determination of heat capacity, enthalpy of mixing and phase diagram description are the main tasks carried out in this thesis. Two systems were analysed with respect to their phase diagrams: the LiF-KF system and the LiF-ThF_4 system. The first system has a known behaviour and was studied in order to verify the novel technique employed. The second system is relevant for the nuclear application as a primary salt for MSR and its behavior is not yet characterized. Both experimental phase diagram points and enthalpy of mixing values were identified for several LiF-ThF_4 compositions and used for the phase diagram assessment. At the same time, experimental determinations of the heat capacity of CsF and ThF_4 pure compounds and of (Li,Rb)F liquid solution were performed. They are part of a systematic investigation on the heat capacity of fluoride salt mixtures performed at ITU.

Finally, the results are summarized and discussed in Chapter 5 and the possible future work is highlighted.

Chapter 1

Molten Salt Reactor Technology

1.1 Nuclear energy

The world's population is expected to increase from about 7 billion people to 10 billion people by the year 2050. This population growth and the improvement of general well-being will lead to an enormous increase of the energy demand in the near future. In this framework and in order to reduce the CO_2 emissions, it appears necessary to reduce the use of fossil fuels. The use percentage of energy supplies that are clean, safe, and cost-effective must increase and nuclear energy can play an important role in providing clean energy for global sustainable development.

In addition to this aspect, the nuclear energy has an excellent energy density, as shown clearly in the Table 1.1. For fuels, the energy per unit volume is a useful parameter. For instance, a low value means reduced transport problems and, of course, less use of resources.

Table 1.1: Comparison in energy density for several fuels. Source: Michel Lung, 2000, AEPN/EFN.

Energy unit of fuel	**Energy content [J]**
1 kg of wood	$7{,}2{\cdot}10^6$ J
1 kg of coal	$1{,}4{\cdot}10^7$ J
1 kg oil	$2{,}1{\cdot}10^7$ J
1 cubic meter of gas	$2{,}1{\cdot}10^7$ J
1 kg of natural uranium	$1{,}8{\cdot}10^{11}$ J

This big difference between the energy content is due to the different type of energy. Except for the uranium, the energy is released after chemical reactions: the burning of coal, oil and gas together with oxygen from the air form new molecules, more stable, which release energy. Considering the uranium, the energy is released after nuclear process, thus the available energy does not depend on the coulombian interaction between nuclei and electrons but on the interactions within the nuclei. This kind of force, called nuclear force, is hundred million time greater than the interactions responsible of the chemical reactions and it explains the large amount of energy generated. Mainly for these reasons the use of nuclear energy is very attractive and the effort in the study of the nuclear system is justified. However, it is good to keep in mind that nuclear energy produces long lived toxic waste, which must be managed with care.

1.2 A brief introduction of the Generation IV Reactors

Nuclear reactors are usually categorized by generation. There are several attributes that can explain the differences between the various generations of reactors and characterize the development of nuclear power reactors.

Among the most important attributes are cost-effectiveness, safety, security, non-proliferation features, and management of the fuel cycle. Based on these parameters, the reactors are classified as:

- **Generation I** refers to the prototype, that shows the feasibility of the chain reaction, and to the first power reactors, such as Shipping Port and Dresden I.

- **Generation II** refers to a class of commercial reactors, which includes most of the commercial reactors currently in operation. The Generation II includes the most common Pressurized Water Reactor (PWR) and the Russian analogue Vodo-Vodyanoi Energetichesky Reactors (VVER), Boiling Water Reactor (BWR), CANadian Deuterium Uranium reactor (CANDU) and Advanced Gas-cooled Reactor (AGR). These designs require relatively large electrical grids, have a defined safety envelope based on Western safety standards, and produce significant quantities of used fuel that require ultimate disposition in a high-level waste repository.

- **Generation III**. This class of reactors are essentially the Generation II reactors with some improvements that have been developed studying the behavior of the previous generation. These important improvements are in areas of fuel technology, thermal efficiency and safety systems and enable to extend the operational life-time of the nuclear power plants.

- **Generation IV** refers to an innovative class of reactors. These nuclear systems are likely to reach technical maturity by 2030. Their design will take cognisance of the progress made in economics and safety. The main goals of these new technologies are:

  - Safety & Reliability. These reactors must provide an excellent level of safety and reliability, which helps to enhance public confidence in the acceptance of nuclear energy. These systems should be passively safe meaning that the reactor would not overheat after a shut-down when there is no coolant available.
  - Sustainability. These reactors must generate energy sustainably and guarantee long term availability of the nuclear fuel. Moreover, it is important to minimize the nuclear waste, especially the portion of long lived actinides, and for this reason a transmutation of these isotopes will be introduced.
  - Economics. To succeed this technology, it is necessary that the life cycle cost is lower compared to other energy sources, e.g., coal power plants.
  - Proliferation resistance. These new reactors must be a very unattractive route for diversion or theft of weapons-usable materials, and provide increased protection against acts of terrorism.

In order to advance nuclear energy to meet future energy needs, ten countries have agreed on a framework for international cooperation in research for a future generation of nuclear energy systems [1]. International experts found the most promising nuclear systems, and six reactor concepts have been selected. These Generation IV concepts are:

- Gas-Cooled Fast Reactor (GFR)

- Lead-Cooled Fast Reactor (LFR)

- Supercritical-Water Reactor (SCWR)
- Sodium-Cooled Fast Reactor (SFR)
- Very-High-Temperature Reactor (VHTR)
- Molten Salt Reactor (MSR)

Among the relevant criteria for the selection of the six systems, a fundamental role was assigned to sustainability. This is the reason that the majority of the chosen systems have a fast spectra and a closed fuel cycle. A brief description of each reactor concepts is made below.

The **GFR** is a system that uses a fast neutron spectrum and closed fuel cycle. The reference reactor is helium-cooled system operating with an outlet temperature of 850°C using a direct Brayton cycle gas turbine for electricity production with high thermal efficiency. Moreover, this reactor offers a waste minimization and efficient use of uranium resources. Further research is needed for fuel and recycling technology development.

The **LFR** is a fast spectrum reactor with a closed fuel cycle. The proposed coolant is molten lead or eutectic lead-bismuth solution. The system is specifically designed for generation of electricity and other energy products, including hydrogen production and desalination of water. This system can be also used as a burner for actinides. The lead offers advantages in terms of sustainability and safety. The large availability of lead enables to guarantee the sustainability of the process and the safety is enhanced by the choice of a relatively inert coolant. Further research is needed for fuel, materials, and corrosion control.

The **SFR** is a fast spectrum reactor with a closed fuel cycle. The difference with the LFR system is the composition of the coolant, which is composed by liquid sodium. The goals are to increase the efficiency of uranium usage by closed fuel cycle. Further research is needed on the recycle technology, economics of the overall system and assurance of passive safety. A test reactor with this concept has been built in France.

The **SCWR** is a thermal reactor concept that operates at high temperature and high pressure. The system has two fuel cycle options: the first is an open cycle with a thermal neutron spectrum reactor, and the second is a closed cycle with a fast-neutron

spectrum reactor. In both options, the coolant is light water above its thermodynamical critical point (374 °C, 22.1 MPa). The advantages of this coolant are the higher thermal efficiency, due to higher outlet temperature, and the simplification of the plant compared to currently used BWRs, due to the fact that the liquid does not change phase in the reactor. The main goal of this reactor is production of low cost electricity.

The **VHTR** is a thermal reactor that uses graphite as moderator and helium gas as primary coolant. This technology uses a once through uranium fuel cycle and is designed to be a very highly efficient system. The outlet temperature exceeds 1000°C and offers the possibility to use the heat for direct hydrogen production, e.g., via sulphur iodine cycle [2]. Due to the high temperature, this system brings significant challenges in terms of fuel and materials developments, as well as safety under transient conditions.

The **MSR** is a unique technology that uses molten salts as coolant and also as fuel. Since the main task of this thesis is the investigation of physico-chemical properties of MSR fuel, useful for the evaluation of safety related features of this reactor concept, a more detailed description of this system is given in the following sections.

For the development of any kind of the above mentioned system two main phases of research were identified. The first, called the 'feasibility phase', examines the feasibility of the key technologies, and the following one, called 'performance phase', undertakes the development of performance data and optimization of the system. Assuming the successful completion of viability and performance research, a demonstration phase of several years is required.

1.3 Description of the MSR system

A schematic layout of a typical Molten Salt Reactor is given in Figure 1.1. In MSR, the fissile material, such as ^{235}U, ^{233}U or ^{239}Pu, is dissolved in a molten fluoride salt and serves as a primary coolant. It is pumped at low pressure through the reactor vessel, where the chain reaction takes place. The heat generated by the fission process is transferred in a heat exchanger to a secondary coolant, which is generally a molten salt also, and the fuel salt flows back to the reactor. The reactor and primary system are constructed from alloy

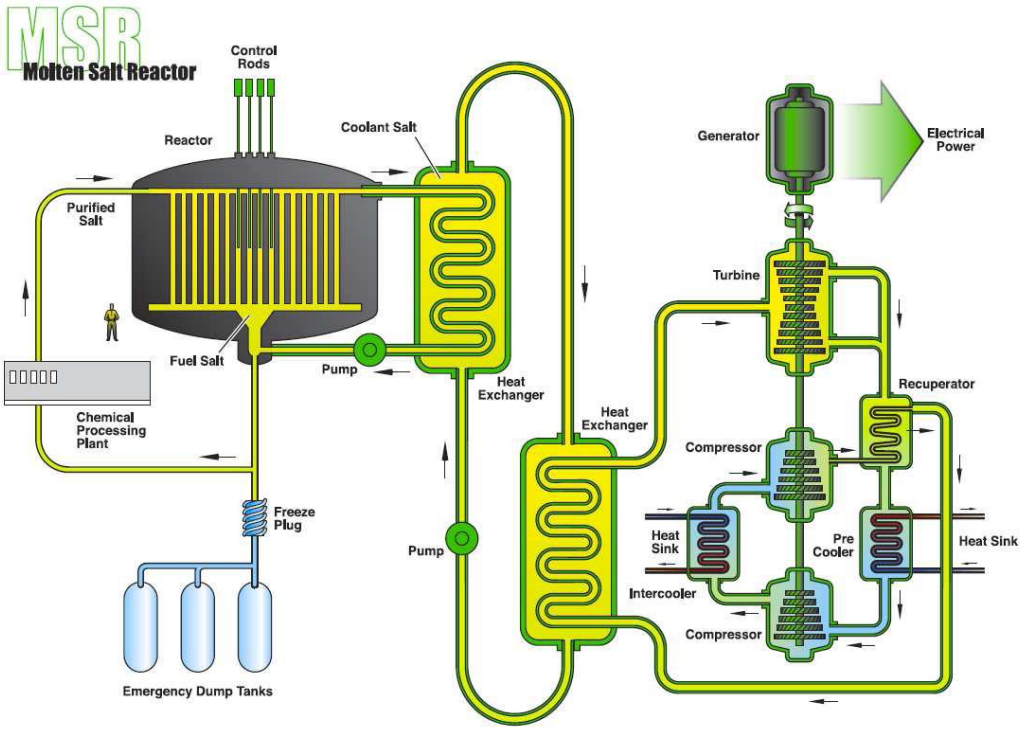

Figure 1.1: Schematic representation of MSR.

based on Hastelloy-N for corrosion resistance purpose. The operating temperature of the MSR is between 800-1000 K, the lower limit determined by the fusion temperature of the salt, whereas the upper one by the corrosion rate of the structural material.

The secondary coolant loop transfers the heat from the primary heat exchanger to a power cycle facility. This intermediate loop is introduced for safety reasons to avoid direct contact between the steam and the fuel. Furthermore, the secondary loop traps the tritium that escapes from the primary system as it tends to migrate across hot heat exchanges and a small clean-up system removes it from the secondary coolant.

Early designs of the MSRs proposed the use of a steam cycle for electricity production but current proposals use a multi-reheat helium or nitrogen Brayton cycle. The helium Brayton cycle has major advantages over the use of a steam Rankine cycle: simplified balance of plant with lower cost, improved efficiency and reduced potential for salt freezing in the heat exchangers. The estimated helium Brayton cycle efficiency is 48% compared to 44% for the steam cycle.

1.3.1 Advantages of the MSRs

Molten salt reactors have several operational and safety advantages over solid fuel designs [3, 4, 5]. Concerning the safety aspects the most important points are summarized below.

The first aspect is that, due to the liquid nature of the fuel salt, the meltdown of the core is substantially irrelevant. Emergency tanks are installed under the reactor and in case of accident the fuel salt is drained automatically to passively cooled tanks. These tanks are designed with the purpose that the fuel stays subcritical under these conditions. Unlike solid-fuel reactors, the MSR has low excess reactivity because the fuel is added as needed. Furthermore, no excess reactivity is needed at reactor start-up to compensate for fuel depletion and to override xenon poisoning. In fact, a continuous removal of the noble gas xenon is done via the off gas system. Since the idea is to perform a continuous clean-up of the fuel salt, no fission products accumulate and thus there is no dead-time of the reactor after shutdown. Due to the possibility to add the fuel continuously, the fissile concentration is easily adjusted and there is no need to have burnable poisons at start-up of the reactor. Neutron absorption from fission products is continuously mitigated by salt clean-up. Beside contributing to a safety of reactor, this fact results in an increase of the fuel burn up.

An important feature of this reactor type is a very strong negative temperature coefficient, especially for the non moderated concept. In general, this feedback coefficient is determined by the properties of the salt and moderator (in case of thermal spectrum reactors), among these the expansion of the salt and the Doppler effect. The final value and the importance of each single factor will depend on the exact design of the reactor.

Another important aspect is the low pressure required to keep the salt liquid. The salts run near atmospheric pressure and only a low pressure vessel is required, unlike the Light Water Reactors (LWR). It means that in case of accident, explosion risks are minimized. The absence of water or sodium, unlike in LWRs and SFR respectively, means that there is not the possibility to have hydrogen production and subsequent explosion. The low vapour pressure of molten fluoride salts reduces also stresses on the vessel and piping.

Concerning the sustainability needed for the Generation IV aims, utilization of the

^{232}Th to ^{233}U cycle produces several orders of magnitude less of transuranic wastes than a conventional once through cycle. Moreover, the terrestrial abundance of thorium is 3 times greater compared with the uranium [6]. The MSR has a good neutron economy and could offer large advantages for burning of transuranic wastes from traditional reactors.

1.3.2 Fuel concepts

To determine the optimal fuel composition several requirements must be fulfilled [7]:

- **Neutronic properties:** low neutron capture cross section for the solvent components.
- **Radiation stability**
- **Thermal and transport properties:** low melting point, thermal stability, low vapour pressure, adequate heat transfer and low viscosity.
- **Chemical properties:** high solubility for the fuel components, compatibility with vessel and moderator materials, feasible salt clean-up.
- **Economic features**: low fuel and reprocessing costs.

The class of compounds that shows the best compromise between all these requirements are the fluoride salts. The first proposal for the fuel, used in Aircraft Reactor Experiment (ARE), was a mixture of NaF-ZrF_4 with dissolved fissile UF_4. These fluorides were preferred because they have relatively high solubility for actinides. When the molten salt technology was transferred to the civilian program and it was recognized that the molten salt would be ideal for thermal breeding of uranium from thorium, the neutron economy in the reactor became a key factor. Hence, in MSBR (Molten Salt Breeder Reactor) new fuel salt was selected based on a very low neutron capture cross section. Lithium and beryllium fluorides would be preferred if high conversion is the objective. This new salt was called FLIBE and it was an eutectic mixture of ^{7}LiF - BeF_2, with a little addition of zirconium fluoride (5%) as oxygen getter. The fissile and the fertile materials were dissolved in this mixture. $^{232}ThF_4$ is a fertile material that was used to produce fissile

$^{233}UF_4$ by a neutron capture and two consecutive beta decays. As secondary coolant the FLIBE mixture was used.

Current MSR designs include also non moderated concepts that use fast neutrons to induce fission. Due to the difference between the cross section in the fast spectrum and in the thermal spectrum, a different choice for the salt can be considered. The most interesting compounds are the alkali halides and alkali earth halides, such as NaF, KF, LiF. At the moment, there are two main approaches for non-moderated MSRs. The first is the Russian MOSART (MOlten Salt Actinides Recycle and Trasmuter) [8], which uses a single-fluid system and is fueled by ^{7}LiF - NaF - BeF_2-AnF_3 (where An is mostly represented by plutonium with small addition of minor actinides). Different conceptual core configurations and molten salt systems, as well as different removal processes for the soluble fission products, are considered. The second one is the French MSFR (Molten Salt Fast Reactor) [9], which is based on the ^{7}LiF - ThF_4 system with the addition of ^{233}U or ^{239}Pu as an initial fissile fuel.

The fluorides are not the only compounds that are considered for the MSR. For instance the REBUS-3700 concept [10] is based on a chloride salt as a fuel. These salts have higher vapour pressures and lower thermodynamic stability at high temperature but they have lower melting points.

All the compounds considered were studied in the past and the research is ongoing. Nevertheless, the choice of the final composition require further knowledge of these systems.

1.4 History of the MSR technology

Investigation of molten salt reactor started in the United States in the 1940s with the aim of developing a nuclear powered airplane. Compared to other solid type fuels, the fuel in MSR is a ionic fluid salt which is stable against radiation damage and the fluid form allows easy extraction of fission products. The attraction of molten fluoride salts for that program was the stability of these salts to high temperatures and to radiation as well. In order to proof the feasibility of molten salt reactor and to investigate the system features,

a small reactor was built at Oak Ridge National Laboratory (ORNL). It is called Aircraft Reactor Experiment (ARE) and it was operated successfully for several days in 1954. The ARE [11] was a thermal spectrum reactor with beryllium oxide as moderator and the fuel salt was a mixture of fluorides, with UF_4 as fissile material dissolved in NaF-ZrF_4 mixture. An extensive research and development program was undertaken in chemistry, materials, high-temperature sensors and other areas.

The developed technology was recognized to be useful also for the civilian power production and in 1956 a group to study the nuclear and economics aspects of the MSR was formed. The results of these studies concluded that molten salt reactor system could be a graphite-moderated thermal reactor operating on a thorium fuel cycle. Two concepts of reactors were evaluated. The first was a single fluid reactor in which fissile (UF_4) and fertile (ThF_4) materials were contained in the same salt and it was the simpler system. The other configuration was a two fluid reactor in which fertile and fissile materials were kept separated. The main advantage of the second configuration is that processing of the fission products from the fuel salt is simplified by the absence of thorium. Furthermore, neutron losses by capture on protoactinium can be minimized as it is effectively diluted in the much larger volume of blanket salt and experiences a lower neutron flux. Hence, the very first design of the reactor, shown in Figure 1.2 (A), was a two fluid concept. A simple sphere containing fissile material was the central molten salt core and it was surrounded by a blanket salt containing ThF_4. Both salts were separated by Hastelloy barrier. In this concept, the moderator was the carrier salt (^{7}Li-BeF_2) itself. By 1960 it was determined that graphite was indeed capable of long term interaction with the salt and thus considered as neutron moderator. A new concept was developed (Figure 1.2 (B)) but the main problem was that the graphite plumbing of hundred tubes proved a large challenge as a crack in one tube means a replacement of the entire core due to its complexity.

The culmination of these researches resulted in a system called Molten Salt Reactor Experiment (MSRE) [12]. The MSRE was a single fluid reactor, chosen to keep the reactor simple and inexpensive, but the fuel salt did not contain thorium. The salt composition was a mixture of uranium, lithium, beryllium and zirconium fluorides. The

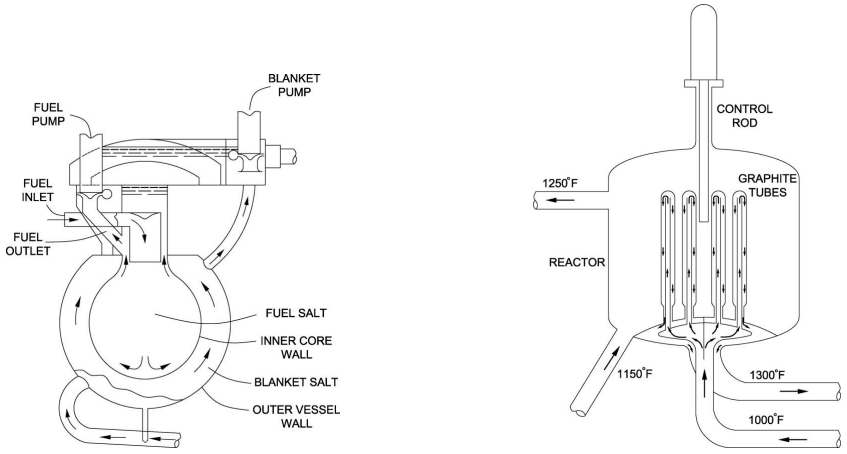

(A) (B)

Figure 1.2: (A) Depiction of the Oak Ridge's two region concept of the 1950s (Reproduced from ORNL-2474) (B) Depiction of the 1960s intermixed Two Fluid MSBR (Reproduced from ORNL-4528).

moderator was graphite and the pipes were realized in a special Nickel alloy (Hastelloy-N) to avoid corrosion problems at high temperature. The maximum power was 8 MW_{th} and the heat generated was dissipated to the atmosphere. The system was critical for the first time in 1965 and it operated successfully for five years. The key parameters of this reactor are summarized in Table 1.2. Operation with MSRE has provided some valuable new information as it operated long enough to be a good test of the practicality of molten-salt reactors and the reactor design showed that handling the high-melting salt is feasible. Fuel chemistry and materials compatibility showed no adverse effects to the reactor environment. Although the operation of the MSRE showed that the design of some equipment and systems could be improved, on overall the MSRE enhanced confidence in the practicality and performance of future molten-salt reactors.

The success of the MSRE enabled to start the study of a thorium power breeder reactor coupled to a reprocessing unit for the on-line extraction of fission products: the Molten Salt Breeder Reactor (MSBR) [13, 14]. Even if the concept looked promising, the project was stopped in the early 1970s leaving still some questions about its feasibility.

The selection of molten salt reactor as one of the six Generation IV reactors in 2002 has contributed to an increase in interest and a renaissance of research. Some recent concepts consider MSR also as a promising candidate as actinides burner.

Table 1.2: MSRE parameters. Data from ORNL -TM-2009/181

Power (heat)	7.4 MW
Fuel salt	65% ^{7}LiF, 29.1% BeF_2, 5% ZrF_4, 0.9 % UF_4
Fuel melting point	434 °C
Fuel inlet temperature	635 °C
Fuel outlet temperature	662,7 °C
Coolant salt	66% ^{7}LiF, 34% BeF_2
Moderator	Graphite
Container	Hastelloy-N (68% Ni, 17% Mo, 7% Cr, 5% Fe)
Critical on U-235	June 1, 1965
Critical on U-233	October 2, 1968
Shut down	December 1969

Table 1.3: Different applications and types of molten salts in nuclear reactors [15].

Reactor type	**Neutron spectrum**	**Application**	**Reference Salt**	**Alternative (s)**
MSR Breeder	Thermal	Fuel	^{7}LiF-BeF_2-AnF_4	
	Fast	Fuel	^{7}LiF-AnF_4	^{7}LiF-CaF_2-AnF_4
		Secondary coolant	NaF-$NaBF_4$	LiF-BeF_2, KF-KBF_4
MSR Burner	Fast	Fuel	LiF-NaF-BeF_2-AnF_3	LiF-NaF-KF-AnF_3, LiF-NaF-RbF-AnF_3
AHTR	Thermal	Primary coolant	^{7}LiF-BeF_2	
VHTR	Thermal	Heat transfer coolant	LiF-NaF-KF	LiCl-KCl-$MgCl_2$
MS-FR	Fast	Primary coolant	LiCl-NaCl-$MgCl_2$	
SFR	Fast	Intermediate coolant	$NaNO_3$-KNO_3	

**An means Th and U.*

1.5 Overview of molten salts in nuclear applications

Molten salts have several applications in the nuclear field as these liquids have been considered as heat transfer or cooling fluids and as fuel in nuclear fission and fusion systems. Fluorides are the most promising as they are stable at high temperature and under high neutron flux, therefore several fluoride molten salts have been investigated in the past. A summary of the different applications of molten salts and the relative reference molten salt compositions is given in Table 1.3. In addition to the application as fuel for MSR, which has been discussed in Section 1.3.2, molten salts are being considered as heat transfer coolants and as primary coolants in other reactor designs. A brief overview of the candidate salts and their properties is given in this section for three interesting nuclear

applications.

Molten salt heat transport systems

Molten fluoride salts are being proposed to transport heat from the Next Generation Nuclear Plant (NGNP) to the Nuclear Hydrogen Initiative (NHI) hydrogen-production plant. The heat transfer loop will use "clean" coolant salt and will operate at high temperatures. The main advantages offered by molten salts over gas heat transport systems are better heat transfer performance, smaller size of the heat transfer loop and increased safety.

Candidate salts must form compounds that have chemical stability at high temperature, melt at moderate to low temperatures (typically lower than 525 °C), are not volatile and are compatible with surrounding materials. Table 1.4 summarizes properties of some candidate coolants for the heat transfer loop, as reported in [16]. Some properties, such as melting point and vapour pressure give directly the information needed for consideration of the salt, while other properties need to be combined to determine the heat transfer performance. Three classes of salts were identified as good candidates: alkali-fluorides, fluoroborate salts, and chloride salts. Salts containing BeF_2 were not considered as this salt is expensive and toxic. In general, fluorides tend to be the best heat transfer fluids, followed by fluoroborates and chlorides. Among these, the LiF-NaF-KF eutectic is a salt with excellent heat transfer properties and it was deeply studied in the past. Nevertheless, other salts are considered as they show lower melting point or they are more economic. Chlorides, which have poorer transfer performance than fluorides, are not excluded from consideration as they have much lower raw material cost. Fluoroborates have low cost and good heat transfer properties but they require additional constraints due to significant pressure of BF_3 vapour over salts at elevated temperatures. Concerning corrosion characteristics, the database for fluoroborates and chlorides is much smaller than the database for fluorides salts, which were successfully used during ARE and MSRE experiments. Further investigations are therefore needed for these systems.

Table 1.4: Summary of the properties of candidate molten salts for heat transfer loop. Data from [16].

Salt	**Composition [% mol]**	**Melting point [°C]**	**Vapour pressure at 900°C [$mmHg$]**	**Heat transfer properties at 700 °C**			
				Density [$g \cdot cm^{-3}$]	**Volumetric heat capacity [$cal \cdot cm^{-3}°C^{-1}$]**	**Viscosity [cP]**	**Thermal conductivity [$W \cdot m^{-1} \cdot K^{-1}$]**
LiF-NaF-KF	(46.5-11.5-42)	454	0,7	2,02	0,91	2,9	0,92
NaF-ZrF_4	(59.5-40.5)	500	5	3,14	0,88	5,1	0,49
KF-ZrF_4	(58-42)	390	1,2	2,8	0,7	<5,1	0,45
LiF-NaF-ZrF_4	(26-37-73)	436	∼5	2,92	0,86	6,9	0,53
LiCl-KCl	(59.5-40.5)	355	5,8	1,52	0,435	1,15	0,42
LiCl-RbCl	(58-42)	313	-	1,88	0,40	1,30	0,36
NaCl-$MgCl_2$	(68-32)	445	<2,5	1,68	0,44	1,36	0,50
KCl-$MgCl_2$	(68-32)	426	<2,0	1,66	0,46	1,40	0,4
NaF-$NaBF_4$	(8-92)	385	9500	1,75	0,63	0,9	0,4
KF-KBF_4	(25-75)	460	100	1,70	0,53	0,90	0,38
RbF-$RbBF_4$	(31-69)	442	<100	2,21	0,48	0,90	0,28

Advanced High Temperature Reactors

Molten salts are nowadays considered as primary coolants for the AHTR (Advanced High Temperature Reactor) concept. In addition to the properties taken into account for heat transfer salts, such as physical properties and chemical factors, the primary coolant salt must show suitable nuclear properties. Neutronics properties are important to evaluate the effect of various salts on the operating conditions of the reactor and the effects of neutron activation. An important criterion for selecting the candidate salts is the evaluation of thermal neutron cross section of elements, which must be lower than 1 barn, while the considered phases must be stable under intense radiation. Table 1.5 presents a summary of properties of some candidate coolant salts, as reported in [17]. Three classes can be identified: alkalifluoride salts, ZrF_4-containing salts and BeF_2-containing salts. The alkali fluorides, which have good transfer properties, are not the best candidate as primary coolant due to the poor neutron performance. For instance, the LiF-NaF-KF system, which is the best candidate as heat transfer coolant, has rather large parassitic capture cross section due to high concentrations of potassium. The best candidate are BeF_2-containing salts, which offer the best neutronic properties combined with very good heat transfer performance. However, these compounds are very expensive. From this perspective ZrF_4-containing salts appear to be the best candidates for low cost coolant.

Fusion reactors

Molten salts are serious candidates as a blanket coolant for fusion energy machines. This liquid must be capable of performing two distinct functions: the absorption of the energy carried by fusion reaction products and consequent transfer of heat generated, and the breeding of tritium. Since tritium can be produced by neutronic reaction with ^6Li, the second requirement is satisfied using a blanket which contains enough lithium. The salt must meet several criteria, most of them similar to those introduced in the previous section, and these requirements must be fulfilled also in presence of large magnetic field. The best candidate salt, in terms of breeding tritium and heat transfer, is the LiF-BeF_2 mixture, called FLIBE [18, 19].

Table 1.5: Summary of the properties of candidate coolants for the AHTR. Data from [17].

Salt	Composition [% mol]	Melting point [°C]	Vapour pressure at 900°C [$mm\,Hg$]	Heat transfer properties at 700 °C				Neutron capture relative to graphite	Moderating ratio
				Density [$g \cdot cm^{-3}$]	Volumetric heat capacity [$cal \cdot cm^{-3} \cdot °C^{-1}$]	Viscosity [cP]	Thermal conductivity [$W \cdot m^{-1} \cdot K^{-1}$]		
$LiF\text{-}BeF_2$	(67-33)	460	1,2	1,94	1,12	5,6	1,0	8	60
$NaF\text{-}BeF_2$	(57-43)	340	1,2	2,01	1,05	7	0,87	28	15
$LiF\text{-}NaF\text{-}BeF_2$	(31-31-38)	315	1,4	2,00	0,98	5	0,97	20	22
$LiF\text{-}ZrF_4$	(51-49)	509	1,7	3,09	0,90	>5,1	0,48	9	29
$NaF\text{-}ZrF_4$	(59.5-40.5)	500	77	3,14	0,88	5,1	0,49	24	10
$KF\text{-}ZrF_4$	(58-42)	390	5	2,80	0,70	<5,1	0,45	67	3
$RbF\text{-}ZrF_4$	(58-42)	410	-	3,22	0,64	5,1	0,39	14	13
$LiF\text{-}NaF\text{-}ZrF_4$	(26-37-37)	436	~5	2,79	0,86	6,9	0,53	20	13
LiF-NaF-KF	(46.5-11.5-42)	454	~0,7	2,02	0,91	2,9	0,92	90	2
LiF-NaF-RbF	(42-6-52)	435	~0,8	2,69	0,63	2,6	0,62	20	8

1.6 Other applications of molten salts

In many areas of the chemical and related types of industry, molten salts are employed as heat carriers. They offer advantages over common heat transfer media and can be used for processes above ~ 400°C. The most popular heat transfer molten salt in chemical and petrochemical industry is called HITEC and it is a ternary mixture of nitrates: KNO_3(53%)-$NaNO_2$(40%)-$NaNO_3$(7%).

A very interesting application is utilizing molten salt as the heat transfer fluid and for thermal storage in solar thermal systems. With salts, it may be possible to increase thermodynamic cycle efficiency and operation temperatures and, moreover, they are cheaper and non-toxic liquids. The major challenge of these liquids is related to their high freezing point, with respect to this application, and complications that can occur due to this phenomena. The salt candidates are mainly nitrate mixtures, which have low corrosion rates, are thermally stable at high temperature range and are relatively inexpensive. The currently reference salt for this solar technology is the mixture of $NaNO_3$(60%)-KNO_3(40%). A small demonstration plant (Archimede), inaugurated in 2010, is testing the use of high-temperature molten salt, as either heat transfer or storage fluid, to improve the plant performance. Moreover, this salt is used in the intermediate circuit of SFRs.

Chapter 2

Thermodynamics of molten salts

One of the most challenging applications of molten salts is its use in the MSR where it is considered as a fuel and, for its good properties, as a heat transfer salt through secondary loop. The research in the field of thermodynamics of the molten salts performed in this study has two main motivations. The first is the basic research in the material science and the second one is the improvement of the thermodynamic database, which is used to assess the safety criteria of the MSR.

For the design of nuclear reactor, it is important to know the behavior of the used fuel. In case of the MSR fuel, which is based on a multi-component system, it is needed to find the optimal composition that fulfills the reactor requirements with respect to the following properties:

- **Melting point.** This is one of the key point in the choice of fuel and coolant composition. The fuel salt, and the coolant salt as well, must show low melting point. It decreases the risk of freezing or the risk of solid precipitates, which could cause local high concentration of fissile material that could become supercritical. To avoid this risk the inlet temperature of the reactor must be always above the melting point and in order to keep an adequate margin of safety it is recommended to be at least 50 K above the melting point. The exact melting temperature of the fuel will depend on the concrete design of the MSR but, to give an idea, the typical inlet temperatures of various MSR concepts are reported in Table 2.1.

Table 2.1: Typical fuel salt inlet and outlet temperatures of some MSR concepts.

MSR concept	T inlet	T outlet	Ref.
MSRE	908 K	936 K	[20]
MSBR	839 K	977 K	[14]
MSR FUJI	840 K	980 K	[21]
MSFR	903 K	923 K	[22]
MOSART	873 K	988 K	[23]

- **Heat capacity.** It determines the amount of heat energy required to change the temperature of a given mass by a certain increase. The heat transfer and the heat storage properties depend strongly on this factor.

- **Vapour pressure.** The vapour pressure is the pressure at which a liquid and its vapour are in equilibrium at a given temperature. The low pressure of the molten-salt fuel system is a beneficial parameter with regard to engineering issues. Since that system can operate at low pressure it offers also an advantage from a safety point of view. Furthermore, considering a multi-component salt with high vapour pressure an undesired phenomena may occurs. The high evaporation of one component causes a dilution of other compounds in the salt mixture and a consequent change in the final composition of the liquid. This leads to a change in the thermodynamic properties, mainly the melting temperature that increases and could approach the safety limit. Systems with low vapour pressure are therefore preferred.

- **Actinides solubility**. The fuel must dissolve, at given temperature, enough fissile material to made the chain reaction possible.

- **Density.** It is an important property to define for candidate coolants, since it affects heat transfer characteristics, e.g., volumetric heat capacity.

- **Viscosity**. It defines the fluid resistance to flow and it is fundamental to the convective heat transport properties. Viscosity is temperature dependent and it depends also on the salt composition. Low viscosity is required.

- **Thermal conductivity.** Thermal conductivity must be evaluated for the purpose

of heat transfer calculations, for instance the design of the heat exchanger. High thermal conductivity is required.

Since fluoride systems best fulfill the above mentioned criteria, they are considered as primary choice for MSR fuel. To optimize the fuel composition, a systematic study of thermodynamic properties is performed in this study. The knowledge of these properties for pure compound can be useful itself but it allows also to optimize the phase diagram of the systems with more than one component, which are the real candidates for MSRs. Since it is impossible to measure every single composition of a multi-component system, an extensive thermodynamic database has been developed at the Institute for Transuranium Elements (ITU). The database provides a large but limited set of experimental values, mostly from URSS research and US research at ORNL between 1950 and 1970 and further investigations are needed. It is indispensable to develop models that can, for instance, describe the phase behavior of binary and ternary systems. The experimental data are in any case essential. They serve to optimize the model and to confirm its correctness.

In this chapter, the basics about thermodynamic functions and how they can describe a mixture are introduced. The description is done focusing on the pure compounds and binary systems, which are the aim of this work and the basis for extrapolation to higher-order systems.

2.1 Pure compound properties

2.1.1 Melting behavior

The melting behavior of a pure compound can be deduced when the stability of each phase (solid, liquid) is known. This knowledge is given by a thermodynamic potential called Gibbs energy or free energy. The Gibbs energy of a compound is defined as:

$$G(T) = H(T) - T \cdot S(T) \tag{2.1}$$

where $H(T)$ is the enthalpy and $S(T)$ is the entropy. Both these thermodynamic functions are temperature (T) dependent. Since the enthalpy is not an absolute quantity, it is related

to its reference value, which is defined as 0 $J \cdot mol^{-1}$ at 298,15 K for pure elements at their standard states. The enthalpy is expressed by the following equation:

$$H(T) = \Delta_f H^0(298) + \triangle H_{298}^T \tag{2.2}$$

which becomes:

$$H(T) = \Delta_f H^0(298) + \int_{298}^{T} C_p(T)\, dT \tag{2.3}$$

where C_p is the heat capacity and $\Delta_f H^0$ is called standard enthalpy of formation since the reference temperature is the standard state temperature (T = 298,15 K). It is equal to the reaction enthalpy of compound formation from the pure elements in their standard states at reference temperature.

The entropy is expressed by the following equation:

$$S(T) = S^0(298) + \int_{298}^{T} \frac{C_p(T)}{T}\, dT \tag{2.4}$$

where $S^0(298)$ is called standard absolute entropy and the reference temperature is again the standard state temperature (T = 298,15 K). Since entropy, in contrast to enthalpy, is an absolute quantity being 0 $J \cdot mol^{-1}$ at 0 K for ideal crystal, it is possible to determine its value at 298,15 K from the low temperature heat capacity measurements.
Combining equations 2.2 and 2.4, the Gibbs energy can be written using the relation below:

$$G(T) = \triangle_f H^0(298) - S^0(298) \cdot T + \int_{298}^{T} C_p(T)\, dT + \int_{298}^{T} \frac{C_p(T)}{T}\, dT. \tag{2.5}$$

Standard entropy, standard enthalpy and heat capacity are known for a large number of pure compounds, thus the calculation of the Gibbs energy is often possible. If this value is known for each phase of the compound, the thermodynamic stability of the compound is described. The phase with the lowest free energy at a given temperature is the stable one.

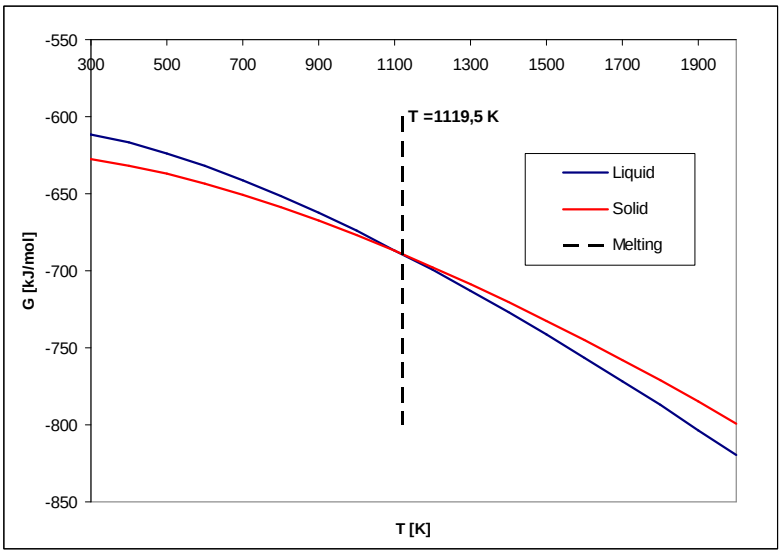

Figure 2.1: Calculated Gibbs energy for solid and liquid phase of LiF. The equations are derived from the known thermochemical data [24].

In the previous relations, the Gibbs energy is represented only as a function of temperature but it is dependent also on pressure and composition. Since for pure substances the composition does not vary and for condensed phases near atmospheric pressure (p$\backsim$1 bar) there is negligible dependence on pressure, the free energy varies greatest with temperature.

As an example curve, the free energy of the liquid and solid phases of LiF is calculated and shown in Figure 2.1. The point where the two curves cross is the melting point and at this temperature the two phases are in equilibrium. Below this point the substance is in the solid phase and above it the substance is in the liquid phase.

2.1.2 Heat capacity

Heat capacity belongs to the most important thermophysical properties of matter. It is a key factor for the assessment of candidate molten salt coolants because the heat transfer is strongly influenced by the heat capacity. It is defined as the amount of heat required to cause the raise of one degree of temperature (SI units, J/K). Widely used are derived quantities, normally: the specific heat capacity, which is the heat capacity per gram of pure substance, and the molar heat capacity, which is the heat capacity per mole of pure substance. In a general form, the heat capacity can be written as:

$$C = \frac{\partial Q}{\partial T}. \tag{2.6}$$

Thermodynamically, the heat capacity is defined under two different conditions: at constant volume, C_V or at constant pressure, C_P. The definitions for the two quantities can be deduced from the first law of thermodynamics:

$$dU = \delta Q - \delta W \tag{2.7}$$

where dU is an infinitesimal change in internal energy and δQ and δW are infinitesimal amounts of heat supplied to the system and work done by the system, respectively. For an expansion or compression work, it could be write like:

$$dU = \delta Q - PdV \tag{2.8}$$

where P is the pressure and dV is the volumetric change. Therefore, if the process is done at constant volume the second term is neglected and the heat capacity at constant volume is defined as:

$$C_V = \left(\frac{\partial U}{\partial T}\right)_V. \tag{2.9}$$

Instead, when one consider processes at constant pressure, the first law of thermodynamics has to be combined with the following equation for the enthalpy:

$$dH = dU + d(PV) \tag{2.10}$$

and the result is the following definition for the heat capacity at constant pressure:

$$C_P = \left(\frac{\partial H}{\partial T}\right)_P. \tag{2.11}$$

Measuring heat capacity at constant volume can be very difficult for liquids and solids, as small temperature changes typically require large pressures to maintain a liquid or solid at constant volume. Instead, it is easier to measure the heat capacity at constant pressure. Several different calorimetric techniques have been developed to determine heat capacity.

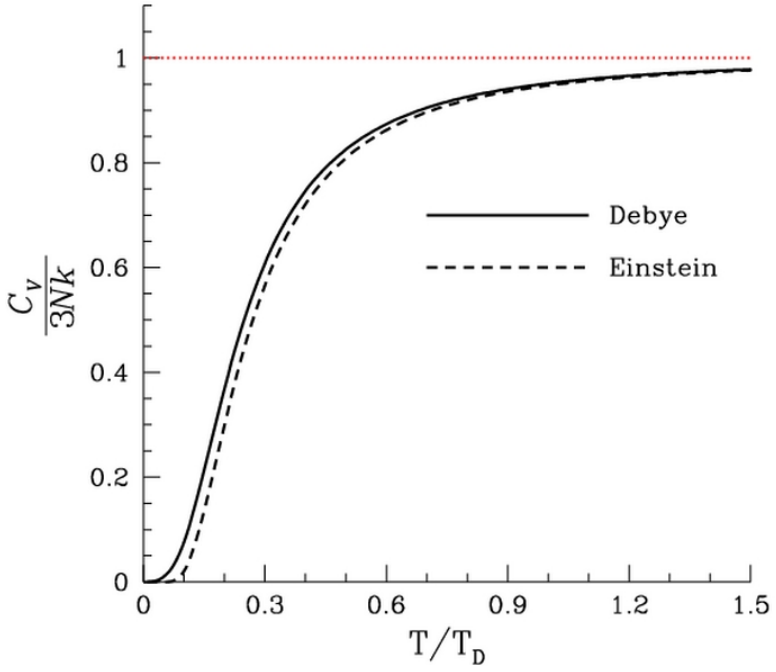

Figure 2.2: Heat capacity as a function of temperature. The comparison between the Einstein model and Debye model is shown.

Probably, the most common are adiabatic calorimetry and relaxation techniques to measure the low temperature heat capacity, and drop calorimetry and Differential Scanning Calorimetry (DSC) to determine the high temperature range, above room temperature.

While in the liquid phase the heat capacity is usually constant or slightly increasing with the temperature, the heat capacity for the solid phase shows a temperature dependence specially in the low temperature range. At absolute zero, the specific heat capacity is also zero and a typical behavior is shown in Figure 2.2. This behavior can be explained by quantum theory using the Einstein model, proposed in 1906, or using the Debye model, proposed in 1912. In practice, the heat capacity is normally measured experimentally and the results are described analytically for a certain range of temperatures in a polynomial form.

2.2 Binary solutions

2.2.1 Melting behavior

Solutions contain more than one component and in these cases the Gibbs energy of a solution will become dependent on its composition as well as on the temperature. Consider a mixture of two components, A and B, where the composition is described by two molar fractions x_A and x_B. The Gibbs energy of such system is a weighted average of the Gibbs energies of pure compounds, plus the Gibbs energy of mixing G_{mixing}, as described below:

$$G^{sol} = x_A \cdot G_A + x_B \cdot G_B + G_{mixing} \tag{2.12}$$

where G_A is the Gibbs energy for the component A and G_B is the Gibbs energy for the component B. The mixing contribution can be distinguished in two parts: an ideal mixing contribution and an excess contribution. As the name suggests, ideal solutions are idealizations of real solutions which have thermodynamic mixing properties analogous to those of a mixture of ideal gas. They are characterized by the following assumptions:

- there is no heat of mixing during the formation of the solution;
- the only contribution to the entropy is the configurational one due to the re-arrangement of the molecules in the system and it accounts for complete random distribution of the molecules.

In this case, the ideal enthalpy of mixing is zero and the mixing free energy is only due to the configurational entropy that can be expressed by the following equation:

$$S_{mixing} = -R \cdot (x_A ln x_A + x_B ln x_B) \tag{2.13}$$

where R is the gas constant ($J \cdot K^{-1} \cdot mol^{-1}$). Since $H_{mixing} = 0$ and $G_{mixing} = H_{mixing} - T \cdot S_{mixing}$, the Gibbs energy of ideal mixing becomes:

$$G_{mixing} = x_A RT\, ln x_A + x_B RT\, ln x_B. \tag{2.14}$$

The molar fraction is a value always lower than 1, thus the mixing Gibbs energy of an

ideal solution is always negative.

If we consider now the real solutions, a term called excess Gibbs energy should be added, as written in the following equation:

$$G_{mixing} = x_A RT\, lnx_A + x_B RT\, lnx_B + G_{excess}. \tag{2.15}$$

Based on the Gibbs energy definition, the excess term can be written as function of thermodynamic excess functions:

$$\Delta G_{excess} = \triangle H_{excess} - T \cdot \triangle S_{excess} \tag{2.16}$$

where the excess functions describe deviations from ideality. Since it is difficult to measure the excess Gibbs energy of a the solution, several thermodynamic models have been developed to describe this term. In the simplest form, the excess Gibbs energy of a real mixture can be represented by a polynomial formalism:

$$G_{excess} = \sum_{n,m} A_{n,m} \cdot x_A^n \cdot x_B^m \tag{2.17}$$

where

$$A_{n,m} = a + b \cdot T + c \cdot Tln(T) + d \cdot T^2 + e \cdot T^3 + ... \tag{2.18}$$

and a, b, c, d, e,... are the parameters to be optimized during the thermodynamic assessment.

2.2.2 Phase diagram

A diagram that depicts existence of different phases of a system at equilibrium as a function of given variables is termed as phase diagram. The so called T-x phase diagram represents phases at equilibrium as function of temperature and composition. The following information can be obtained from a knowledge of a phase diagram.

- To determine which phases are present at specific composition and temperature and

to determine their quantities.

- To indicate solubility limit of one compound in another, in case solution is formed.
- To indicate the temperature at which different phases undergo transition, decompose or start to melt.
- To determine a crystallization path of a given melt.

Gibbs energy curves determine the most stable state for a system and the phase diagram can be constructed using a graphical method. To construct the phase diagram it is necessary to find the equilibrium point between different phases which must satisfy the equilibrium condition that imposes the equality of the chemical potentials of two components in the system. The foundation of the graphical method is called "common tangent rule" and states that compositions of the two coexisting phases lie at the points of common tangency of the Gibbs energy curves. First the Gibbs energy of each phase combination is plotted as function of composition. The other parameters, such as temperature and pressure, are kept fixed. The equilibrium condition is satisfied by drawing a line that forms a common tangent to the different phase curves. The points where the tangent touches the two curves are equilibrium points.

Figure 2.3 shows the construction of a phase diagram for a simple system if the Gibbs energy of each phase is known. The red line and the blue line represent the Gibbs energy of the liquid solution and the Gibbs energy of the two solids as a two-compound mixture, respectively. They are plotted as a function of composition for various isothermal cuts.

The first graph shows that, at T=A, the two curves cross only at one point at B end-member. For the rest of the phase diagram the Gibbs energy of liquid solution is more negative than the solid mixture and hence is the stable one. At B component the two phases are in equilibrium and this point corresponds to the melting temperature of B end-member. In this case, the common tangent line coincides with the meeting point 1 between the two curves.

At T=B, the two curves cross in two points. The points where the common tangent line cross the two curves are the equilibrium points. In this case there are two traceable

lines: one that links points 2 and 3, where point 2 represents the liquidus point, and the other that coincides with point 4, which is the melting point of A end-member.

In the third graph, the situation is analogue to the previous one and two liquidus compositions are determined by points 5 and 7.

The last graph shows that the Gibbs energy of solid phase is lower than the Gibbs energy of the liquid solution touching at point where three phases are in equilibrium: solid A, solid B and liquid. This is called eutectic point. The knowledge of these equilibrium points for each temperature allows the construction of the phase diagram, as illustrate on the right side in the Figure 2.3.

Phase diagrams may have very different shape depending on the compounds that form the mixture. Consider for simplicity the behavior of two component systems in which equilibrium exists between solid and liquid phase and where the components are completely miscible in the liquid state. Two representative phase diagrams are given in Figure 2.4. They are respectively phase diagrams of the LiF-KF system and LiF-ThF_4 system, which have been studied in this work. The LiF-KF system is an example of one of the simplest possible binary phase diagram since the only solid phases are the pure end-members. Points A and B represent melting points of the pure components and the two curves that start in these points are called liquidus curves. They represent the composition of solutions which are in equilibrium with the solid component at different temperature. The two curves cross in the point C where both solid components can exist in equilibrium with a solution of definite composition. This point lies at lower temperature than the melting point of either component and is called eutectic point. At all points above the liquidus curves the liquid phase is in equilibrium and at all the points below the eutectic point the system is a solid mixture.

The second phase diagram in Figure 2.4 shows a more complex situation where stable solid intermediate compounds are formed. The points C, D, E are called peritectic points and represent the limit of the existence of the generic compound A_xB_y. For instance, the point D is the limit of the existence of the $LiTh_2F_9$ compound, which upon decomposition forms liquid solution of a D composition and solid $LiTh_2F_9$.

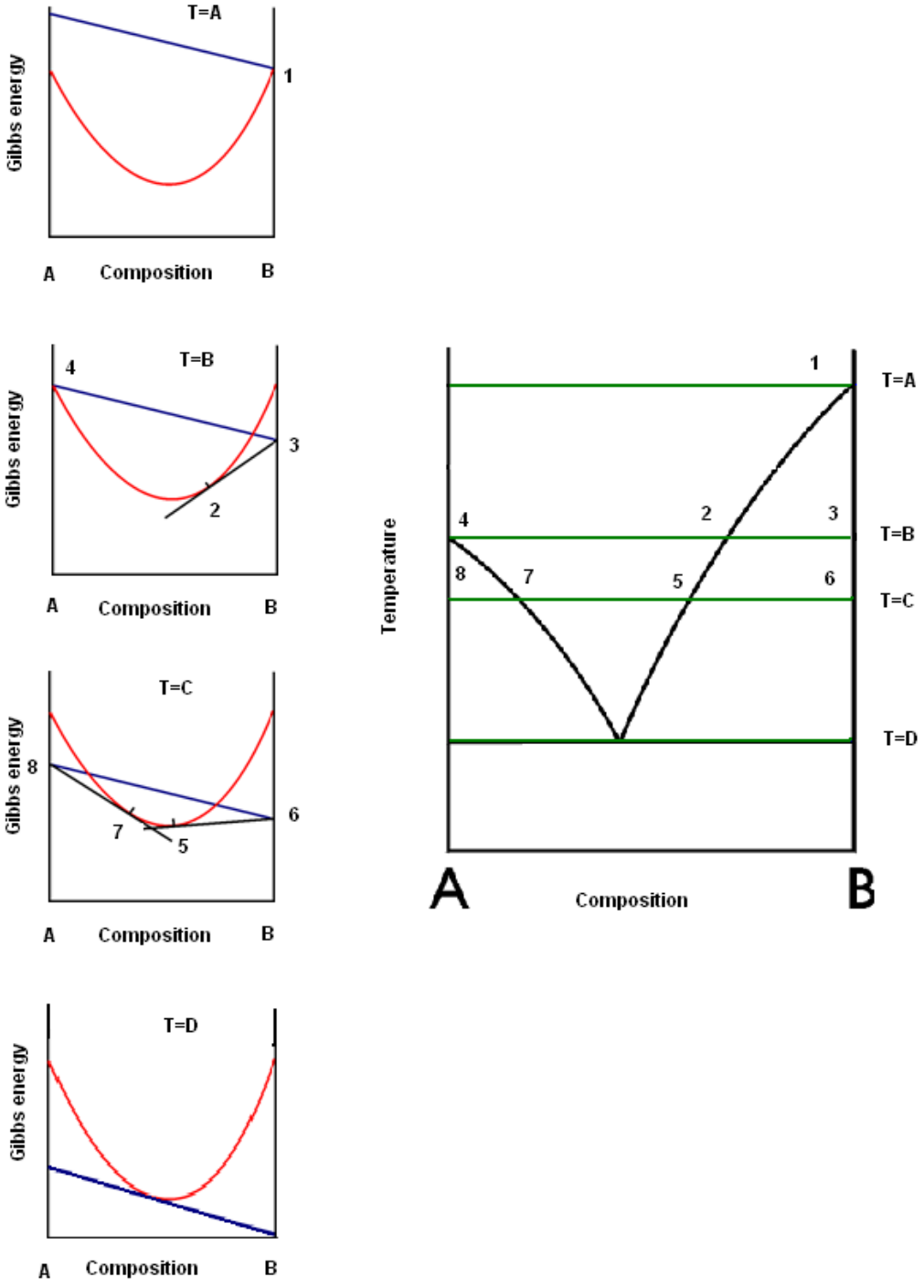

Figure 2.3: Left: Depiction of the Gibbs energy vs. composition curves for a A-B binary system at four different temperature.
Right: Phase diagram for the A-B binary system constructed by the common tangent method.

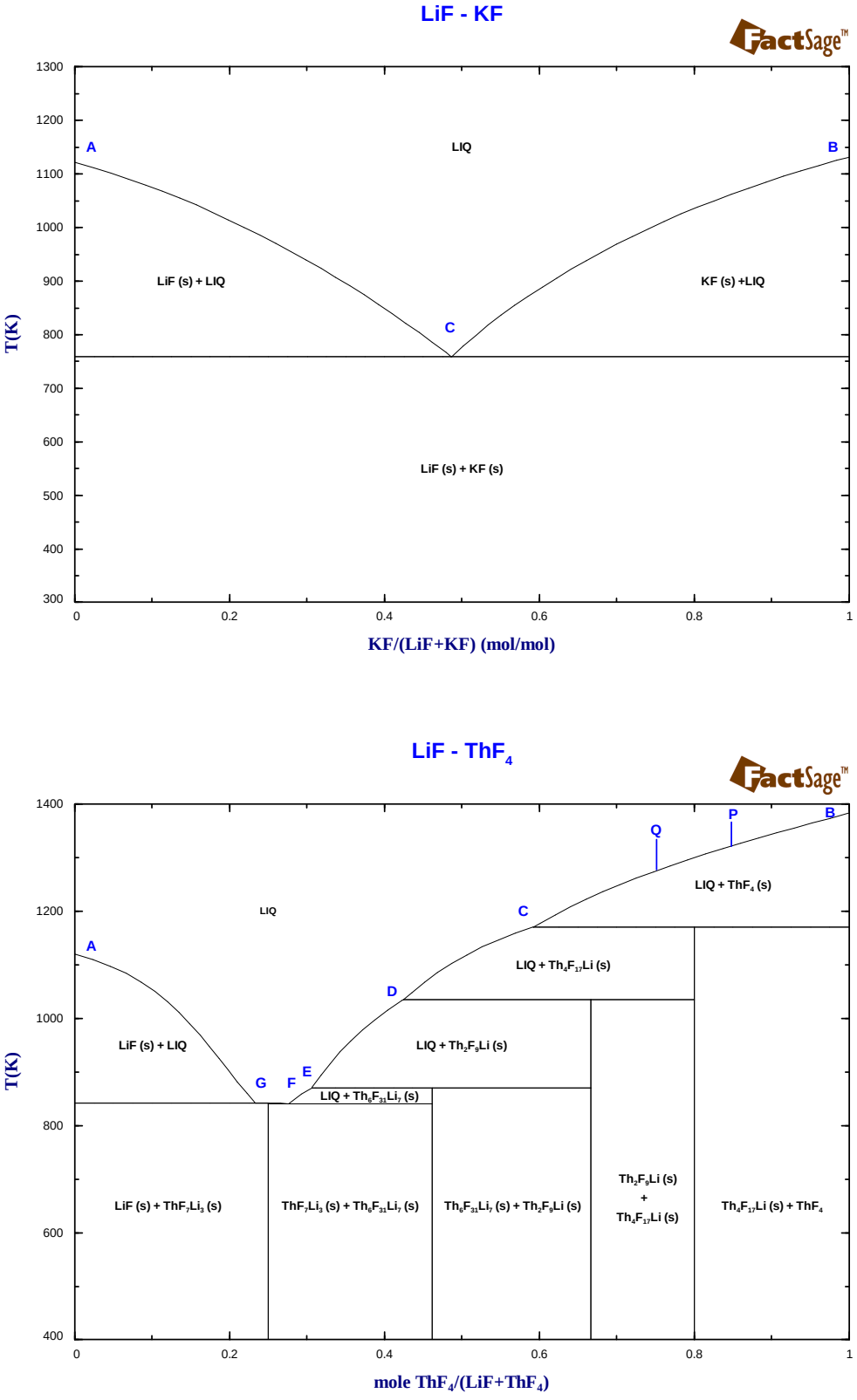

Figure 2.4: Phase diagrams of two systems studied in this work. Upper: Phase diagram of LiF-KF system. Bottom: Phase diagram of LiF-ThF_4system.

It is interesting to observe the behavior during the cooling for points P and Q indicated in the figure. For the point P, the cooling can be shown on the phase diagram as a vertical line until the curve BC. At this point, the ThF_4 begins to precipitate and the cooling follows the curve BC towards C. In C the temperature is equal to the maximum temperature for the stability of the compound $LiTh_4F_{17}$ and the ThF_4 reacts at this point with the liquid to form this intermediate compound. The final result is a mixture of ThF_4 and $LiTh_4F_{17}$ since there is not enough quantity of LiF to react completely with ThF_4.

If we consider now the point Q, the behavior will be the same until the point C. Then, the quantity of LiF in the solution is sufficient to consume all the ThF_4 present and the cooling follows the curve CD while $LiTh_4F_{17}$ precipitates. As soon as the peritectic point D is reached, the separation of $LiTh_4F_{17}$ compound and $LiTh_2F_9$ compound occurs. The systems described are just two case among the numerous existing systems, but they are useful to understand almost every phase diagram.

As mentioned before, the amount of data that would be required for a complete description of every single system is enormous and the development of models is then indispensable. The assessment of the phase diagrams is usually done using the CALPHAD method, described for the first time by Kaufmann and Bernstein [25]. The principle is that a phase diagram is a representation of the thermodynamic properties of a system and it can be obtained by minimization of the Gibbs energy. All the available experimental and theoretical data (solidus and liquidus transitions, heat capacity, mixing enthalpy of solution, etc.) are used to assess a Gibbs energy model, which contains adjustable parameters. The optimization is done in order to obtain the best fit between the calculated phase diagram and the available data.

Chapter 3

Experimental part

3.1 Handling of fluoride salts

Generally, alkaline and alkaline-earth fluorides have tendency to absorb water molecules. For this reason, the handling of fluorides must be done in dry environment, e.g., inside argon glove boxes, where a very low concentration of water is ensured. In case of this study, sample were handled in glove boxes with water concentration lower than 50 ppm using a constant argon flow, or lower than 2 ppm using an argon purifier. In order to obtain the compound as pure and dry as possible, the substances were subjected to a purification treatment, which consisted of a heating cycle at 350 °C for several hours. This treatment is done in an oven under argon flow to avoid oxidation or reaction with the air. The purity of the salts is then checked with the Differential Scanning Calorimeter (DSC) method for the identification of the melting temperature which is generally very sensitive to any kind of impurities.

In addition, some fluoride compounds show a tendency to oxidize and they require special purification processes to turn the oxides into fluorides. Among this compounds, the most relevant for this work is ThF_4 and the purification method is explained in the following sub-section.

3.1.1 Purification method for ThF_4

The preparation of molten salt mixtures must be done using fluorides containing a minimum content of water, oxides or oxy-fluorides. Otherwise, they can change the mixture chemical composition and induce a change in the physico-chemical properties. The purification methods were developed at ORNL and most of them are based on high-temperature treatment with a gas mixture containing hydrogen fluoride (HF) or fluorine gas (F_2). Since these gases are very corrosive and thus difficult to handle, an alternative method to convert oxides into fluorides was proposed [26, 27]. Instead of HF or F_2, the purification is done using the ammonium hydrofluoride NH_4HF_2. The chemical reaction that occurs during the ThF_4 purification, is the following:

$$ThO_2 + 4NH_4HF_2 \longrightarrow ThF_4 + 4NH_4F + 2H_2O \tag{3.1}$$

The reaction occurs during a heating process and the maximum temperature must not exceed 400 °C to avoid the formation of undesired compounds. The purification of the compound used in this work was done by mixing unpurified ThF_4 with NH_4HF_2 in the ratio (1 : 3). The powder obtained was then heated up in a closed container at 250 °C for 12 hours. To allow the evaporation of ammonium fluoride and water, a second heating cycle was performed in an open container. Both heating cycles were done in an Ar/ H_2 atmosphere to eliminate oxygen presence.

The results of the purification process were tested with the DSC technique and showed good purity of the obtained compound indicating an average melting temperature at T = 1378,2 K, in close agreement to literature value at T=1383 K [28]. The efficiency of the purification process is clearly visible from the comparison of the same batch of salt measured before and after the treatment (Figure 3.1). After the purification, only one peak at the ThF_4 melting temperature is visible, while before a second peak was observable. Moreover, the purified ThF_4 has an higher melting temperature closer to the literature value.

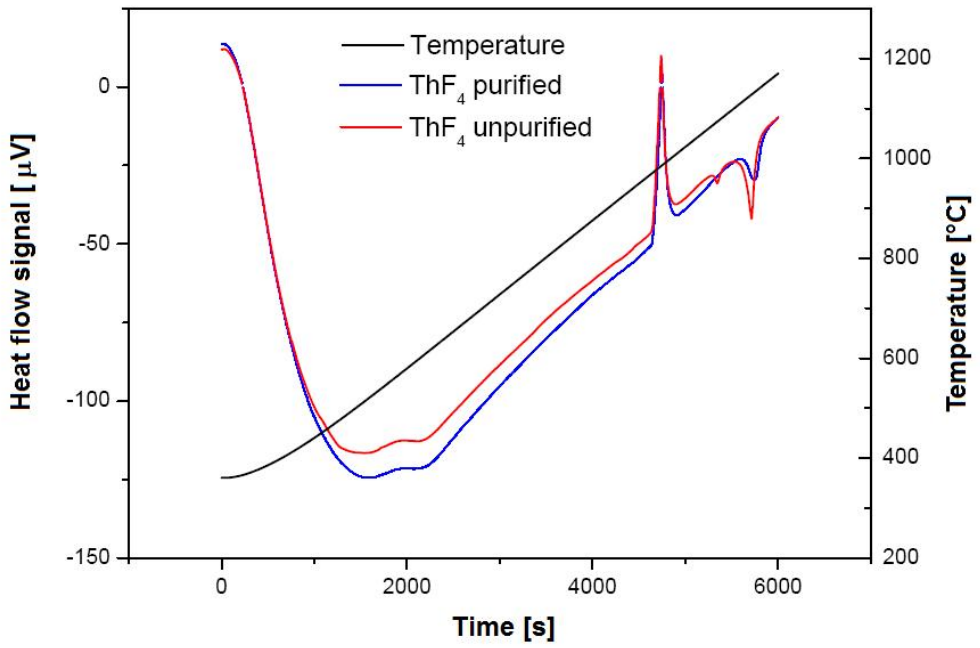

Figure 3.1: Comparison between the signal output, corresponding to an heat flow, obtained using the DSC technique for ThF_4. The red line is the result obtained measuring the ThF_4 before the purification process, while the blue line is the result obtained on the same batch of ThF_4 after the purification process.

3.1.2 Encapsulation technique

The alkali fluorides are among the most stable compounds but at high temperatures the vapours can be very corrosive against several materials, especially with presence of water vapours. At high temperature they even corrode platinum which is the main component of the thermocouples used in our calorimetric devices. Experience shows that, after few high temperature cycles, the instrument detector is damaged, thus it is necessary to provide a sort of barrier between the fluoride vapours and the detector. It was crucial to develop an encapsulation technique. The main requirements that the crucible must meet are:

- Compatibility with the instrument dimensions;
- Compatibility of the material of the crucible with the fluorides at high temperatures;
- Ability to contain the released vapours;
- Absence of big deformation during the measuring (in case of DSC crucible design).

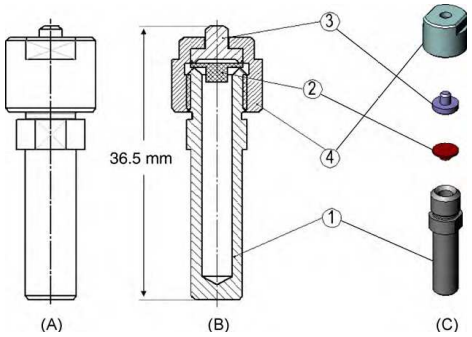

Figure 3.2: Schematic representation of the developed DSC crucible. (A) Scheme of the side of the developed DSC crucible; (B) Scheme of a cut of the crucible; (C) Depiction of the various parts of the crucible: (1) stainless steel main body, (2) nickel sealing, (3) stainless steel closing stopper, (4) stainless steel bolt.

Based on these criteria, two encapsulation techniques were developed in the past at ITU for the Differential Scanning Calorimeter [29] and for the Drop Calorimeter [30]. A brief summary about these methods is given in the following two sections.

Encapsulation technique for Differential Scanning Calorimeter

For this instrument it is required that the dimensions of the crucible fit perfectly with the sample holder in order to maintain a very good thermal contact. Since the gap between the crucible and the detector tube is minimal, the crucible must be strong enough to avoid big deformation with increasing temperature. To fulfill this requirement the crucible is realized from stainless steel which is however corroded by fluoride at high temperature. This issue is solved with an internal liner made from different material, such as nickel or boron nitride, able to resist to the corrosion.

The scheme of the crucible is shown in Figure 3.2, and consists of four parts. The main body and the cap are made from stainless steel and the crucible can be closed easily by screwing. To ensure the crucible tightness there is a nickel sealing that, due to its softness, is squeezed between the main body and the stopper by a bolt, which is made from stainless steel. The stopper and the main body have sharp edges, which are in tight contact with the sealing and ensure the tightness.

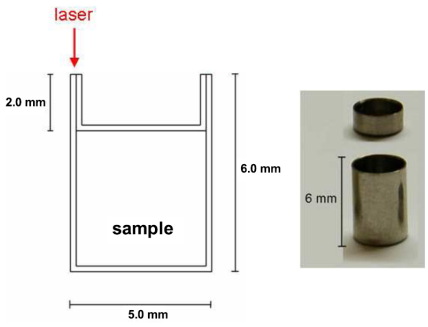

Figure 3.3: A schematic presentation and a picture of the nickel crucible designed for Drop Calorimeter measurements.

Encapsulation technique for Drop Calorimeter

The encapsulation technique for the Drop Calorimeter is different to that of the DSC because the dimension requirements are more limited on size. The design of the developed crucible is shown in Figure 3.3. It consists of two cylindrical parts: the main body of the crucible that is filled with the studied sample, and a lid that fit perfectly in the bigger crucible. Both parts are made of nickel, which is inert against studied fluorides. Due to its softness and small dimensions, the screw closure is impossible and the best found solution is the laser welding. For the welding a Trumpf laser is available in the laboratory. It is a Nd-YAG HLD4506 laser of 4.5 kW maximal power that can operate either in continuous or in pulse mode in the range of milliseconds. For the regularity of the weld and its strength a continuous mode is selected.

Once the crucible is filled with the material to be studied and closed with the lid, it is placed into an apparatus for welding. The apparatus consists of three main parts, shown in Figure 3.4. The optical device (A) is connected to an optical fiber and directs and focuses the laser beam on the edge of the crucible. To ensure the position precision during the welding the optical device is kept fixed. The crucible is held inside a vessel, which has an outlet connected to a vacuum pump and an inlet connected to ambient pressure. Vacuum is necessary to avoid oxidation of nickel at high temperature and to reduce the encapsulated gas pressure. The vessel is placed on a movable platform used to position the laser and the crucible is connected with a turning device, which rotates the crucible during welding.

The good quality of the weld is checked through a microscope and also by means of a thermic treatment afterwards. This treatment is a simple heating to a temperature higher than the maximum temperature that will be reached during the measurements and it lasts several hours in order to reproduce the measuring condition. After this procedure the crucible weight is checked and if there are significant losses, typically more than 1 mg, the crucible is not considered tight and it is discarded.

3.2 Differential Scanning Calorimeter

The Differential Scanning Calorimeter (DSC) is a technique which is part of a group of thermal analysis techniques which are based on the detection of temperature changes between the sample and reference crucibles upon heating.

The DSC instrument used in this study is a SETARAM MHTD 96 and is made of a furnace for heating or cooling the sample at constant rate and a detector monitoring the heat flow change between the crucibles. The furnace is cylindrical and the heating element is a graphite tube with copper ends for the current intakes. A sealed alumina tube provides an insulation between the furnace and the experimental chamber. The DSC detector is made from alumina with two compartments for crucibles (Figure 3.5); the reference and the sample crucible. Both crucibles are surrounded by a series of interconnected thermocouples. The thermocouples used are of S-type and are constructed using one wire of Platinum and one wire of 90% Platinum and 10% Rh. These thermocouples are suited up to 1400 °C. The experimental chamber is gas tight and for all measurements was kept under Argon atmosphere to avoid the oxidation of stainless steel at high temperature, used as encapsulating material for crucibles.

The sample and reference crucibles are both maintained at the temperature predetermined by the program. During a thermal event in the sample, such as a phase transition, the temperature difference between the sample and the reference increases as the reference crucible continue to heat, whereas the sample one is delayed before its full transformation. Hence, a heat flow between the two crucibles is observed and recorded as a peak. The area under the peak is directly proportional to the enthalpy of the transition and its direction

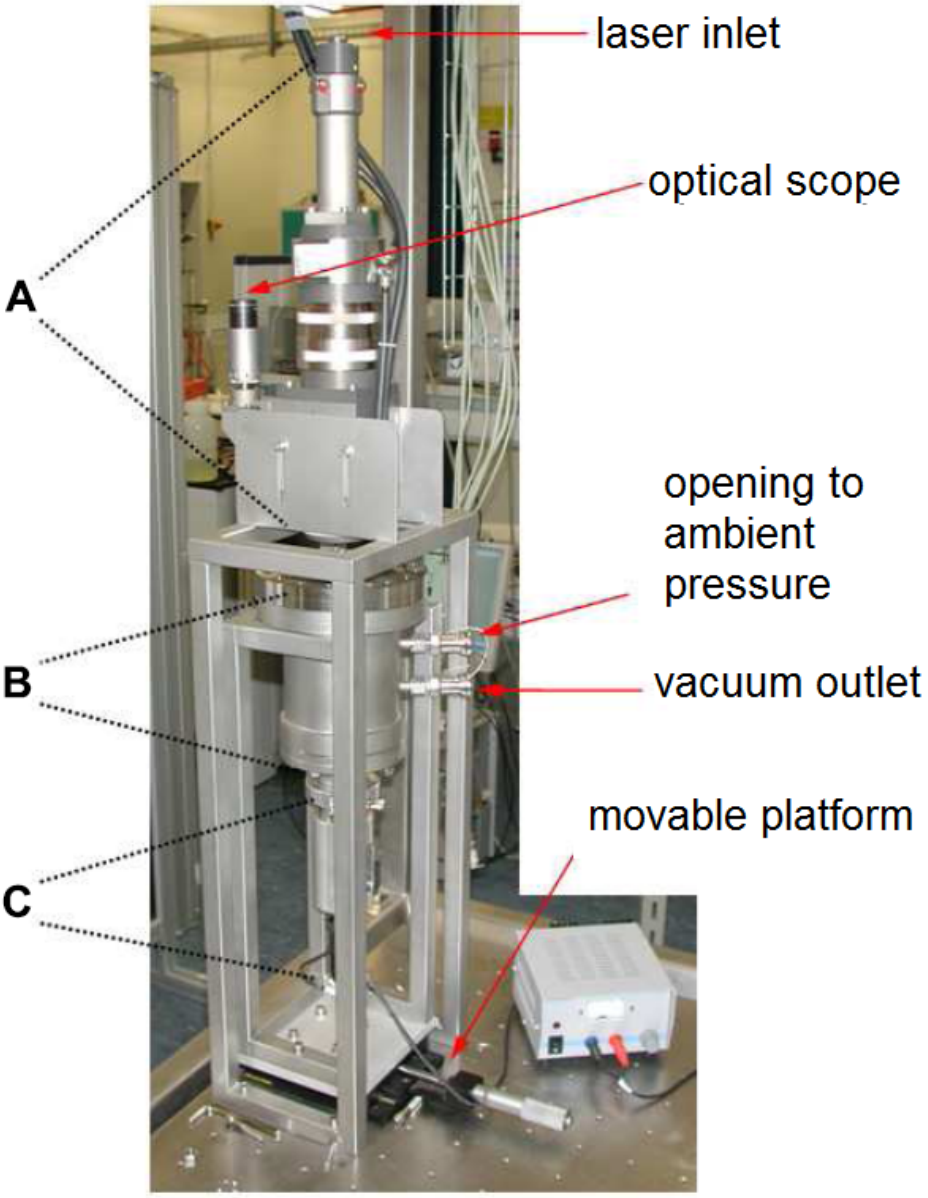

Figure 3.4: Picture of the device used for the laser welding.

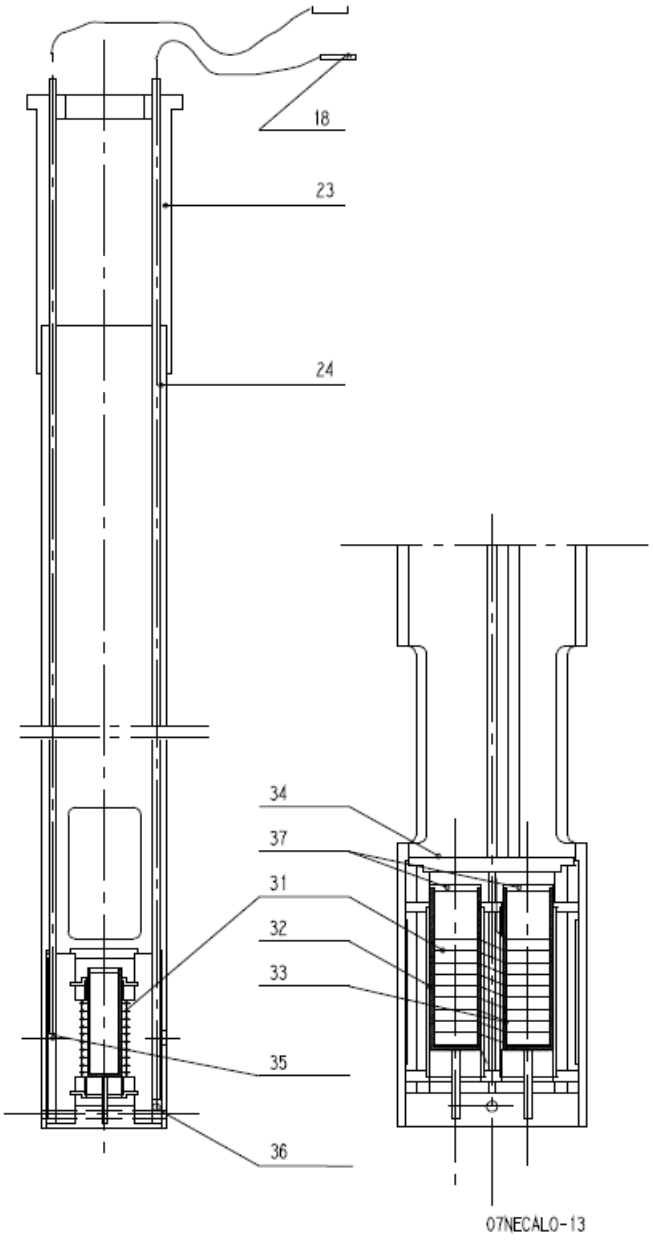

Figure 3.5: Section of the DSC detector.

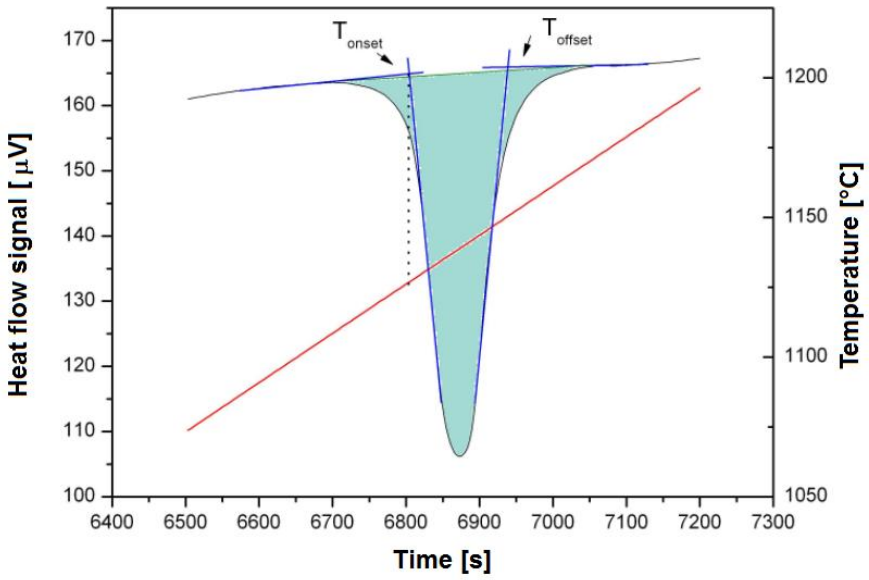

Figure 3.6: DSC result for the melting of ThF_4 performed in this work to verify the purity of the compound. The determination of the onset temperature and the peak area are shown.

indicates if the thermal event is endothermic or exothermic.

A typical DSC output is a spectrum that represents the temperature and heat flow trend over time and an example of ThF_4 melting is shown in Figure 3.6. From the study of this spectrum it is possible to determinate the phase transition temperature and the heat change for this transition. The temperature transition is identified as an onset of the peak (T_{onset}) determinated by the intersection of the base-line with the tangent to the peak's inflection point, as shown in the figure. The heat exchanged during the transition is the peak area and it can be determined by a simple integration.

3.2.1 Temperature calibration

The temperature measurement is performed by a thermocouple fitted under the crucible containing sample. This measurement is done near the sample but a little shift from the temperature on the sample is possible. This is due to the thermal gradient and the time delay needed for the heat to cross the crucible wall. To suppress this discrepancy the calibration is done under the same conditions as for the experiment and is done every time when the experimental conditions change significantly, e.g., change of the

Table 3.1: Standard reference materials used in this study for temperature calibration. Data from National Institute of Standard and Technology.

Substance	Melting point (°C)	Purity (%)
Indium	156,598	99,9+
Tin	231,94	99,99
Lead	327,47	99,9+
Zinc	419,53	99,9999
Aluminum	660,33	99,9
Silver	961,780	99,9+
Gold	1064,18	99,99
Copper	1084,62	99,9

detector or its repositioning. The parameters influencing the temperature correction are the temperature, the scanning rate, the type of crucible, the type of inlet gas and the exact position of the detector. Since the type of crucible and inlet gas are kept the same, the calibration is done as a function of temperature and scanning rate.

Standard materials with well known point of fusion are used for the calibration. These metals must have high purity and different melting points in order to cover the needed range of temperature. Materials used in this study are listed in Table 3.1. All these standards have been heated at different rates, from 2 K/min to 12 K/min, and the melting temperature has been recorded. For each standard the difference between the measured temperature and the theoretical temperature is plotted as a function of the heating rate as shown in Figure 3.7. These points are then fitted linearly according to:

$$T_{meas} - T_{real} = \Delta T_0 + b \cdot r \tag{3.2}$$

where the terms $\triangle T_0$ and b are identified as an intercept of the fit and its slope, respectively. The $\triangle T_0$ and b terms are further plotted as a function of temperature and fitted again with the suitable curve, reported in Figure **??**.

Substituting Equation 3.2 with the obtained curves the full calibration curve for the detector becomes:

$$T_{meas} - T_{real} = 6 \cdot 10^{-6 \cdot} T^2 + 0.008 \cdot T + 3.3724 + r \cdot (2.839 - 0.015 \cdot T) \tag{3.3}$$

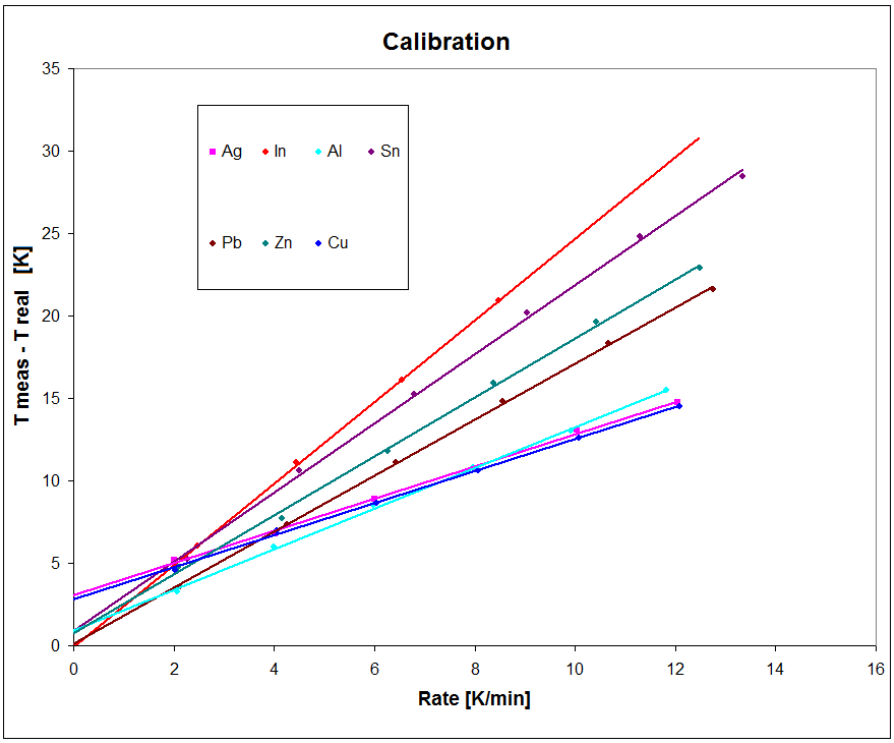

Figure 3.7: Difference between measured and real temperature as a function of heating rate for different standard material.

where T is the temperature of the measurement expressed in Kelvin and r is the heating rate expressed in K/min.

3.2.2 Energy calibration

The energy calibration is essential to measure the enthalpies of mixing or transitions of investigated samples. The DSC output is an electrical signal (heat flow) expressed in microvolt and it has to be transformed in a thermal power expressed in milliwatt. For this purpose the sensitivity of the detector that determines the relation between the output signal and the real heat is needed. It is defined as:

$$S = \frac{A_{ref} \cdot M_{ref}}{\triangle H_{ref} \cdot m_{ref}} \tag{3.4}$$

where A_{ref} is the area of the heat flow peak related to a specific enthalpy change (e.g., melting) ($\mu V \cdot s$), M_{ref} is the molar mass of the material (g/mol), $\triangle H_{ref}$ is the enthalpy change (J/mol) and m_{ref} is the mass (g). Once the sensitivity is determined, the enthalpy

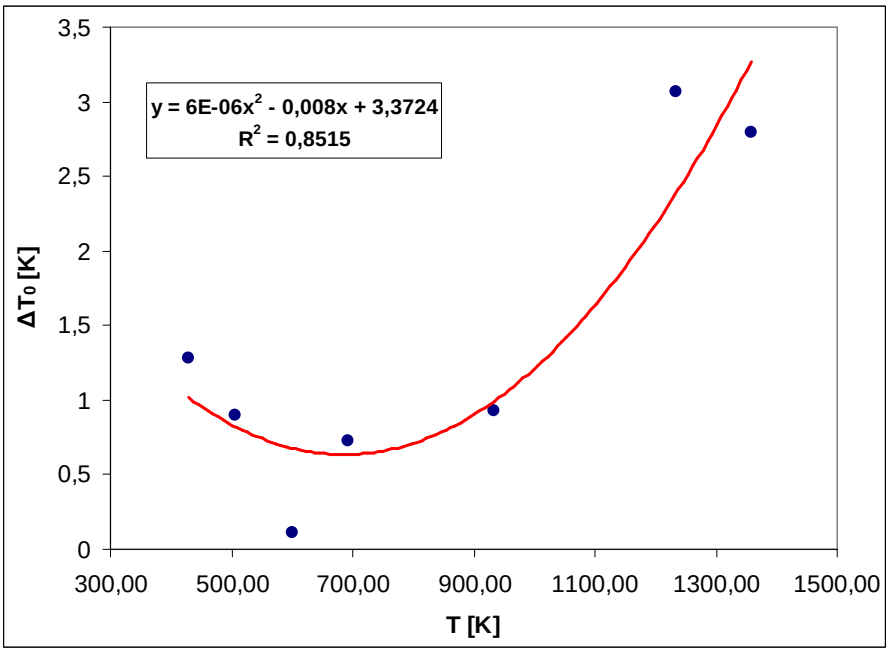

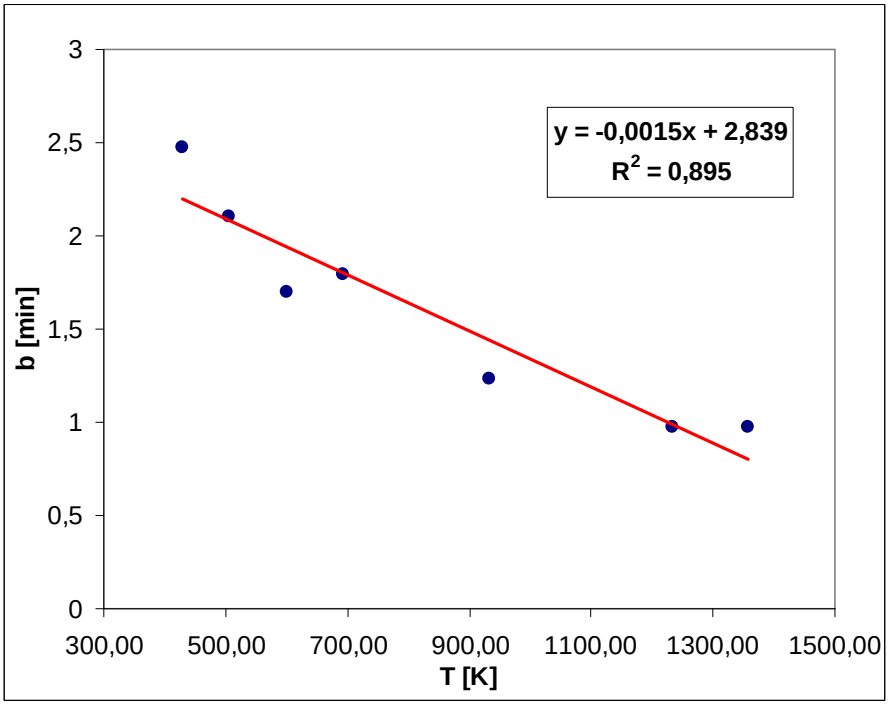

Figure 3.8: Polynomial fit for the term $\triangle T_0$ and linear fit for the term b

of fusion or the enthalpy of mixing of a studied material is calculated according to analogue equation:

$$\triangle H_{sample} = \frac{A_{sample} \cdot M_{sample}}{S \cdot m_{sample}} \tag{3.5}$$

where A_{sample} is the area of the heat flow peak related to a specific enthalpy change in the sample ($\mu V \cdot s$), M_{sample} is the molar mass of the sample (g/mol), S is the sensitivity obtained with Equation 3.4 and m_{sample} is the mass of the sample (g).

To determine the sensitivity several experiments were carried out using materials with known enthalpy of fusion. During these measurements it was observed that the sensitivity shows some variations even keeping the same experimental conditions. This discrepancy is due to the real conditions of the detector, which are slightly different in every thermic cycle. Under a quantitative point of view, these variations are small but for some experiments performed in this work they could be the key factor increasing the uncertainty.

In order to obtain the sensitivity as accurate as possible, a different method was applied. In this case, the standard material is placed in the reference crucible and measured in the same cycle with the sample. In this way, it is possible to directly compare the area of the reference, thus its sensitivity, and the area of the sample. For our experiment the selected reference material was pure silver because its melting point is close to the melting point of the analysed systems, thus in the region with very similar sensitivities, however far enough to distinguish the two observed peaks. A typical output is shown in Figure 3.1. To test this novel method, several experiments were carried out with three different compounds of known enthalpy of fusion and similar melting points: LiF, KF and NaCl. For each of this compound, several measures have been performed and the ratio between the sample sensitivity and reference sensitivity has been calculated. The average value of these results is:

$$R_{samp/ref} = 0,935 \pm 0,03. \tag{3.6}$$

This correction factor is used when the sample has a melting point relatively close to the compounds used for this determination.

3.3 Drop Calorimeter

Drop calorimetry is a common technique for obtaining heat capacity above room temperature. A sample, at temperature T_1(usually room temperature), is dropped into a calorimeter that is maintained at higher temperature T_2. The measured heat is equal to the enthalpy increment of a dropped sample from T_1 to T_2 and repeating such measurement for several different T_2, an enthalpy is obtained as a function of temperature. The heat capacity is then derived according to:

$$C_p = \left(\frac{\partial H}{\partial T}\right)_P . \tag{3.7}$$

The instrument layout is very similar to the DSC calorimeter descripted in the previous section but in this case the two crucibles are placed differently. The calorimeter is equipped with a big cylindrical alumina crucible where the sample drops and the reference crucible is placed below. Both crucibles are surrounded by 28 S-type thermocouples that provide the heat flow signal.

The Drop Calorimeter is equipped with an automatic multi-sample introducer in order to make consecutive introduction of several samples without manual operations. A program is used that consists in three consecutive steps. The first step is the heating from ambient temperature to the desired temperature with a heating rate of 10 K/min, followed by the period of temperature stabilization, lasting usually 4 hours. After an adequate stabilization time, the measuring sequence begins. During this period, samples and references are dropped with delay of 30 minutes, enough time to re-equilibrate the temperature and the heat flow signals.

As the sample is colder than the environment, an extra heat must be delivered to keep the pre-set temperature. The output is a peak of the heat flow signal and the area of this peak is proportional to the enthalpy increment of the sample. This value can be obtained if the sensitivity of the calorimeter is known. Therefore, between two different sample drops, a reference material is measured. The sensitivity for the sample is the average value from the two surrounding reference values. The reference has a well-known heat capacity and in this study sapphire and platinum were used. For these materials the heat

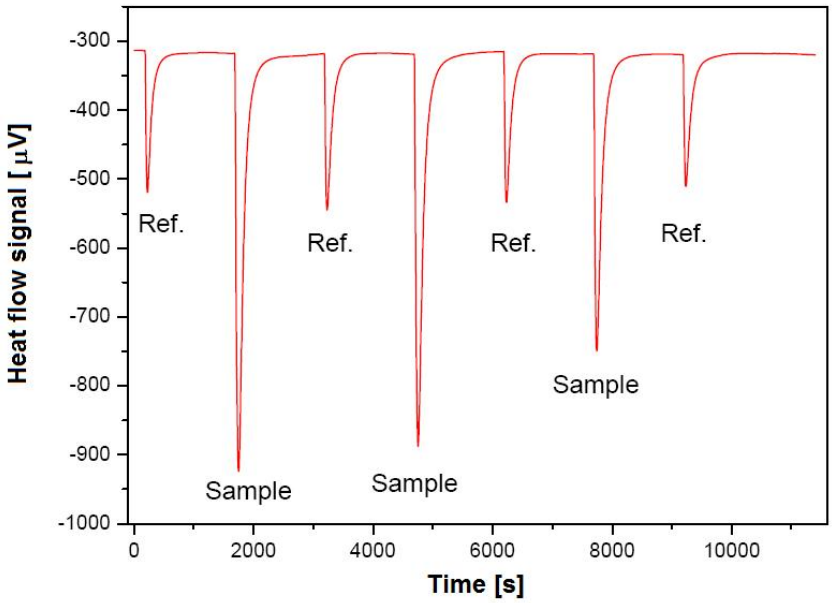

Figure 3.9: A typical measuring sequence performed with the Drop Calorimeter. The enthalpy increment of the exact composition $(Li_{0,5}Rb_{0,5})F$ is recorded using a sapphire reference at T=948 K.

capacities were taken from [31] and [32], respectively, and are reported in Appendix A. The output of one measurement is then a succession of several peaks as shown in Figure 3.9.

Samples used for this work were pellets of fluoride salts encapsulated as described in Section 3.1.2. The results obtained from the analysis contain two information: the enthalpy increment of the fluoride salt and the enthalpy increment of the nickel, which is the material for the crucible. To obtain the value for the analysed fluorides, the contribution of nickel must be subtracted. A complete characterization of the nickel enthalpy within the whole temperature range was done in [33] and is reported in Appendix A.

3.3.1 Temperature calibration

The temperature calibration is needed also for the drop calorimetry. The procedure is the same as for the DSC technique, described in Section 3.2.1. In this case, the calibration as a function of the scanning rate is not necessary as the measuring method is isothermal. Nevertheless, to identify the "zero rate" temperature shift, the difference between the real and measured temperatures is again plotted as a function of heating rate for each

reference but only the intercept of the lines is taken into account. The results are shown in Figure 3.10 and the calibration curve is:

$$T_{meas} - T_{real} = 1,8395 - 0,0010 \cdot T \tag{3.8}$$

It is interesting to see that in case of the DSC (Figure **??**) the $\triangle T_0$ function was fitted with a second order polynomial, whereas in case of the Drop detector rather linear dependency was observed. This could be explained by the different geometry of the two detectors.

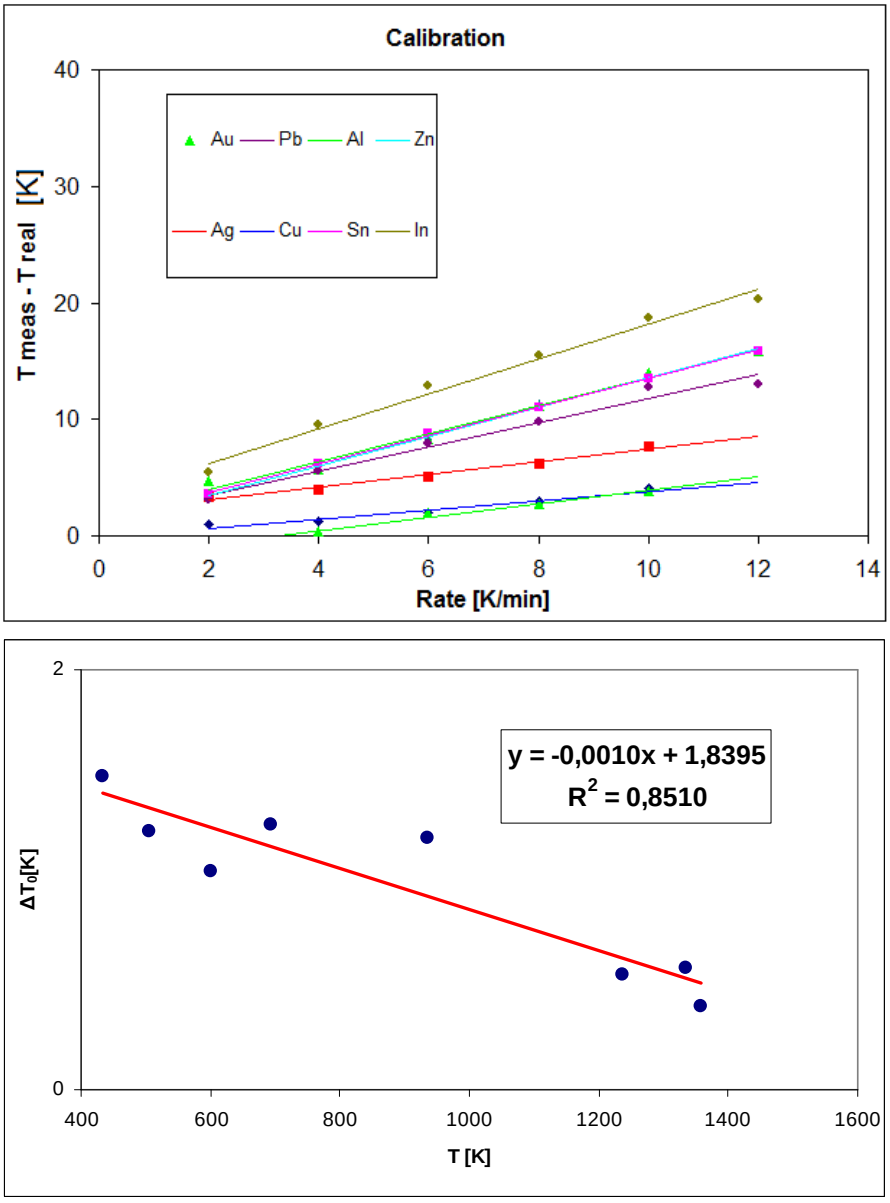

Figure 3.10: Calibration results for the Drop Calorimeter.
Upper graph: Difference between measured and real temperature as a function of heating rate for each reference.
Bottom graph: Linear fit for the term $\triangle T_0$ determined from the previous graph.

Chapter 4

Experimental results

In this chapter, the results obtained during this work are presented. The thermodynamic characterization of fluoride salts was the main aim of the study and was carried out in parallel on several systems, which are described separately below. Experimental determination of heat capacity and phase diagram description are the two main purposes. Heat capacities of three systems were measured using the drop calorimetry: CsF in the solid phase, ThF_4 in the solid phase and the $(Li_{0,5}Rb_{0,5})F$ liquid phase. Concerning the phase diagram determination, equilibrium points, excess heat capacity and excess enthalpy of mixing of various systems were the three thermodynamic properties investigated. The data were then used to assess the LiF-KF and LiF-ThF_4 phase diagrams. Furthermore, the Li_3ThF_7 pure compound was synthesized and its fusion enthalpy was determinated by the DSC technique.

4.1 LiF - KF system

The LiF-KF system is a simple eutectic system which has been studied in the past by several authors. The experimental phase diagram points were obtained for the first time using the visual-polythermal method by Bergmann and Dergunov [34]. Their results show an eutectic point at 765 K and 1:1 composition. A different technique was used later by Aukrust et al. [35] in their measurements finding very close results. They used thermal analysis and high temperature filtration supplemented by visual observation. In both

cases, only the liquidus points were provided.

The phase diagram points are not the only data available about this system. The excess enthalpy of the (Li,K)F binary mixture was also studied in several works [36, 37]. The more recent data by Hong and Kleppa [38] were measured using a twin microcalorimeter. In this apparatus, the two salts are kept separated until the desired temperature is reached. Then the salts are brought into contact and the mixing occurs while the enthalpy change of this process is being recorded. The knowledge of this set of data combined with the equilibrium points allows better determination of the phase diagram as information on the behaviour of the liquid phase is known.

A discrete quantity of data is known on LiF-KF system, therefore it has been used in this work to proof the applicability of the new technique to determine the mixing enthalpy. Moreover, new data for the heat capacity of the (Li,K)F liquid solution have been experimentally determined and introduced in the final assessment of the LiF-KF phase diagram.

4.1.1 Preparation of the sample

First thing to do whenever working with fluorides, which are hygroscopic, is the purification of the salts. This process is a simple drying of powdered material for several hours at 350 °C in order to remove the residual moisture and its effectiveness is checked through the DSC method. A DSC output that shows only one sharp peak upon melting is a sign of a good purified material that needs to be confirmed by the identification of the melting temperature as the peak onset temperature. The results obtained for the two purified end-members of the studied LiF-KF system are reported in Figure 4.1. The melting temperatures are in good agreement with the literature data, with a maximum error of ± 5 K. Since the purity of the pure compounds is important to obtain reliable data of the studied binary system, every batch of prepared salt was tested before use for the experiment.

As discussed in Section 3.1.2, the sample must be encapsulated to avoid a vapour release during heating, thus a stainless steel crucible with a BN liner is used. For successful measurement of the enthalpy of mixing, it is important to avoid a contact between the two salts before they melt. Otherwise, solid reactions can occur and alter the enthalpy value.

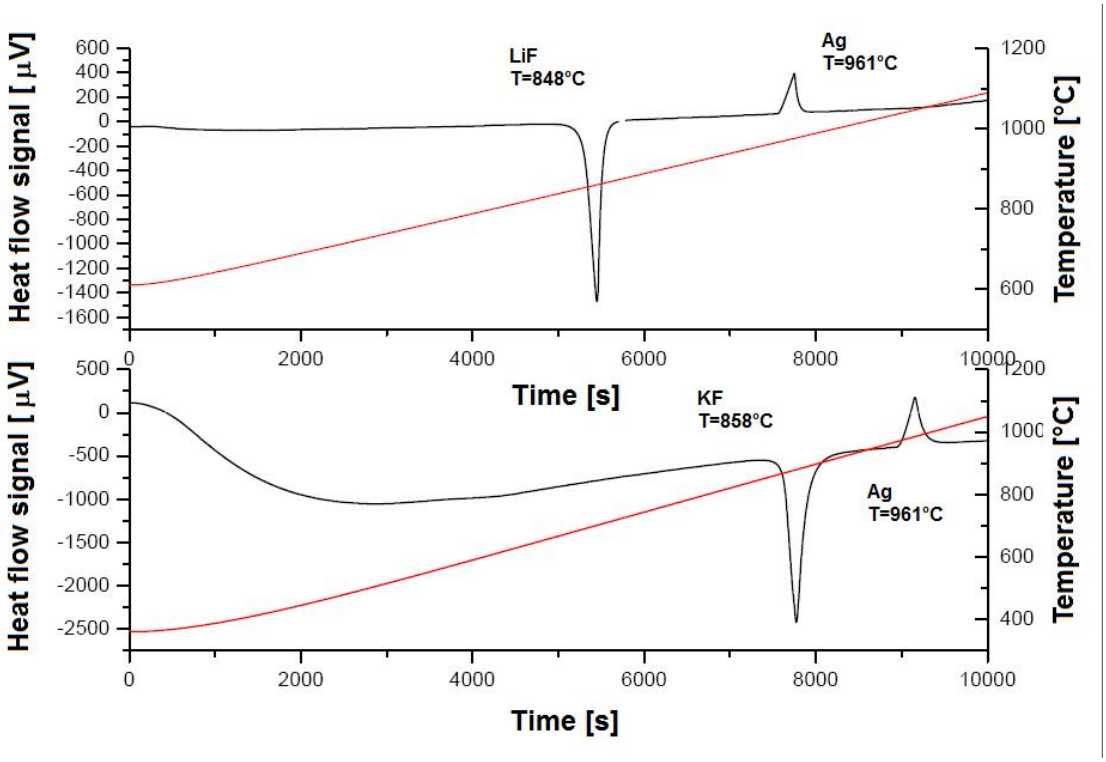

Figure 4.1: DSC results for LiF (upper graph) and KF (bottom graph).

For this purpose a new technique has been adopted. The compounds are compressed into pellets in order to be more compact and the two pellets are placed into the crucible as shown in Figure 4.2. In the bottom part the compound with the lower melting point is placed, in this case LiF, whereas above the higher melting end-member is placed. The two salts are kept separated by a thin Ni liner, which must have a diameter big enough to avoid the contact between the pellets but allowing the liner movement inside the crucible. When LiF melts (T = 1121 K), the Ni liner falls down into the crucible together with the KF pellet which starts to dissolve in LiF. If the dissolution is fast enough, the three events that occur (the melting of LiF, the melting of KF and the mixing of the two compounds) are shown as a single thermal event by the DSC. Since the mixing occurs approximately at the same time when the LiF melts, the mixing enthalpy value refers to a temperature equal to the LiF melting temperature.

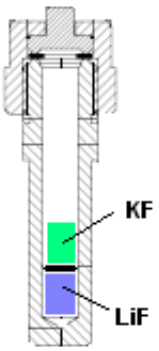

Figure 4.2: Representation of the technique to measure the enthalpy of mixing. The pellet of the system end-members are kept separated by a Ni liner and they get in touch upon melting of LiF.

4.1.2 Experimental data

Enthalpy of mixing data

Using the technique described in the previous section, several compositions of the LiF-KF system were prepared in order to describe the mixing enthalpy of the (Li,K)F liquid solution as a function of composition. The measurements were done using a Differential Scanning Calorimeter (DSC). A standard program was used for each measurement that consists of four thermic cycles until 1373 K with the same heating rate, 10 K/min, but different cooling rate. The enthalpy of mixing is obtained during the first heating when the formation of the solution occurs. The first peak recorded, upon the LiF melting temperature, is the sum of the LiF enthalpy of fusion, the KF enthalpy of fusion and the enthalpy of mixing. Therefore, the desired value of mixing enthalpy is obtained from the total DSC signal subtracting the fusion contributions of the end-members. Unfortunately, the enthalpy of mixing is the smallest quantity and little variations in the determination of the peak area lead to considerable differences in the mixing enthalpy value. Therefore, a technique with internal silver standard, as described in Section 3.2.2, was applied. The results obtained are reported in Table 4.1 and plotted in Figure 4.3. The points are quite well described by the following fitting:

Table 4.1: Measured values for the enthalpy of mixing of LiF-KF system. The absolute error is calculated based on the sensitivity uncertainty.

Molar fraction KF	$\triangle H_{mixing}$**[J/mol]**	**Error [J/mol]**
0,4771	-4113	808
0,5609	-4348	800
0,4420	-4196	805
0,6542	-3950	814
0,1901	-2412	867
0,2669	-3662	823
0,8028	-3341	836
0,3415	-3935	814
0,9029	-2949	850

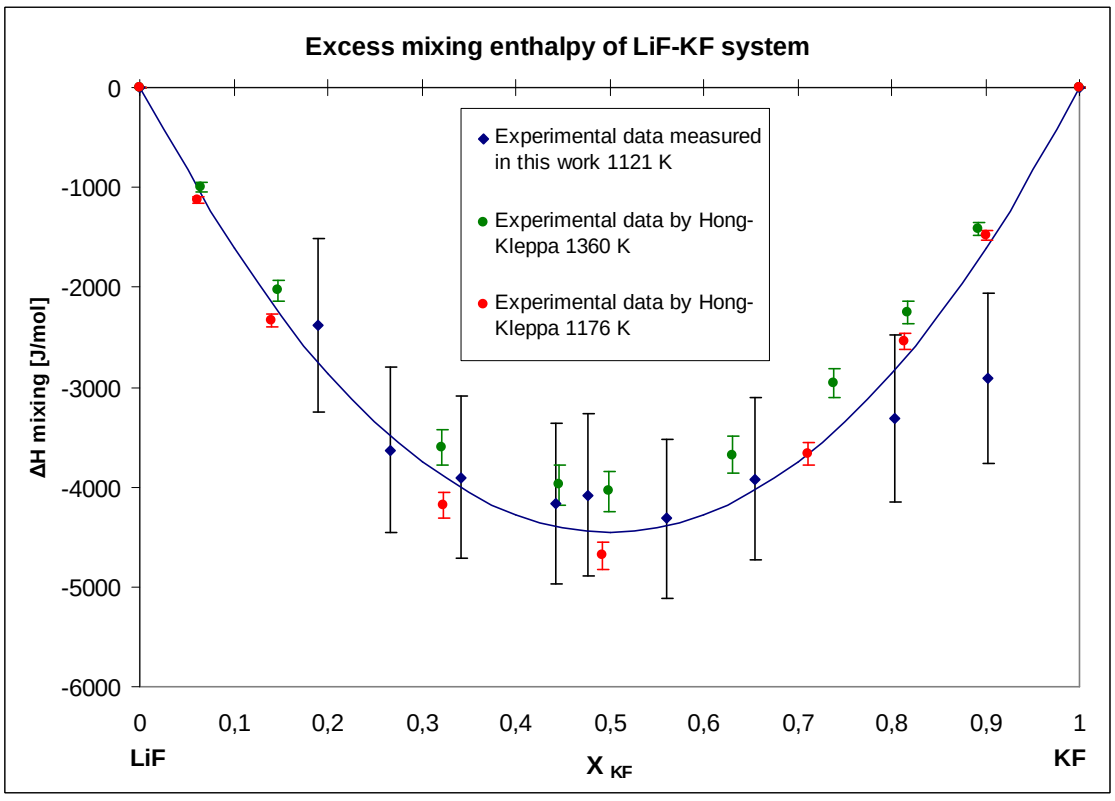

Figure 4.3: Comparison between the enthalpy of mixing data available for the LiF-KF system. ♦ Data measured in this work at T= 1121 K. ● Data from Hong and Kleppa [38] at T=1360 K. ● Data from Hong and Kleppa [38] at T=1176K.

$$\triangle H_{mixing} = -17847 \cdot X_{LiF} \cdot X_{ThF_4}. \quad (4.1)$$

The error bars are calculated based on the sensitivity uncertainty, determinated during the energy calibration and reported in Equation 3.6. Quantitatively, the error is bigger compared to work of Hong and Kleppa [38], but in their study they used a direct method for the enthalpy determination. Nevertheless, the comparison with the existing literature data shows a good agreement and suggests that the new technique is able to give reliable data of the mixing enthalpy with the right order of magnitude.

Phase diagram points

After the first heating the final solution is formed, thus the subsequent thermic cycles provide the information about the phase equilibria of the given composition. For each analysed composition, except for the eutectic composition and the end-members, two peaks were obtained. Considering the heating process, the first peak shows an onset temperature identified as eutectic temperature, while the second peak shows an offset temperature identified as liquidus temperature. This second signal takes the form of a shoulder and sometimes is difficult to be identified. The cooling curves can be useful for this purpose and help to better identify the liquidus points as they show much sharper peaks of the DSC output. The different shape of the signal upon heating ad upon cooling is shown in Figure 4.4. During the cooling process, the temperatures were not deduced directly as the onset temperatures of the peaks due to supercooling effect. The points were obtained by extrapolation to zero of the straight line interpolating the points measured at different rates. In this way, the melting temperatures of the pure end-members of the LiF-KF system were calculated and the values obtained were in perfect agreement with the values obtained upon heating.

The points measured are reported in Table 4.2 and shown in Figure 4.5, where they are compared with the data obtained by Aukrust [35] showing a very good agreement.

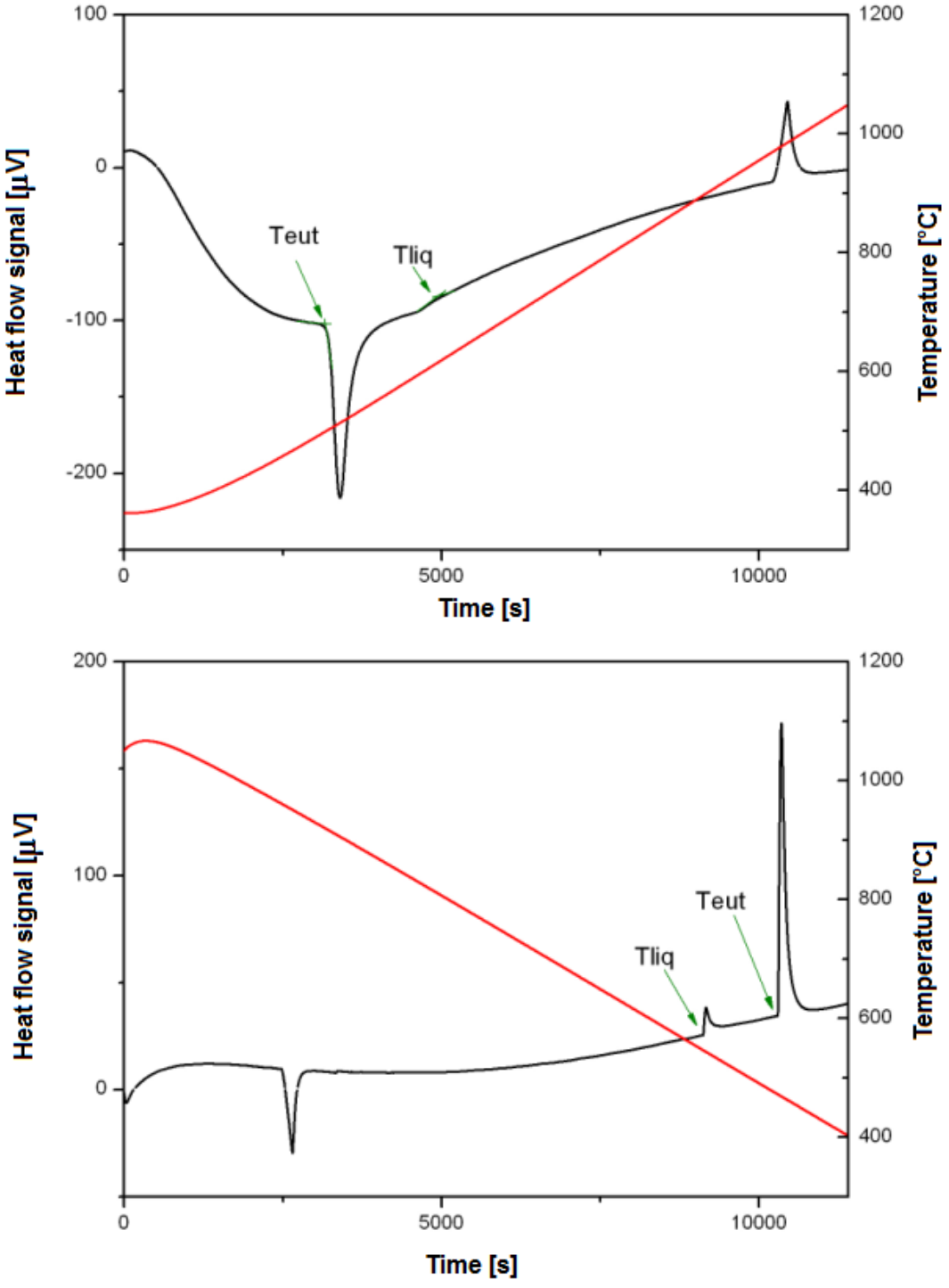

Figure 4.4: Typical DSC output obtained for the LiF-KF system upon heating (upper graph) and upon cooling (bottom graph).

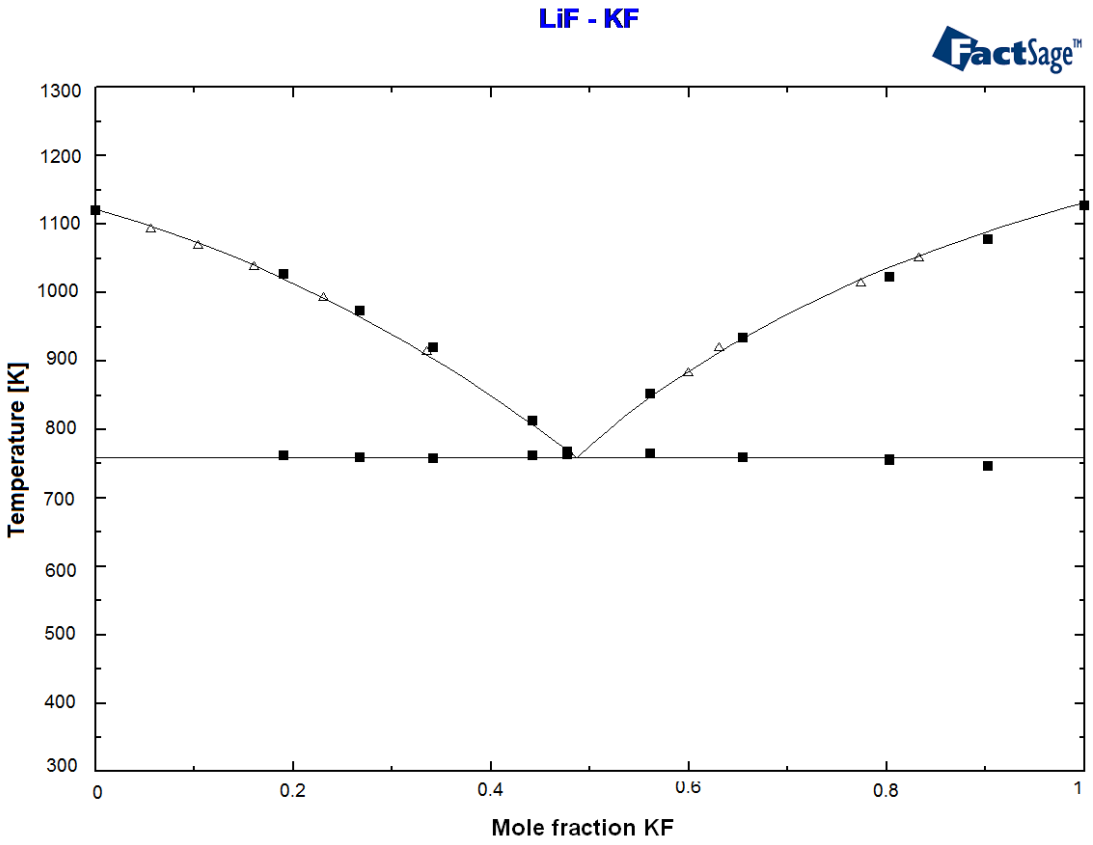

Figure 4.5: The calculated phase diagram of the LiF-KF system. ■ Data measured in this work. △ Data measured by Aukrust [35].

Table 4.2: Equilibrium points of LiF-KF system measured in this work.

Molar fraction KF	**T [K]**	**Equilibrium**
0	1118,9	*LiF melting point*
0,1901	761,6	*Eutectic*
	1026,6	*Liquidus*
0,2669	758,1	*Eutectic*
	972,2	*Liquidus*
0,3415	757,3	*Eutectic*
	919,5	*Liquidus*
0,4420	760,7	*Eutectic*
	811,8	*Liquidus*
0,4771	762,1	*Eutectic*
	767,1	*Liquidus*
0,5609	763,4	*Eutectic*
	851,3	*Liquidus*
0,6542	757,8	*Eutectic*
	933,0	*Liquidus*
0,8028	755,6	*Eutectic*
	1027,6	*Liquidus*
0,9029	745,9	*Eutectic*
	1077,3	*Liquidus*
1	1126,9	*KF melting point*

Excess heat capacity data

The excess heat capacity at constant pressure is an excess properties that can be derived theoretically from the excess enthalpy. It is defined as follows:

$$C_P^{excess} = \frac{\partial H^{excess}}{\partial T}. \tag{4.2}$$

This excess heat capacity is the difference between the molar heat capacity of the non-ideal binary solution and the molar heat capacity of the perfect ideal solution. For the ideal solution, the heat capacity can be calculated using the Neumann-Kopp rule and it is defined like a simple weighted average of the heat capacity of the two pure compounds:

$$C_P^{id} = x_A \cdot C_P^A + x_B \cdot C_P^B \tag{4.3}$$

where x_A and x_B are the molar fractions, which describe the generic mixture of two components A and B, whereas C_P^A and C_P^B are the heat capacities of these generic compounds.

Some solutions show a behavior identical or very close to ideality but others can be characterized with excess contributions. This property, like the mixing enthalpy, can be useful to determine the Gibbs energy of a solution and thus is important for the assessment of the phase diagram.

Concerning the LiF-KF system, no heat capacity measurements of the (Li,K)F liquid solution were found in literature. In order to describe this thermodynamic function within the whole range of composition, three intermediate compounds were prepared with the following LiF molar fraction: X_{LiF}=0,25; X_{LiF}=0,50; X_{LiF}=0,75. The samples were measured using a Drop Calorimeter and the derived heat capacity results are shown in upper graph of Figure 4.6 together with the LiF and KF end-members, measured in this work as well. These values are then compared with the heat capacity of the ideal solution which is defined in Equation 4.3 and corresponds, in a Cp-X graph, to a straight line between the heat capacity values of end-members. The points are fitted in a polynomial form as follows:

$$C_P^{excess} = A \cdot X_{LiF} \cdot X_{KF} \tag{4.4}$$

where X_{KF} is the molar fraction of KF, X_{LiF} is the molar fraction of LiF and A is the parameter to be optimized. The bottom graph of the Figure 4.6 shows the excess value and its fit. It is obvious that a significant shift from the ideal behavior was observed.

4.1.3 Assessment of the phase diagram

The experimental data obtained and described in the previous sub-sections were used to optimize the phase diagram of the LiF-KF system using the FactSage software. A simple polynomial model for the excess Gibbs energy was chosen, due to its simplicity, and is described by the following equation:

$$\triangle G_{excess} = \sum_{n,m} X_{LiF}^n \cdot X_{KF}^m \cdot [A^{n,m} + B^{n,m} \cdot T + C^{n,m} \cdot T \cdot ln(T)] \tag{4.5}$$

where there are three parameters $A^{n,m}$, $B^{n,m}$ and $C^{n,m}$ that can be modelled based on the known properties. Considering as first approach $n = m = 1$, the equation becomes:

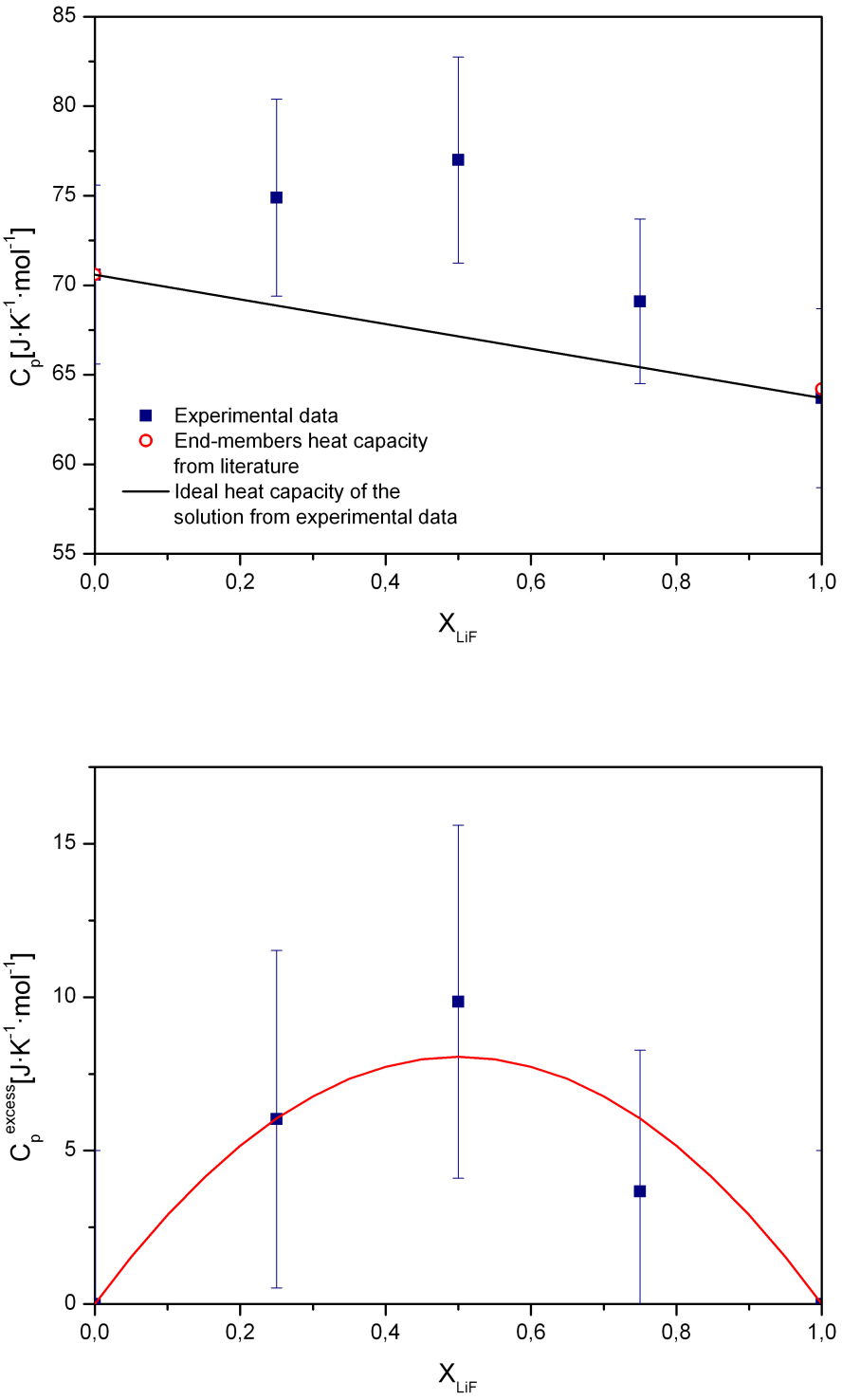

Figure 4.6: Heat capacity data obtained for three different compositions of the (Li,K)F liquid solution. The excess values are obtained subtracting the ideal heat capacity contribution.

$$\triangle G_{excess} = X_{LiF} \cdot X_{KF} \cdot [A + B \cdot T + C \cdot T \cdot ln(T)] \tag{4.6}$$

The parameters A, B, C are selected based on the relations with the real physical properties that can be deduced from the Gibbs energy: excess entropy, mixing enthalpy and excess heat capacity. The expression of these functions, using the polynomial model for the excess Gibbs energy description, is given in the following three equations:

$$\triangle S_{excess} = \left(\frac{\partial \triangle G_{excess}}{\partial T}\right)_P = X_{LiF} \cdot X_{KF} \cdot [-B - C \cdot (ln(T) + 1)] \tag{4.7}$$

$$\triangle H_{mix} = \triangle G_{excess} + T \cdot \triangle S_{excess} = X_{LiF} \cdot X_{KF} \cdot [A - C \cdot T] \tag{4.8}$$

$$C_P^{excess} = \left(\frac{\partial \triangle H_{mix}}{\partial T}\right)_P = X_{LiF} \cdot X_{KF} \cdot [-C] \tag{4.9}$$

Since the excess entropy value is not available for this system, the entropy was optimized during the phase diagram assessment, while the other two values were taken from experimental results. Starting from this setting, the excess entropy is optimized to best fit the phase diagram points.

The first optimization done showed an unsatisfactory agreement between the calculated enthalpy of mixing and the available data. The temperature dependence of the function calculated from such assessment was excessive compared with the experimental evidence and, in order to reduce the gap between the curves at different temperature, the excess heat capacity had to be reduced. In the second iteration, a different fit for the excess heat capacity was taken, considering the lowest possible fit which remains within the experimental error bars. Using this new assumption a re-assessment was done and provided a more satisfactory result. Both cases are shown Figure 4.7 for a direct comparison.

The Gibbs energy model described with one interaction, $n = m = 1$, leads to a symmetrical shape of the phase diagram. The experimental points show instead that the eutectic point does not lie exactly at $X_{LiF} = X_{KF} = 0,5$ but it is slightly shifted. To

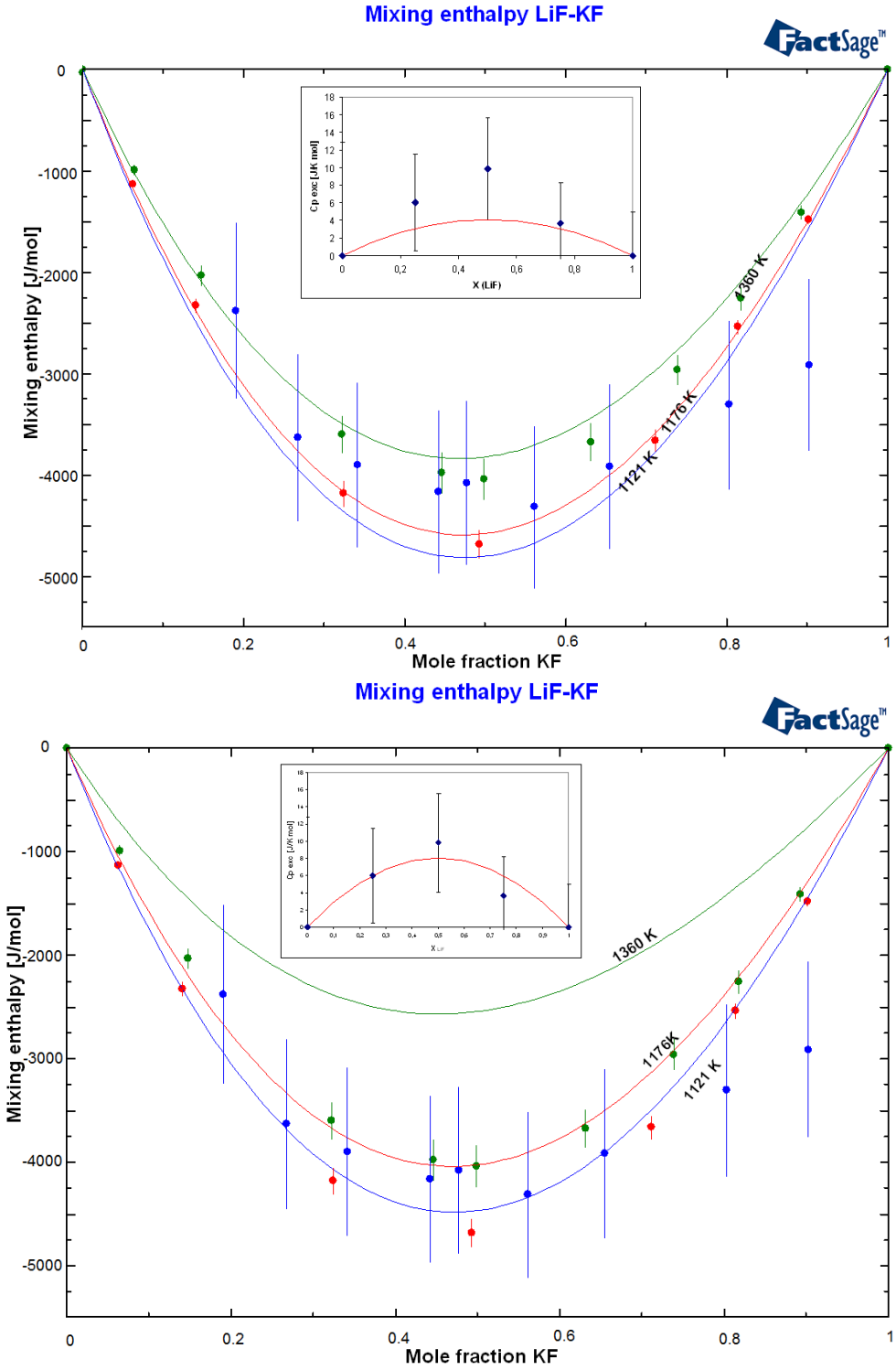

Figure 4.7: Comparison between the two different optimizations done in this work for the LiF-KF system. The calculated enthalpy of mixing is plotted for the two cases with different excess heat capacity. Green line and green points: calculated enthalpy of mixing at T=1360 K and data by Hong and Kleppa [38] at the same temperature. Red line and red points: calculated enthalpy of mixing at T=1176 K and data by Hong and Kleppa [38] at the same temperature. Blue line and blue points: calculated enthalpy of mixing at T=1121 K and data measured in this work.

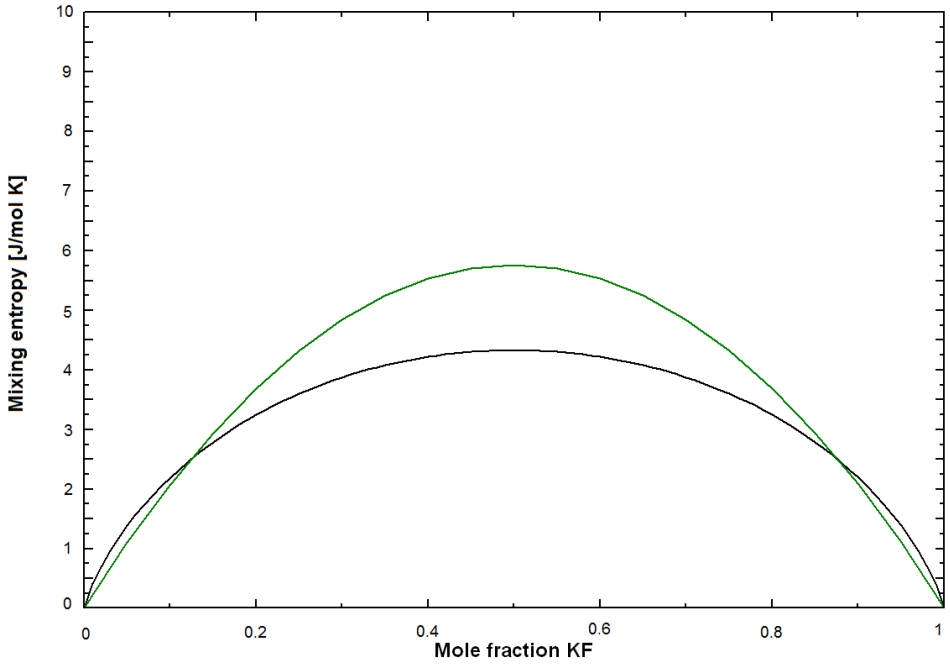

Figure 4.8: Entropy of the (Li,K)F liquid solution. Green line: Ideal solution entropy. Black line: calculated entropy function at T=1121 K.

include this observation in the model, two interactions are added that take into account different weighting for the LiF and KF molar fractions. The final assessment, given in Figure 4.5, is derived by the following equation:

$$\triangle G_{excess} = X_{LiF} \cdot X_{KF} \cdot [-37600 + 137,32 \cdot T - 16,4 \cdot T \cdot ln(T)]$$

$$-X_{LiF}^2 \cdot X_{KF} \cdot 2000 + X_{LiF} \cdot X_{KF}^2 \cdot 2000 \tag{4.10}$$

The eutectic point is identified at T= 757 K and $X_{KF} = 0,4866$. The entropy function was also calculated at T=1121 K and is shown in Figure 4.8. It is compared with the ideal contribution, the configurational entropy, showing a realistic value with a small shift from the ideality.

Concluding, the addition of the excess heat capacity data to the previously published model [39] does not change substantially the shape of the phase diagram but was useful to confirm its correctness and to improve the description of the Gibbs energy model, which

Table 4.3: Invariant equilibria points for the LiF-ThF_4 system.

Molar fraction ThF_4	Invariant temperature	Equilibrium
0,234	841 K	Eutectic
0,276	840 K	Eutectic
0,306	870 K	Peritectic
0,425	1035 K	Peritectic
0,592	1170 K	Peritectic

is essential for better extrapolation to higher order systems.

4.2 LiF-ThF_4 system

Salts containing thorium will probably assume a role of increasing importance as fuel for the MSR technology. Among the various systems, the LiF-ThF_4 system has a special relevance because it is the primary choice for the Molten Salt Fast Reactor fuel [9]. Therefore it is of big importance study this system in order to obtain its thermodynamic description, which is useful for the safety assessments and the reactor design calculations.

The most recent experimental data for the LiF-ThF_4 phase diagram were obtained by Thoma et al. [40]. One congruently melting compound ($3LiF \cdot ThF_4$) and three incongruently melting compounds ($7LiF \cdot 6ThF_4$, $LiF \cdot 2ThF_4$, $LiF \cdot 4ThF_4$) were found, using the thermal analysis coupled with X-ray analysis of the crystalline phases [41] confirming the compounds formulas. Based on these data, the optimization of the phase diagram was done recently [42] and the assessment is shown in Figure 2.4. It consist of five invariant equilibria summarized in Table4.3.

Later study by the same authors [43] considers the intermediate compound $LiF \cdot ThF_4$ instead of the compound $7LiF \cdot 6ThF_4$. The use of this different compound is justifiable based on the isostructurality with the analogue compound in the LiF-UF_4 system, originally reported as $Li_7U_6F_{31}$. It has been shown by single crystal studies [44] to have the composition $LiUF_5$, implying the same structure for the thorium compound $LiThF_5$. This assumption leads to a different assessment of the phase diagram presented by Van der Meer et al. [45] and shown in Figure 4.9. The correct intermediate compound has not been yet clarified and new experimental data may be useful for this purpose and

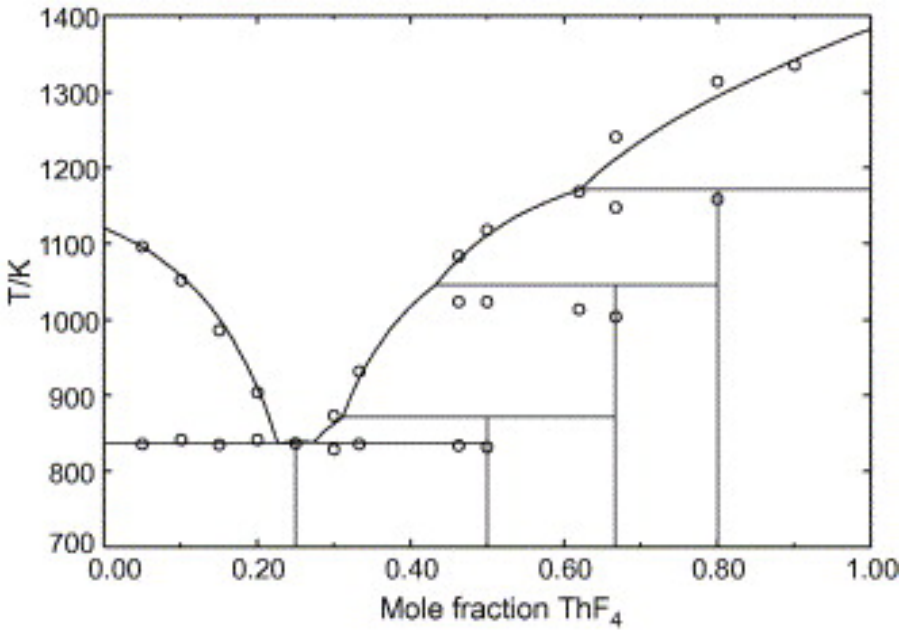

Figure 4.9: Assessed LiF-ThF_4 diagram considering the intermediate compound $LiF \cdot ThF_4$ [45]. ∘ Experimental data from Thoma et al. [40].

consequently for the determination of the phase diagram.

The assessments published in the past were based on the phase diagram points reported by Thoma et al. [40], which were at that time the only available experimental data found in literature. The absence of other thermodynamic data, such as mixing properties, leads to a Gibbs energy model that has many degrees of freedom. It means that there is an increased probability that the model is inaccurate. The main aim carried out in the present work for this system was the improvement of the Gibbs energy model adding new experimental data, the mixing enthalpy, and the improvement of the phase diagram description based on new experimental data on the phase transitions. Additionally, the fusion enthalpy of the congruently melting compound Li_3ThF_7 intermediate compound has been measured and taken into account during the assessment.

4.2.1 Experimental data

Enthalpy of mixing data

The enthalpy of mixing of the (Li,Th)F_x liquid solution was measured using the same technique introduced and described in details on the case of the LiF-KF system. The two

end-members (LiF and ThF_4) were purified, compressed into pellets and placed inside the DSC crucible. In the bottom part was placed the LiF, which has the lower melting point, and the two pellets were kept separated with a Ni liner. Since the ThF_4 is a radioactive salt, the preparation of the sample was done completely within a glove box.

The same procedure used for the LiF-KF system was used to measure this system but a slightly different program was used. The four thermic cycles were performed until 1523 K, to reach the ThF_4 melting point, and after the first heating an isothermic zone at high temperature was introduced. This allowed complete mixing of the two fluorides in case they would not mix completely upon LiF melting. The determination of the excess enthalpy for the LiF-ThF_4 system was more challenging than the previous one. Unlike the LiF-KF system, the end members have very different melting points: T=1121 K for the LiF and T=1383 K for the ThF_4. When LiF melts, ThF_4 is still far from its melting point and it must dissolve from the solid phase during mixing. The process is ruled in this case by the solubility velocity. If the dissolution is fast enough, only one peak is observed during the first heating and the mixing occurs at temperature near the LiF melting point. This is the optimal case and the enthalpy of mixing is derived from the peak area subtracting the enthalpy of fusion value of the two end-members (the ThF_4 fusion enthalpy was extrapolated to melting temperature of LiF).

It was sometimes the case that the mixing did not occur in a proper way and two or even three peaks were observed during the heating. The first peak appeared at LiF melting temperature, the second one near the ThF_4 melting temperature and sometimes a third one was observed when the crucible was kept at high temperature ($\sim$1523 K) for a fixed time. The interpretation of these different cases can be very tricky and in general no data on mixing enthalpy were deduced from these measurements. However, it was observed in some experiments that the first peak at LiF melting temperature had an area corresponding only to the enthalpy of fusion of LiF. Probably, the two end-member were not in contact until the ThF_4 melting temperature is reached and then the ThF_4 melts. During the melting, the mixing occurs showing a single peak which was considered as the sum of ThF_4 enthalpy of fusion and the mixing enthalpy. The values obtained are not directly comparable with the previous ones because they refer to a different temperature,

Table 4.4: Measured values for the enthalpy of mixing of the LiF-ThF_4 system. Two sets of data are reported respectively for T=1121 K and T= 1383 K. The absolute errors are calculated based on the sensitivity uncertainty.

Data at T=1121 K

Molar fraction ThF_4	$\triangle H_{mixing}$**[J/mol]**	**Error [J/mol]**
0,3137	-8808	812
0,4423	-10139	832
0,1052	-4852	843
0,2151	-7566	805
0,2774	-8760	795

Data at T=1383 K

Molar fraction ThF_4	$\triangle H_{mixing}$**[J/mol]**	**Error [J/mol]**
0,1286	-4967	14
0,1820	-5807	63

at the ThF_4 melting point.

The mixing enthalpy data measured in this study are reported in Table 4.4 separately for the two temperatures and are plotted in Figure 4.10.

As done for the LiF-KF system, the errors were calculated based on the sensitivity uncertainty but for this system the percentage error is lower mainly due to the larger absolute value of mixing enthalpy. Due to the discussed experimental difficulty, limited number of points were taken into account for the analysis showing a clear trend. The data were fitted with the best curve in the following form:

$$\triangle H_{mixing} = A \cdot X_{LiF} \cdot X_{ThF_4} \tag{4.11}$$

where X_{LiF} is the molar fraction of LiF, X_{ThF_4} is the molar fraction of ThF_4 and A is the parameter to be optimized. The curves obtained for the two sets of data are:

$$\triangle H_{mixing} = -42696 \cdot X_{LiF} \cdot X_{ThF_4} \ @\, T = 1121K \tag{4.12}$$

$$\triangle H_{mixing} = -40983 \cdot X_{LiF} \cdot X_{ThF_4} \ @\, T = 1383K. \tag{4.13}$$

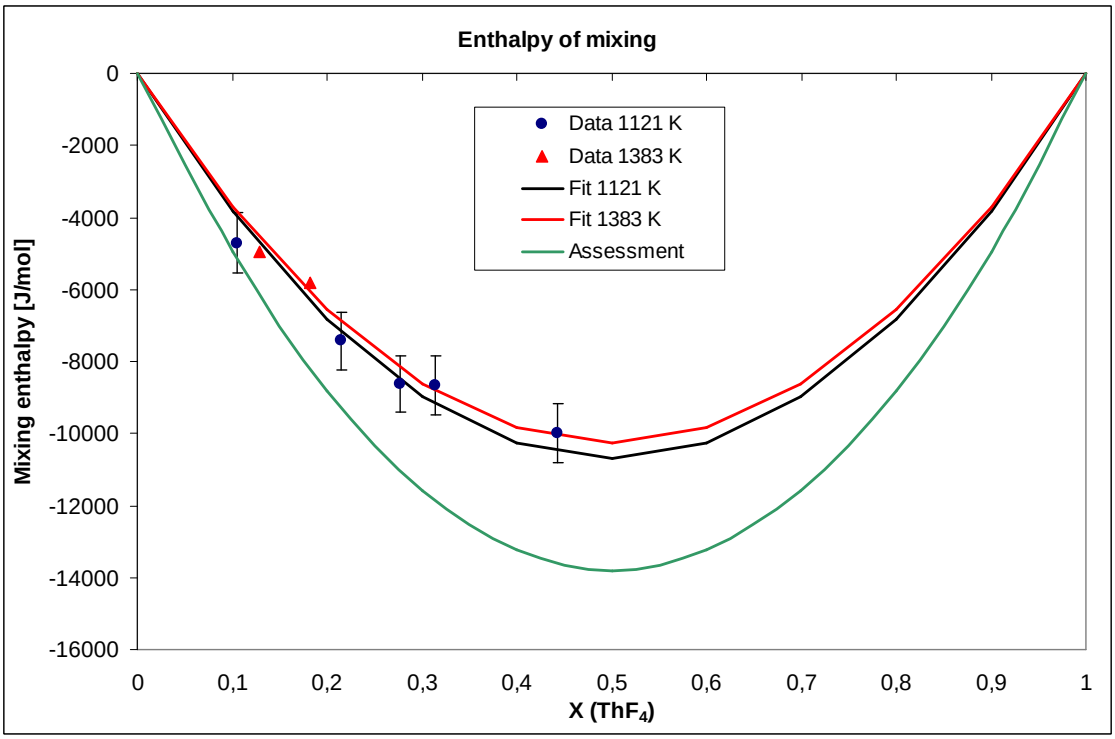

Figure 4.10: Enthalpy of mixing data for the LiF-ThF_4 measured in this work.
Blue points and blue line: Data at T=1121 K and the mixing enthalpy calculated.
Red points and red line: Data at T=1383 K and the mixing enthalpy calculated.
Green line: Enthalpy of mixing calculated from the assessment in [42] at T=1120 K.

Figure 4.10 shows the enthalpy of mixing calculated from the Gibbs energy model found in the recent assessment [42] and reported for T = 1121 K. It is obvious that these values are significantly lower than the experimental data. Therefore, a re-assessment of the phase diagram was done the present work taking into account the novel mixing enthalpy data.

Phase diagram points

In order to understand the various equilibria in the LiF-ThF_4 phase diagram, several measurement were done varying the mixture composition. All composition were treated with the same program, which consists of four heating cycles until 1523 K. During the first heating the formation of the intermediate compounds occurs, while the consequent cycles are used to identify the phase diagram equilibria. Thus, the phase transition temperatures are measured three times for the same crucible. The final values, reported in the phase diagram, are the average value of these different cycles and it was observed that the points were almost identical. This observation is good for the accuracy of the measurements and confirms that the mixing is complete and that no other reactions occur. The cooling curves were not taken into account for this system because of very pronounced supercooling effect that causes a strong temperature shift.

The points measured are given in Table 4.5 and shown in Figure 4.11. They are superimposed to the assessment of the phase diagram taken from [42] and a good agreement is evident.

Furthermore, the presence of a transition near T= 840 K in the range between X=0,46 and X=0,5 was observed and this should be visible only if the assessment considers the $LiThF_5$ compound instead of the $Li_7Th_6F_{31}$ compound. To avoid wrong interpretations, which could be related to the uncertainty in the determination of the composition, three samples with very similar composition were measured. All these results show the presence of the eutectic transition. Therefore, according to our experimental data, the intermediate compound should be $LiThF_5$ and the assessment in Figure 4.14 should be preferred.

A behaviour of an unknown origin was observed in the range between X= 0,6 and X= 0,7 where an unexpected transition at T= 945 K, suggesting e.g the existence of an unknown phase, was observed. However, a more careful analysis of the DSC spectra for

Table 4.5: Phase diagram equilibria of the LiF-ThF_4 system measured in this work.

Molar fraction ThF_4	**T [K]**	**Equilibrium**
0	1118,9	*LiF m. p.*
0,0638	831,6	*Eutectic*
	1097,8	*Liquidus*
0,1052	836,1	*Eutectic*
	1057,4	*Liquidus*
0,1286	835,2	*Eutectic*
	1036,5	*Liquidus*
0,182	835,9	*Eutectic*
	959,2	*Liquidus*
0,2151	834,5	*Eutectic*
	889,7	*Liquidus*
0,2495	831,3	Li_3ThF_7 *congruent m. p.*
0,2774	832,4	*Eutectic*
0,3137	825,0	*Eutectic*
	873,9	*Liquidus*
0,3208	828,0	*Eutectic*
	881,1	*Liquidus*
0,3412	826,3	*Eutectic*
	870,5	*Peritectic*
	973,4	*Liquidus*
0,361	834,3	*Eutectic*
	879,5	*Peritectic*
	982,8	*Liquidus*
0,3752	827,8	*Eutectic*
	875,3	*Peritectic*
	991,0	*Liquidus*
0,3907	831,8	*Eutectic*
	875,8	*Peritectic*
0,3907	1001,8	*Liquidus*
0,4103	831,9	*Eutectic*
	879,2	*Peritectic*
	991,3	*Liquidus*
0,4377	831,4	*Eutectic*
	873,4	*Peritectic*
	1064,6	*Liquidus*
0,4423	833,4	*Eutectic*
	880,2	*Peritectic*
	1057,5	*Liquidus*
0,4703	824,5	*Eutectic*
	874,3	*Peritectic*
	1043,9	*Peritectic*
	1097,8	*Liquidus*

Molar fraction ThF_4	**T [K]**	**Equilibrium**
0,4809	819,6	*Eutectic*
	871,6	*Peritectic*
	1053,1	*Peritectic*
	1109,2	*Liquidus*
0,4894	830,8	*Eutectic*
	872,0	*Peritectic*
	1040,4	*Peritectic*
	1121,6	*Liquidus*
0,5214	861,7	*Peritectic*
	1038,1	*Peritectic*
	1134,6	*Liquidus*
0,6084	860,3	*Peritectic*
	945,2	*Unknown*
	1048,4	*Peritectic*
	1162,2	*Liquidus*
0,6211	853,1	*Eutectic*
	945,2	*Unknown*
	1049,0	*Peritectic*
	1159,1	*Liquidus*
0,6487	942,4	*Unknown*
	1047,6	*Peritectic*
	1171,4	*Liquidus*
0,6573	935,1	*Unknown*
	1059,4	*Peritectic*
	1194,5	*Liquidus*
0,7143	1028,0	*Peritectic*
	1181,4	*Peritectic*
	1230,1	*Liquidus*
0,7809	1188,0	*Peritectic*
	1274,6	*Liquidus*
0,8417	1159,3	*Peritectic*
	1296,7	*Liquidus*
0,9083	1138,0	*Peritectic*
	1328,5	*Liquidus*
1	1386,0	ThF_4 *m. p.*

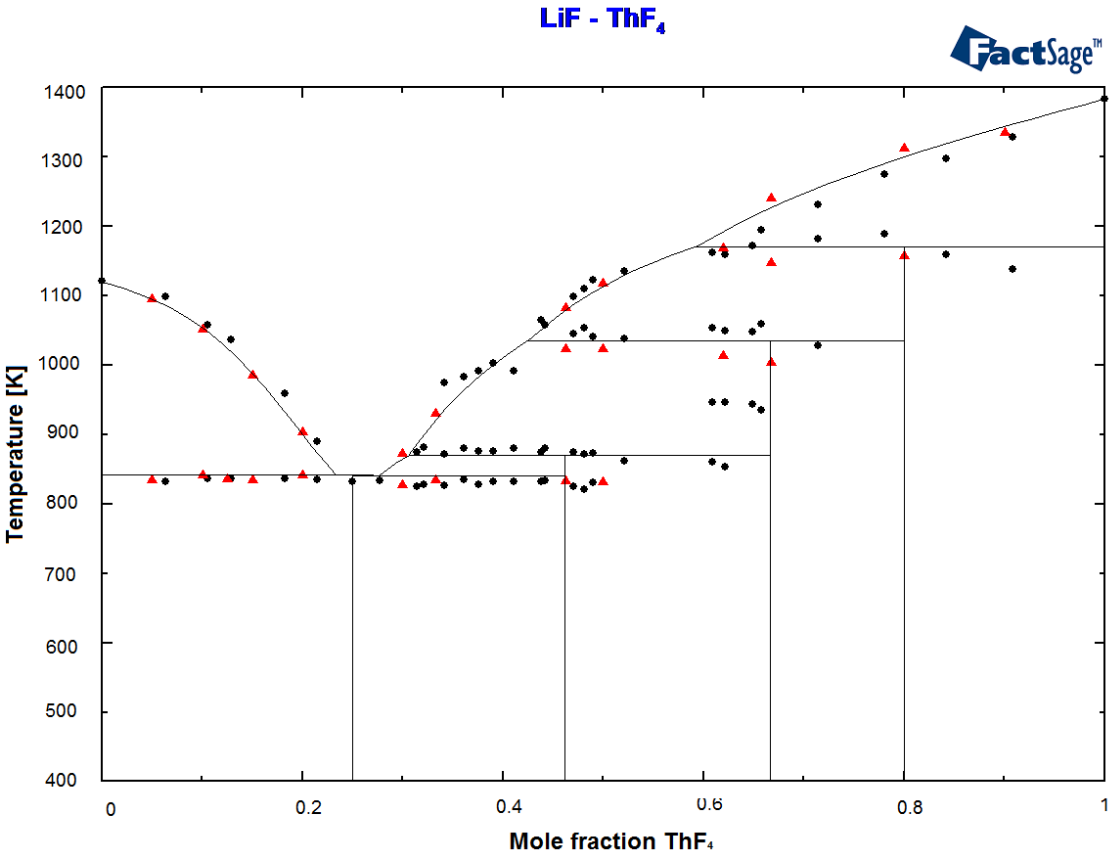

Figure 4.11: Phase diagram of the LiF-ThF_4 system optimized in [42]. ▲ Experimental data measured by Thoma et al. [40] • Experimental data obtained in this work.

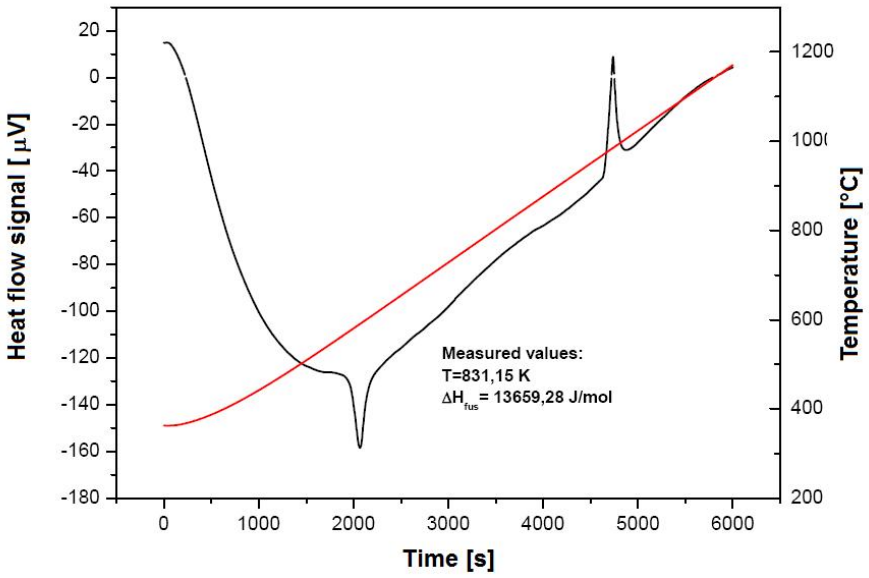

Figure 4.12: DSC output of Li_3ThF_7 compound. The first peak represents the melting of this compound and its area correspond to the enthalpy of fusion. The second peak is the melting of the silver used as internal reference.

all these four experiments has shown the existence of a little peak near the ThF_4 melting point. The peak, which does not occur for the other points, is visible upon heating and also upon cooling. Further investigation is needed to establish the source of this signal, maybe due to a small unreacted quantity of ThF_4 or to an unknown compound.

4.2.2 Congruently melting compound Li_3ThF_7

As part of the work performed on the LiF-ThF_4 system, the intermediate compound Li_3ThF_7 was synthesized. This compound shows a congruent melting point at T=831 K, as measured in this study, and it was prepared by mixing stoichiometric quantities of LiF and ThF_4. The mixture obtained was then heated for 2 hours at T=1373 K and in that time mixing in the liquid phase occurs completely. The aim was to prepare the pure Li_3ThF_7 compound which is planned to be used in the future for several measurements, such as the determination of its heat capacity.

The purity of the compound was checked by means of both the X-ray technique and the DSC technique. The results obtained by the DSC analysis (Figure 4.12) confirm the behaviour of the Li_3ThF_7 compound in terms of melting point and heat of fusion. The

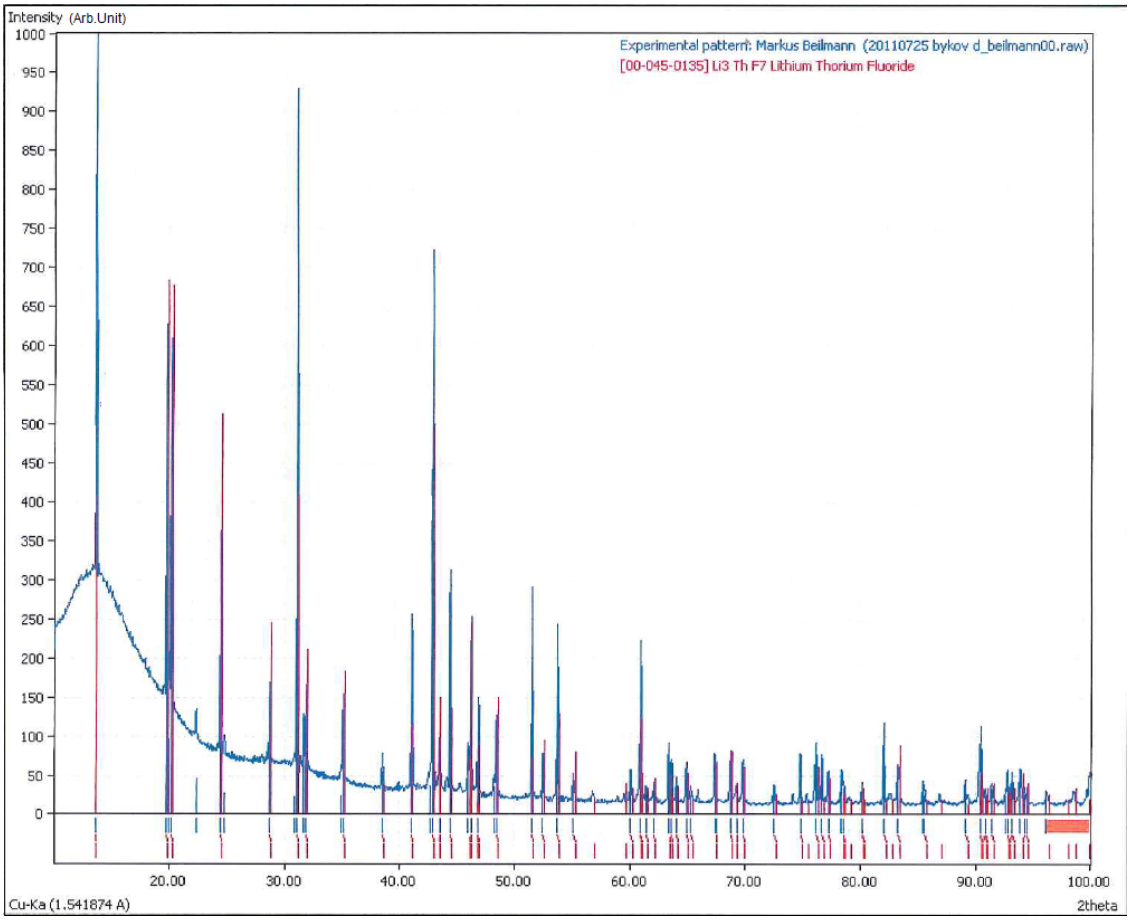

Figure 4.13: X-ray analysis of the Li_3ThF_7 compound. Blue line: Experimental pattern measured. Red line: Data from the database [47].

measured heat of fusion is comparable with the literature data by Gilbert [46] who found a value of 14602 J/mol.

The X-ray technique allows to determine the arrangement of atoms in the crystal using the diffraction of X-rays. The output of this analysis is a diffractogram where the X-ray intensity is plotted against the angle between the detector, the X-ray source, and the sample surface. The result obtained for the Li_3ThF_7 compound is shown in Figure 4.13 and was compared with the literature X-ray spectra [47] indicating the same crystalline structure.

4.2.3 Assessment of the phase diagram

Combining the new experimental data measured in this work, a re-assessment of the phase diagram has been done using the FactSage software. As already discussed, this

system is more complex than the LiF-KF system since stable solid intermediate compounds are formed. A database which contains the thermodynamic properties for the pure compounds and all intermediate compounds is needed for the calculation. The thermodynamic properties of the pure compounds LiF and ThF_4 were derived from literature, respectively from [24] and from [45], whereas the thermodynamic functions of intermediate compounds are not known and were obtained by optimization. Estimations of these values, used as starting values for the assessment, were calculated as weighted average of the properties of pure compounds. The heat capacities were estimated by Neumann-Kopp rule from its LiF and ThF_4 end-members, until additional data become available, and the optimization was done changing standard enthalpy of formation and standard absolute entropy. As discussed in the Section 4.2.1, the intermediate compound $LiThF_5$ was preferred during the modeling in order to explain the observed transition in the range from X=0,46 to X=0,5. All thermodynamic properties obtained in this work are reported in Appendix A.

The binary (Li,Th)F_x liquid solution was described using a simple polynomial model for the excess Gibbs energy, which is expressed by the following general equation:

$$\triangle G_{excess} = \sum_{n,m} X_{LiF}^{n} \cdot X_{ThF_4}^{m} \cdot [A^{n,m} + B^{n,m} \cdot T + C^{n,m} \cdot T \cdot ln(T) + D^{n,m} \cdot T^2 + ...] \quad (4.14)$$

where the parameters $A^{n,m}$, $B^{n,m}$, $C^{n,m}$, $D^{n,m}$,... are optimized during the thermodymanic assessment. Since most of the mixing enthalpy points have been measured at T=1121 K, the assessment was focused on this temperature.

In Section 4.2.1, the enthalpy of mixing points were fitted with a symmetric curve ($n = m = 1$), reported in Equation 4.12, which was used in this assessment as a starting value. However, it did not describe properly the shape of the phase diagram. In fact, the analysis of the experimental phase diagram points shows clearly an asymmetric component, thus further interactions have been added. In total, two asymmetric interactions were introduced, each with different weights on the two end-members, and the resulting fit of the mixing enthalpy was still in agreement with the experimental data. Due to the

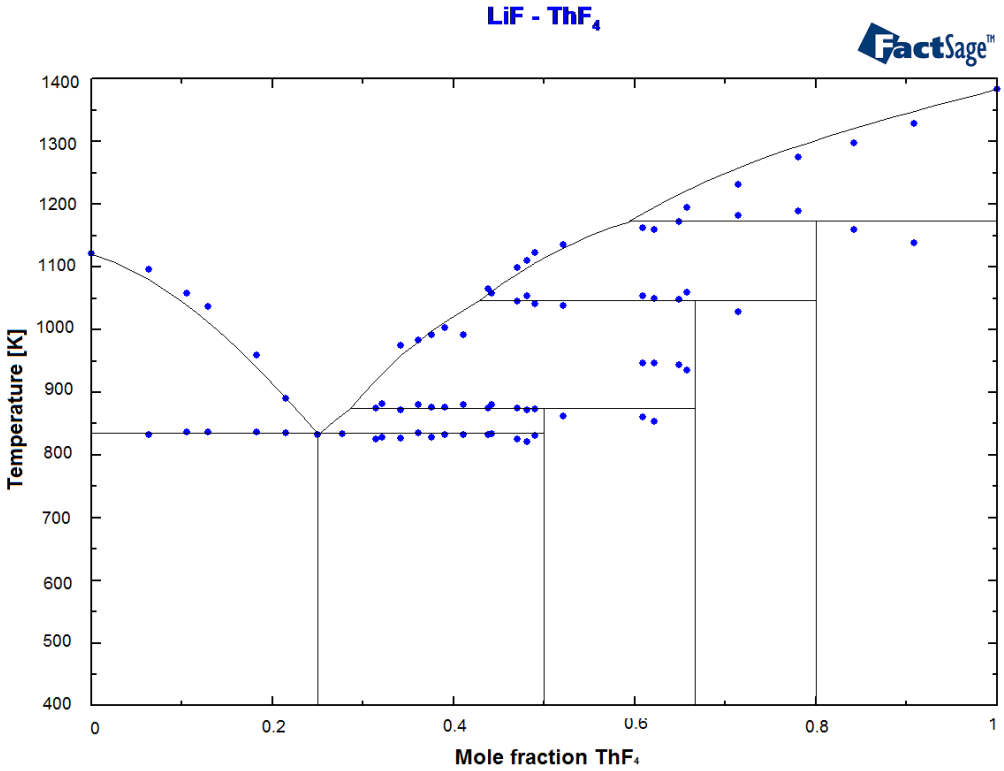

Figure 4.14: Phase diagram of LiF-ThF_4 system which has been re-assessed in this work. • Experimental data obtained in this work.

absence of other data, such as the heat capacity of the liquid solution, only the parameters A and B were used for the modeling. The excess Gibbs energy model which best fits with the experimental data was found to be:

$$\triangle G_{excess} = X_{LiF} \cdot X_{ThF_4} \cdot [-1200] + X_{LiF}^2 \cdot X_{ThF_4} \cdot [-61500 + 10 \cdot T]$$

$$+X_{LiF} \cdot X_{ThF_4}^3 \cdot [-15000]. \tag{4.15}$$

The equation reported leads to the phase diagram shown in Figure 4.14 , which is in good agreement with the experimental points, reported as well. It is the best obtained compromise between the different sets of data considered. In fact, in addition to phase diagram points, the model shows a good agreement with the enthalpy of mixing data measured in this work. This function was calculated as well, and the result is shown in Figure 4.15. It is compared with the analogue function calculated with the previous

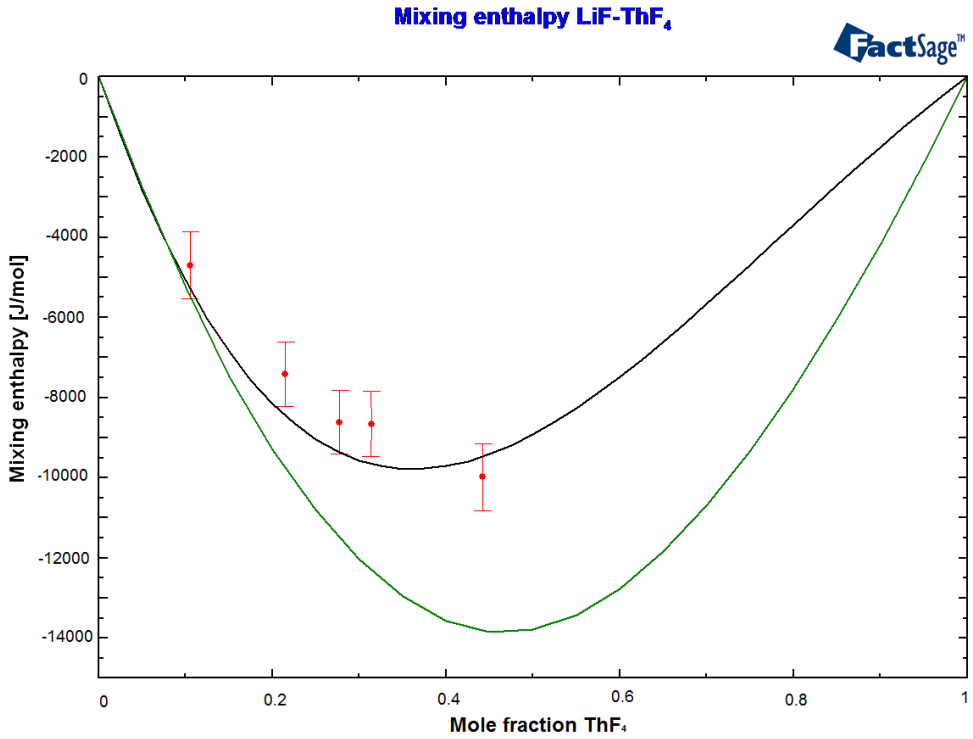

Figure 4.15: Enthalpy of mixing function of LiF-ThF_4 calculated from the new assessment (black line) and from the previous one (green line). • Data measured in this work.

assessment [42] and a significant difference is evident. It can be thus concluded that the new assessment is able to better describe the experimental mixing enthalpy data. Moreover, the entropy of the (Li,Th)F_x liquid solution was calculated from the assessment and a behaviour, shown in Figure 4.16, not far from ideality was observed.

Further investigation isare still needed to improve the description of this system and make the model compatible with all the data. The enthalpy of fusion of the compound Li_3ThF_7 was measured in this work, as described in the previous section, and the result was compared with the value calculated from the assessment. The values for the Li_3ThF_7 compound are reported below:

$$\triangle H_{fus}(exp) = 13660\ J \cdot mol^{-1} \tag{4.16}$$

$$\triangle H_{fus}(calc) = 22850\ J \cdot mol^{-1} \tag{4.17}$$

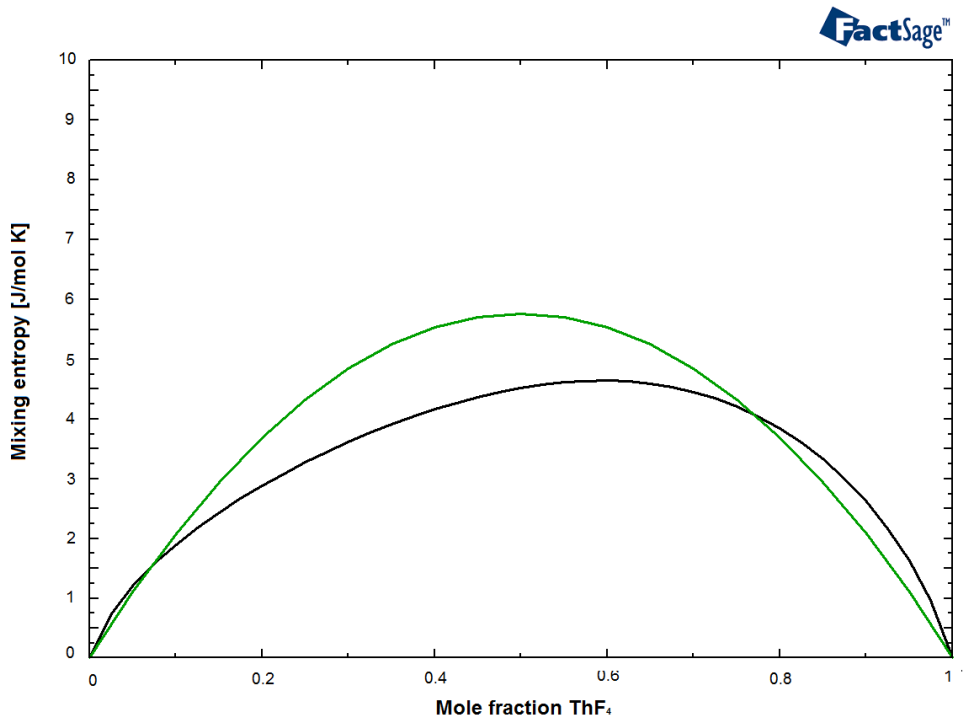

Figure 4.16: Entropy of the (Li, Th)F_x liquid solution. Green line: Ideal solution entropy. Black line: calculated entropy function at T=1121 K.

Two different actions are suggested in order to reduce the gap between the values: i.e., the excess heat capacity of the solution or the heat capacity of the compound can be modified. Both the properties have never been measured, thus it is not obvious how to establish the selection of the two functions. Since the measurement of these quantities is planned for the near future, interventions were not taken.

4.3 CsF heat capacity

To determine the experimental heat capacity of CsF, an extensive work has been carried out at ITU. The work includes the determination of the high temperature heat capacity of the liquid phase and solid phase and the low temperature heat capacity. Studies on CsF thermodynamic properties are important for the MSR technology because this salt is the stable phase of the Cs fission product, which is formed in the reactor during the operation time [7]. It is difficult to remove it from the molten salt mixture because of its solubility in the fuel, thus is expected to accumulate in the salt mixture. The presence

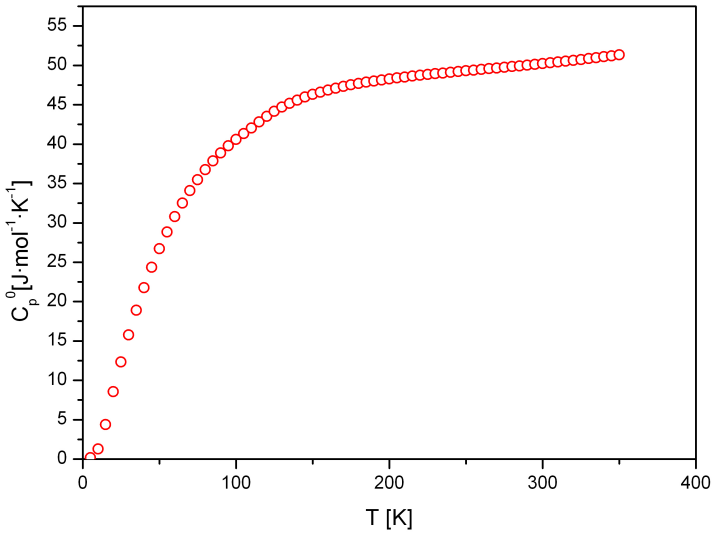

Figure 4.17: Heat capacity data of CsF measured from 5 K to 350K.

of this impurity must be accounted as it influences the final behaviour of the fuel and therefore the thermodynamic description of this single component is important.

4.3.1 Experimental data

Low-temperature heat capacity

The low temperature heat capacity data were measured recently at ITU using the adiabatic calorimeter. In this instrument, the sample, confined in a vacuum-tight vessel and thermally insulated from the environment, is supplied with a fixed amount of energy resulting in an increment of the sample temperature. The heat capacity is calculated from the ratio of the supplied energy and the temperature increase. The low temperature data measured at ITU are shown in Figure 4.17.

High temperature heat capacity

The heat capacity measurements of CsF above the room temperature were performed using the Drop Calorimeter described in the Section 3.3. The samples were CsF pellets (70-80 mg) prepared from pure CsF and encapsulated in Ni crucibles. Four crucibles were loaded in the calorimeter sample holder for each measurement, which consists of four

Table 4.6: Enthalpy increment from reference temperature to measuring temperature for the solid phase of CsF. The measurements are taken from 400 K to 960 K.

Temperature [K]	**H(T)-H(298 K) [J/mol]**	**Error [J/mol]**
402,9	5257	435
429,4	7093	779
455,5	8230	1494
481,6	9553	1586
507,4	13215	36 7
533,2	14618	3743
558,9	15688	2730
584,2	16413	3966
609,9	20125	4008
634,9	21876	4582
660,1	23889	2667
685,3	25554	3628
710,4	24402	2574
735,5	25568	2088
760,6	29482	3764
785,8	29401	4411
810,5	3233	4052
835,6	35048	4617
860,9	39190	3599
885,4	38635	3851
910,7	42894	3514
935,1	44312	2437
960,2	52340	8334

sample drops and five reference drops.

For the solid phase, the increment enthalpies were measured from 400 K to 960 K with step of 25 K and the values are listed in Table 4.6. The values reported are the average values between the four samples measured at given temperature and the standard deviation gives the error of the measurement. Usually, each measurement was repeated at least two times to reduce the uncertainty. The results are plotted as a function of temperature and compared with the data of Macleod [48], in fair agreement, as given in Figure 4.18. It is also important to observe that, unlike the work by Macleod, the measurements were performed using a very small quantity of CsF (100 mg instead of 10 g). The possibility to use this technique with small amounts of sample makes it very interesting from the perspective of measuring radioactive materials, which have usually limited availability.

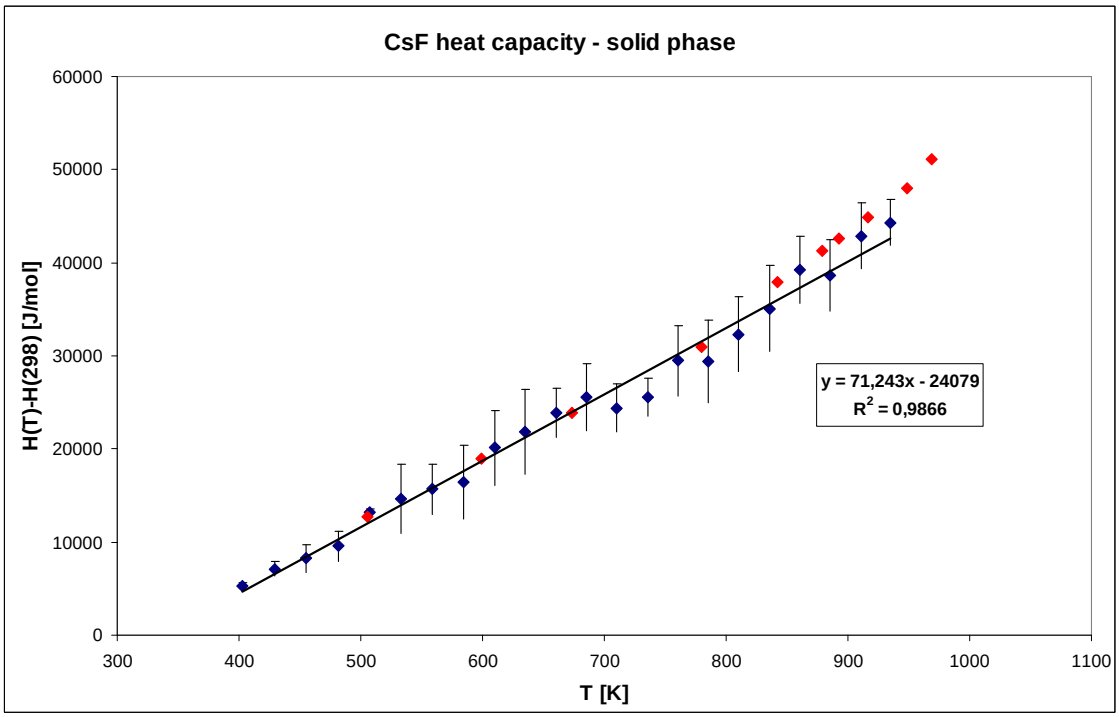

Figure 4.18: Enthalpy values plotted as a function of temperature in the solid phase range of CsF. The slope of the trendline is the heat capacity of the compound. ♦ Data measured in this work ♦ Data measured by Macleod [48]

To obtain the heat capacity of CsF, the measured enthalpy data were at the first stage fitted linearly and the slope of this trendline gives:

$$C_P = 71,24 \ \ J \cdot mol^{-1} \cdot K^{-1}.$$

Since this value is constant and very high at room temperature, compared to the low temperature observation ($C^0_{p,298} = 50,19 \ \ J \cdot mol^{-1} \cdot K^{-1}$), the enthalpy data had to be fitted with higher order polynomial function. Thus, the heat capacity was fitted using a Maier-Kelly type second order polynomial equation, which has the general form given below:

$$C^0_p(T) = A + B \cdot T + C \cdot T^{-2} \tag{4.18}$$

and the coefficients which best fit the experimental data are:

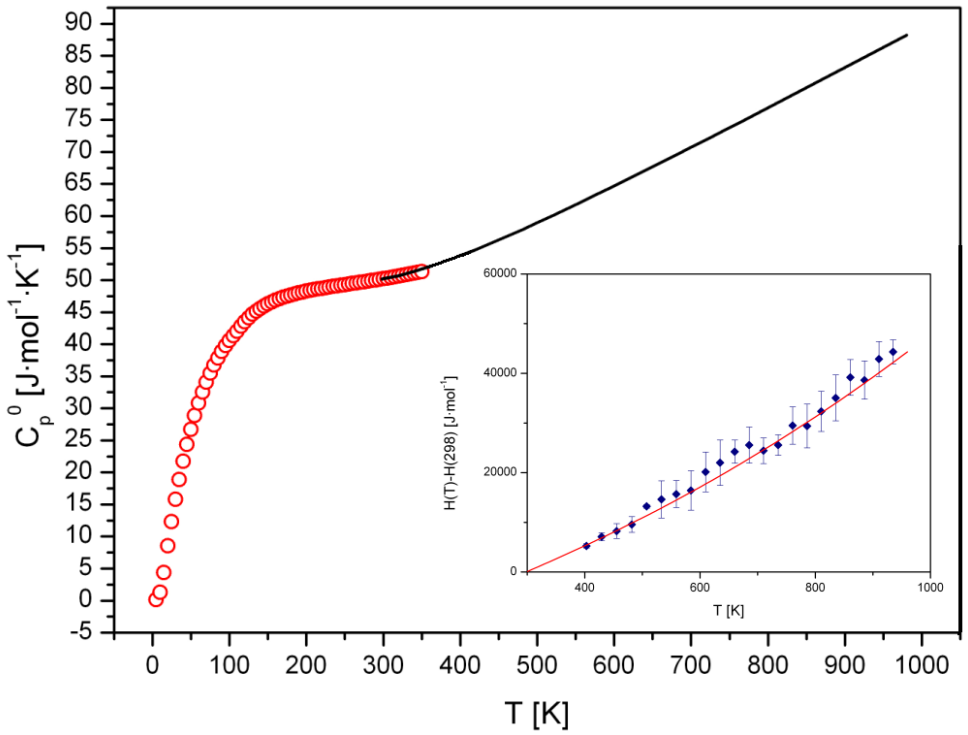

Figure 4.19: Solid phase heat capacity and enthalpy increment (inset graph) of CsF. ○ Low temperature heat capacity data. Black line: High temperature heat capacity fit. ♦ High temperature enthalpy increment data. Red line: High temperature enthalpy fit.

$$A = 24,291 \pm 7,646 \;\; J \cdot mol^{-1} \cdot K^{-1} \tag{4.19}$$

$$B = 6,4607 \cdot 10^{-2} \pm 1,6683 \cdot 10^{-2} \;\; J \cdot mol^{-1} \cdot K^{-2}$$

$$C = 589981 \pm 242592 \;\; J \cdot mol^{-1} \cdot K$$

The resulting heat capacity of CsF is shown in Figure 4.19, where the corresponding enthalpy fit is also plotted (inset graph) together with the experimental enthalpy increment data.

For the liquid phase, the enthaply increments were measured from 1030 K to 1385 K and are reported in Table 4.7. The final heat capacity value obtained for the liquid phase is:

Table 4.7: Enthalpy increment from reference temperature to measuring temperature of CsF liquid phase. The measurements are taken from 1030 K to 1385 K.

Temperature [K]	**H(T)-H(298 K) [J/mol]**	**Error [J/mol]**
1033,6	68746	3429
1083,7	75341	1709
1133,5	78178	2783
1183,2	79845	7222
1233,0	83674	2144
1282,8	85773	6377
1257,8	83736	3090
1208,2	83383	3149
1108,7	76890	2552
1059,0	73227	3951
1158,3	81876	1423
984,3	69914	3209
1332,2	95186	6357
1382,3	98011	3133

Table 4.8: Comparison between the enthalpy of fusion of CsF measured in this work and from literature **[24]**.

ΔH_{fus} obtained by Drop Calorimeter	**ΔH_{fus} obtained by DSC calorimeter**	**ΔH_{fus} from literature [24]**
21400 ± 3000 J/mol	22100 ± 2000J/mol	21700 J/mol

$$C_P = 70,56 \pm 5,5 \ \ J \cdot mol^{-1} \cdot K^{-1}$$

which is in perfect agreement with the work of Macleod [48] that reports a value for the heat capacity of $C_P = 69,47 \ \ J \cdot mol^{-1} \cdot K^{-1}$.

Using the two enthalpies equations obtained from the experimental results, the enthalpy of fusion was calculated as difference between the enthalpy in solid and liquid phase at the CsF melting temperature (Figure 4.20). This value was confirmed by the DSC analysis, measuring the same sample used for the heat capacity determination. At the end, the enthalpy of fusion was compared with the literature value [24] and the results are summarized in Table 4.8, indicating very good agreement between the two used technique.

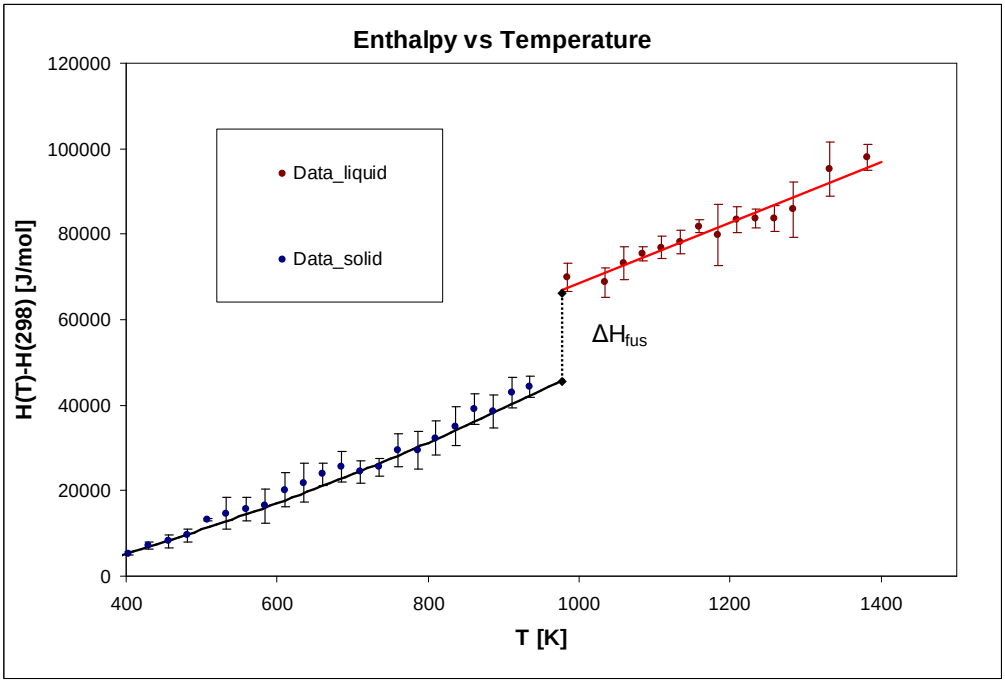

Figure 4.20: Enthalpy results in the whole range between 400 K and 1400 K of CsF. The enthalpy of fusion is represented with the dotted line.

4.4 ThF_4 heat capacity

Despite its importance in the future nuclear fuel, the ThF_4 available data on heat capacity and enthalpy of fusion are lacking. There are no published experimental data on the heat capacity at high temperature, the only available data are preliminary enthalpy measurements by Dworkin from 1200 K to 1420 K. These results were used by Wagmann [49] to obtain an equation for the solid state from 298,15 K to 1383 K giving :

$$C_{p,sol}[J \cdot K^{-1} \cdot mol^{-1}] = 122,1 + 8,37 \cdot 10^{-3} \cdot T - 1,255 \cdot 10^{6} \cdot T^{-2} \tag{4.20}$$

and for the liquid state:

$$C_p = 133,9\, J \cdot K^{-1} \cdot mol^{-1}. \tag{4.21}$$

The enthalpy of fusion adopted is also based on unpublished data by Dworkin:

$$\triangle H_{fus} = 41800\, J \cdot mol^{-1} \tag{4.22}$$

These values are commonly assumed for the thermodynamic calculations, such as the assessment of the phase diagram, but new experimental analyses are needed to confirm them. The aim of the study on ThF_4 properties was the experimental determination of the ThF_4 heat capacity in the liquid and solid phase. When these two properties are known, the determination of the enthalpy of fusion is possible, as done for the CsF presented in the previous section. However, due to time constrains and technical difficulties related to encapsulation, only measurements on ThF_4 solid phase are presented in this thesis.
A key factor to achieve the objective is the purity of the salt, which must be free from oxy-fluorides or other impurities. Several tests were carried out to find the right procedure to purify the ThF_4 and the goal was recently reached using the purification method described in Section 3.1.1. Moreover, the ThF_4 has a relatively high melting point and the samples are subjected to high temperature during the measurements. To avoid leaks of fluoride vapours, it necessary to guarantee perfect tightness of the crucible used for analysis which was continuously checked monitoring its weight after each measurement. The study is still ongoing but first results for the ThF_4 solid phase were obtained in this study and are described in this section.

4.4.1 Experimental data

The enthalpy increment measurements of the ThF_4 solid phase were performed for wide range of temperature, from 320 K to 1290 K with step of 25 K. The results obtained are listed in Table 4.9 and plotted in Figure 4.21. The measured data (black points) were preliminary fitted, for simplicity, with a straight line assuming no temperature dependence of the heat capacity. The fit obtained is satisfactory and corresponds to the following heat capacity:

$$C_{p,sol} = 173,02\, J \cdot K^{-1} \cdot mol^{-1}. \tag{4.23}$$

which is much higher than the value obtained from Equation 4.20, as clearly shown in

Table 4.9: Enthalpy increment from reference temperature to measuring temperature for the solid phase of ThF_4. The measurements are taken from 320 K to 1290 K.

Temperature [K]	H(T)-H(298 K) [J/mol]	Error [J/mol]
322,9	3965	1551
376,3	10524	813
429,3	16057	4049
481,8	27753	3019
533,2	37651	6737
584,6	45255	8520
635,3	60958	6879
685,7	59415	5045
736,0	70227	4589
786,1	85485	12677
835,9	99376	9256
886,1	105431	8978
935,9	112862	7842
985,8	116185	7699
1035,7	133129	10689
1085,7	143346	12724
1135,6	140693	8061
1185,8	144134	16816
1235,8	152592	8472
1286,2	166233	9201

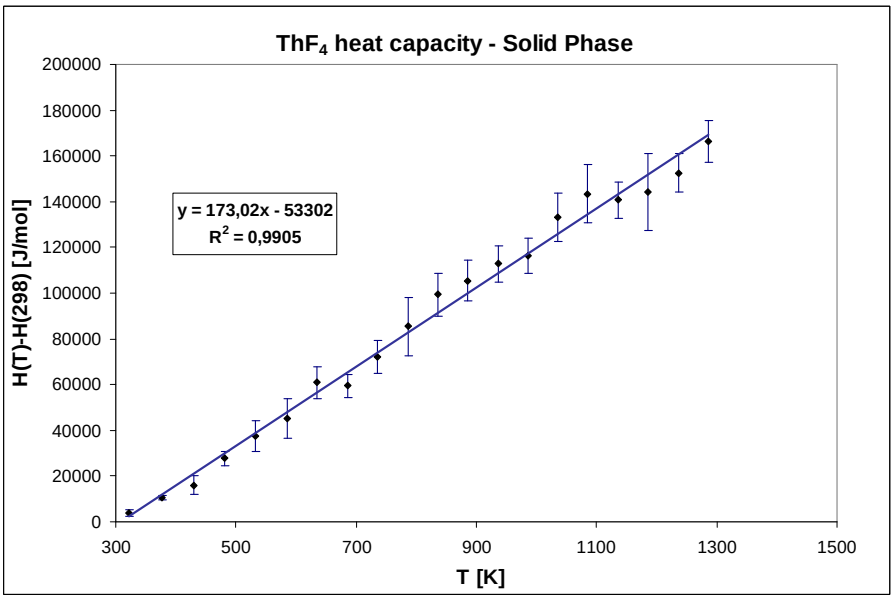

Figure 4.21: Enthalpy values plotted as a function of temperature in the solid phase range of ThF_4. ♦ Data measured in this work.

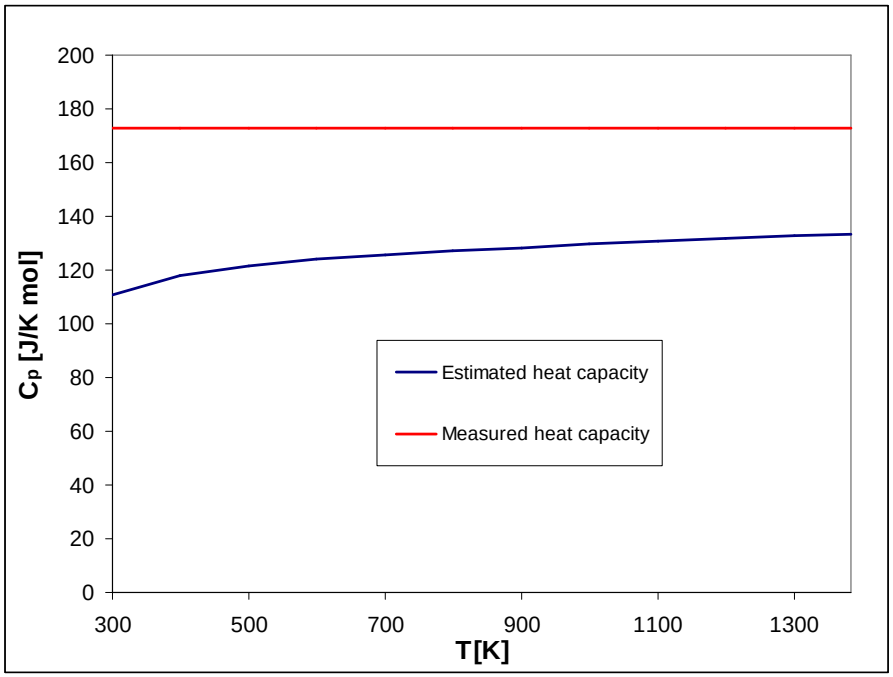

Figure 4.22: Comparison between the experimental heat capacity and the estimated heat capacity of ThF_4 [49].

Figure 4.22, where the two capacities are compared. The estimated equation for the solid state heat capacity is based on the preliminary work by Dworkin. However, as reported in [50], experimental difficulties were encountered during these measurements, which could have affect this evaluation, and the results have not been published. As explanation of heat capacity deviation, the presence of impurities was also taken into account and investigated. However, such significant deviation is not likely according to the precise melting point measurements. Nevertheless, further chemical analysis is being performed to justify the quality of the measured sample.

4.5 LiF-RbF excess heat capacity

The study of this system is part of a larger project pointing to a full description of all the interesting binary and ternary fluorides systems. Heat capacity measurements were done at ITU for some intermediate compositions of the generic system LiF-MF (M=Na, K, Cs). The comparison between the excess heat capacity was studied and it indicates a direct link between the cation size and the excess heat capacity. In order to conclude the

Table 4.10: Enthalpy increment from reference temperature to measuring temperature for the $Li_{0,5}Rb_{0,5}F$ liquid solution. The measurements are taken from 930 K to 1290 K.

Temperature [K]	H(T)-H(298 K) [J/mol]	Error [J/mol]
935,7	58997	2183
960,7	60914	1383
985,6	64002	3345
1010,5	65978	3356
1035,6	69634	4605
1060,6	67522	3107
1085,6	69858	3849
1110,6	73260	3949
1135,5	76112	4439
1160,6	76328	1282
1185,7	78955	4789
1210,7	80403	4243
1235,7	84501	2298
1260,9	85494	4950
1286,0	88799	3348

determination of the excess heat capacity of this series and confirm the observed trend, the "missing" LiF-RbF system was subject of this work.

4.5.1 Experimental data

Since in the previously studied systems LiF-NaF, LiF-KF, LiF-CsF the maximum deviation from ideality was found at 1:1 ratio of the end-members, the LiF-RbF (1:1) compound was primarly studied in this work. The intermediate composition LiF-RbF (1:1) was synthesized and several pellets, with an average salt weight of 100 mg, were prepared. The sample was checked using the DSC technique. According to the phase diagram of the LiF-RbF system, two transitions should be visible during the heating process and it was confirmed in our analysis. The temperatures obtained were very close to the ones predicted by the phase diagram, thus the composition of the intermediate $Li_{0,5}Rb_{0,5}F$ was justified. Also for this system the sapphire was used as reference and the increment enthalpies were measured for the liquid phase from 930 K to 1290 K with step of 25 K. The average values for each temperature are listed in Table 4.10 and the data are plotted in Figure 4.23. The obtained heat capacity of the $Li_{0,5}Rb_{0,5}F$ liquid solution is:

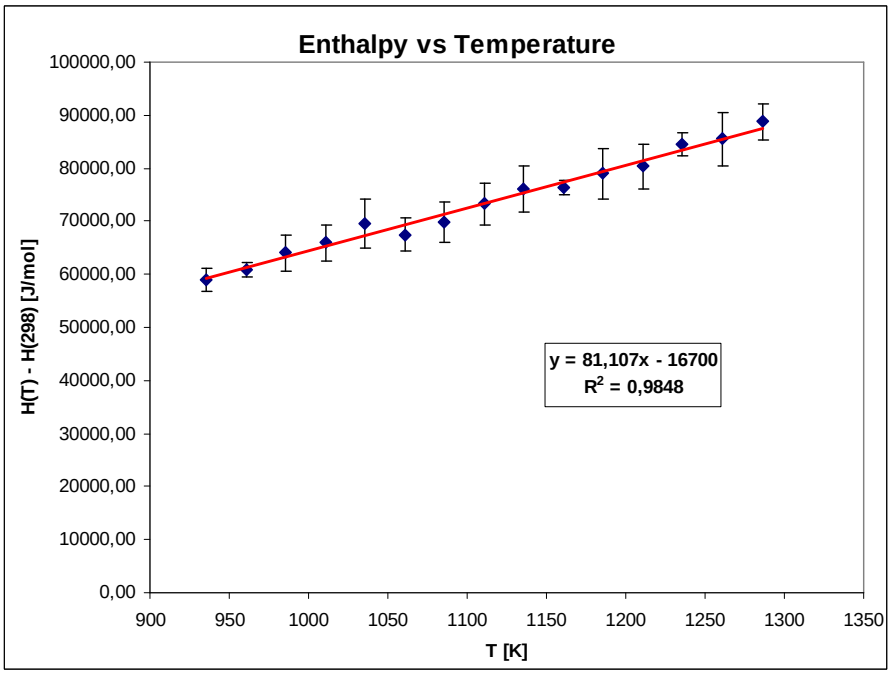

Figure 4.23: Enthalpy increment measured plotted as function of temperature for the LiF-RbF system. The measurements were performed in the liquid phase between 930 and 1290 K.

$$C_P = 81,11 \;\; J \cdot mol^{-1} \cdot K^{-1} \tag{4.24}$$

This value was compared with the ideal heat capacity of the mixture, obtained by Neumann-Kopp rule, and the excess value was derived. The knowledge of this property could be used, as done for the LiF-KF system, to optimize the phase diagram introducing this parameter in the Gibbs energy model.

Furthermore, it is interesting to observe how the excess heat capacity value changes in the analysed series of systems. The results derived from this study were added to the results already available, concluding the description of the generic system consisting of LiF and another alkali fluoride. The excess heat capacities are compared in Figure 4.24 and confirm the initial assumption that with increasing radii difference between the cations in the system the excess heat capacity increases. Probably due to the larger strain existing in the compound, the heat capacity of the solution increases and deviates more from the ideal behaviour. In order to verify the presence of a correlation, the excess heat capacity for the 1:1 composition was plotted as a function of the ionic radii difference between the

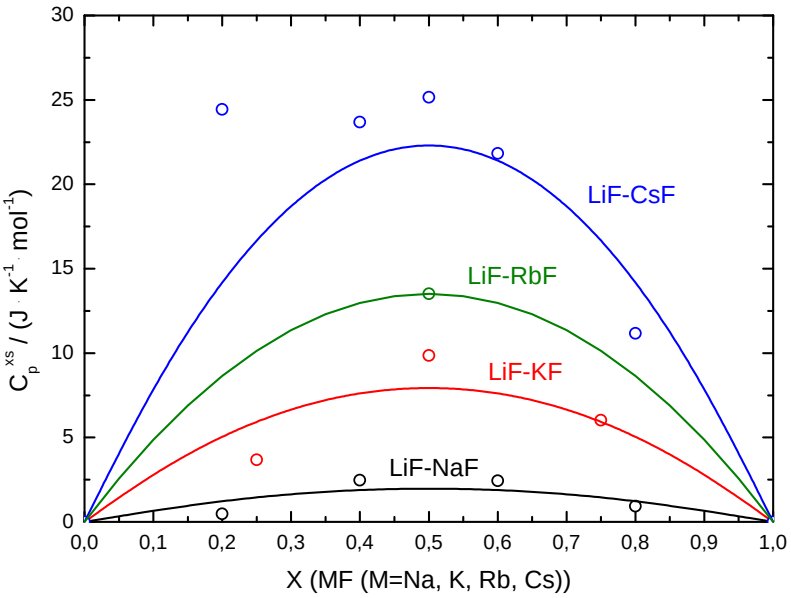

Figure 4.24: Comparison between the excess heat capacity in the generic system LiF-MF (M=Na, K, Rb, Cs).

two alkaline compound as given in Figure 4.25, showing a systematic trendline.

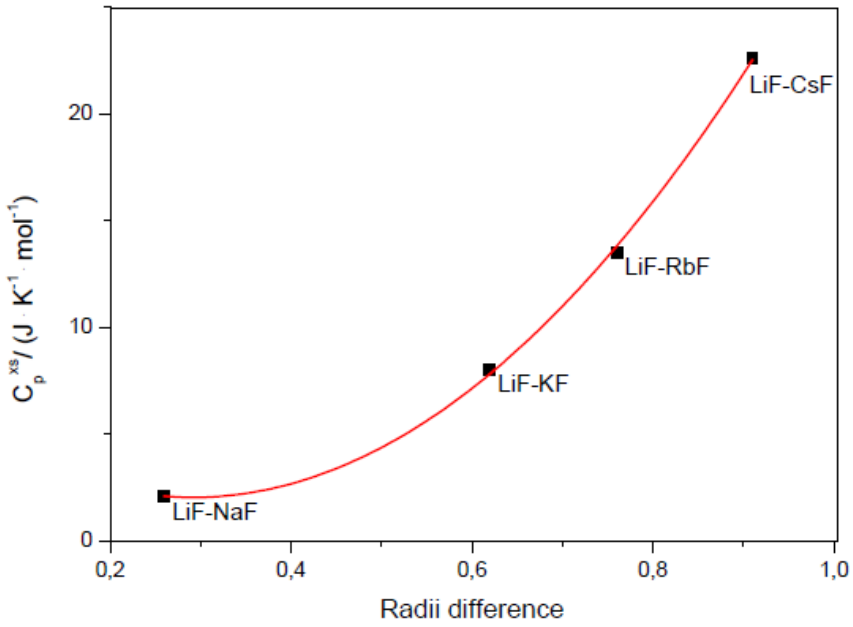

Figure 4.25: Excess heat capacity for the 1:1 compositions within the LiF-AlkF series as a function of the ionic radii difference. The ionic radii data are taken for octahedral coordination from [48].

Chapter 5

Conclusions

The main task of this work was the study of thermodynamic properties of molten salts for nuclear applications. The investigations were carried out entirely on fluoride salts, which are currently the most relevant salts as potential fuel for the Molten Salt Reactor. Since these salts are hygroscopic and their vapour release is very corrosive, a special care is required during handling of fluorides and during the measurements. Two techniques, DSC and drop calorimetry, were employed in this work to measure thermodynamic properties (heat capacity, equilibrium data, enthalpy of mixing, enthalpy of fusion) of some fluoride systems in order to improve the current dataset. To properly describe the phase diagrams, the experimental work was coupled with modeling of the phase relations accomplished according to CALPHAD method.

A challenging task was the measurement of the enthalpies of mixing of binary systems, which required the development of a new method compatible with the DSC technique. Since this method requires a more accurate determination of the instrument sensitivity, a new energy calibration was applied and tested.

The following systems were investigated in this study and the following main conclusions were drawn.

The LiF-KF system was studied with the main aim to verify the possibility to use the novel method for the determination of the enthalpy of mixing. The results were satisfactory since it was possible to identify the right order of magnitude of this value obtaining a good agreement with the literature data. Moreover, new excess heat capacity

data of the (Li,K)F liquid phase were measured recently in ITU and together with the mixing enthalpies were used to improve the Gibbs energy model for the description of the phase diagram, which has been re-assessed in this study as well.

Using the same technique, the LiF- ThF_4 system was studied for its importance in nuclear applications. Experimental values for enthalpy of mixing were measured for the first time and, at the same time, the experimental phase diagram points were collected. Some difficulties were experienced during the mixing of LiF and ThF_4 end-members forming the mixture, which have rather different melting points. Despite this, it was possible to measure some points useful for the enthalpy of mixing description. Combining the two sets of mentioned data (enthalpies of mixing and phase diagram points), a re-assessment of the phase diagram was performed. Based on the experimental evidences, the intermediate compound $LiThF_5$ was preferred during the modeling and the final result offers a good agreement with all the experimental data. Moreover, the congruently melting compound Li_3ThF_7 was synthesized and analysed by X-ray diffraction and DSC technique, showing high purity. Further investigations on this ternary compound would be of interest for the improvement of the thermodynamic modeling. In fact, in absence of experimental data, the heat capacity of all intermediate compounds was assumed to be ideal during the modeling. Experimental determination of this quantity and excess heat capacity of the (Li,Th)F_x liquid solution may contribute to the improvement of the final description of the LiF-ThF_4 system. Concluding, the analysed system was improved considering novel experimental data, however further investigations of thermodynamic properties of intermediate compounds are recommended.

The heat capacity of pure CsF heat capacity was measured over an extended temperature range, from 5 K to 1400 K, combining different sets of data obtained by low temperature adiabatic calorimetry and drop calorimetry. The obtained results were comparable with the literature values, which are available in a smaller temperature range. Since this salt is one of stable form of Cs fission product and will most likely accumulate during the operation of MSR, the obtained results are relevant for the prediction of fuel behaviour during the reactor life-time.

A study of ThF_4 has been started in order to investigate the thermodynamic properties

(heat capacity and heat of fusion) of the pure salt. No experimental data are available in literature and the data commonly assumed are based on an unpublished work. The achieved good purity of ThF_4 and the encapsulation techniques developed in the past were key factors that permitted a successful determination of thermodynamic properties of this compound. First results of heat capacity were obtained in this work for the solid phase, showing rather big value compared with the estimated one (increased by 30 %). Further investigations are needed in the future to support this experimental value which, if confirmed, will change substantially the thermodynamic description of e.g., the LiF-ThF_4 system. For the same reason, new experimental data on liquid heat capacity are of interest as well.

Last but not least, the excess heat capacity of the $Li_{0,5}Rb_{0,5}F$ compound was measured in order to finalize the description of the generic system LiF-MF (M=Na, K, Cs, Rb). The obtained value was in perfect agreement with the trend shown by the other systems previously analysed and confirms the initial assumption. The excess heat capacity is influenced by the size difference between the cations, and increases with it. Thermodynamic re-assessment of these alkali fluoride binary mixtures, considering this significant excess heat capacity contribution, is needed in future work as this quantity has a big impact on Gibbs energy determination.

Appendix A

Thermodynamic properties used in this work

Table A.1: Heat capacity equations C_P [$J \cdot K^{-1} \cdot mol^{-1}$] for the reference materials used for the Drop Calorimeter.

Reference materials	**Heat capacity**	**Ref.**
Synthetic sapphire (α-Al_2O_3)	C_P =257,4076 - 1,715·10^{-1}·**T** + 4,542·10^{6}·**T**$^{-2}$ + 1,290·10^{-4}·**T**^{2} - 4,608·10^{-8}·**T**^{3} + 6,318·10^{-12}·**T**^{4} - 5,476·10^{4}·**T**$^{-1}$ - 1,325·10^{8}·**T**$^{-3}$	[31]
Pt	C_P =24,251 + 5,376·10^{-3}·**T**	[32]

Table A.2: Enthalpy coefficients [$J \cdot mol^{-1}$] of nickel in the high temperature range used for the drop encapsulation technique. Data taken from [33].

Temperature range	**a**	**b·T**	**c·T^2**
298,15 K - 700 K	-6283,27	23,6126	0,00432
700 K - 1728 K	-6769,54	19,087	0,012

Table A.3: Thermodynamic data for pure compound and intermediate compound used in this study for the phase diagram assessments: $\Delta_f H^0(298)$ [kJ·mol^{-1}], $S^0(298)$ [J·K^{-1}·mol^{-1}] and heat capacity coefficients C$_p$[J·K^{-1} · mol^{-1}].

Compound	$\Delta_f H^0(298)$	$S^0(298)$	**a**	**b·T**	**c·T^2**	**d·T^{-2}**	**e·T^3**
LiF (s)[a]	-616,931	35,660	43,309	$1{,}631 \cdot 10^{-2}$	$5{,}047 \cdot 10^{-7}$	$-5{,}691 \cdot 10^{6}$	-
LiF (l)[a]	-598,654	42,962	64,183	-	-	-	-
KF (s)[a]	-568,606	66,547	68,757	$-5{,}775 \cdot 10^{-2}$	$7{,}540 \cdot 10^{-5}$	$-7{,}667 \cdot 10^{5}$	$-2.388 \cdot 10^{-8}$
KF (l)[a]	-554,374	67,769	71,965	-	-	-	-
ThF_4(s) [b]	-2097,900	142,05	122,173	$8{,}37 \cdot 10^{-3}$	-	$-1{,}255 \cdot 10^{6}$	-
ThF_4(l) [b]	-2064,491	156,629	133,9	-	-	-	-
Li_3ThF_7(s)[c]	-3959,393	249	252,100	$5{,}730 \cdot 10^{-2}$	$1{,}514 \cdot 10^{-6}$	$-2{,}962 \cdot 10^{6}$	-
$LiThF_5$(s)[c]	-2724,531	178,6	165,481	$2{,}468 \cdot 10^{-2}$	$5{,}047 \cdot 10^{-7}$	$-1{,}824 \cdot 10^{6}$	-
$LiTh_2F_9$(s)[c]	-4830,331	320,76	287,655	$3{,}305 \cdot 10^{-2}$	$5{,}047 \cdot 10^{-7}$	$-3{,}079 \cdot 10^{6}$	-
$LiTh_4F_{17}$(s)[c]	-9032,631	603,86	532,001	$4{,}979 \cdot 10^{-2}$	$5{,}047 \cdot 10^{-7}$	$-5{,}589 \cdot 10^{6}$	-

[a] Data taken from [24].
[b] Data taken from [28].
[c] Data obtained by optimization.

References

[1] "A technology roadmap for generation IV nuclear energy systems" (2002) , U.S. DOE Nuclear Energy Research Advisory Committee and the Generation IV International Forum, <http://www.gen-4.org/PDFs/GenIVRoadmap.pdf>.

[2] Mathias, P. M. and Brown, L. C. "Thermodynamics of the Sulfur-Iodine Cycle for Thermochemical Hydrogen Production", presented at the 68 th Annual Meeting of the Society of Chemical Engineers, Japan 23 March 2003.

[3] Le Blanc, D. (2010) "Molten salt reactors: A new beginning for an old idea", *Nuclear Engineering and Design* , vol. 240, p. 1644-1656.

[4] Rosenthal, M.W., Kasten, P.R. and Briggs, R.B. (1970) "Molten Salt Reactors - History, Status, and Potential", *Nuclear Applications and Technology*, vol. 8.

[5] Luzzi, L., Di Marcello, V. and Cammi, A. (2012) "Multi-Physics Approach to the modeling and analysis of Molten Salt Reactors", Chapt. 1, Nova Science Publishers, Inc., New York.

[6] Hore-Lacy, I. (2009) *"Thorium". In: Encyclopedia of Earth*, World Nuclear Association, Eds. Cutler J. Cleveland, <http://www.eoearth.org/article/Thorium>.

[7] Grimes, W.R. (1970) "Molten Salt Reactor chemistry", *Nuclear Applications and Technology*, vol. 8 , p. 137-155.

[8] Ignatius, V., Feynberg, O., Gnidoi, I., Merzlyakov, A., Smirnov, V., Surenkov, A., Tretiakov, I. and Zakirovet, R. (2007) "Progress in Development of Li,Be,Na/F Molten Salt Actinide Recycler & Transmuter Concept", Proceedings of ICAPP 2007, Nice, France.

[9] Merle-Lucotte, E., Heuer, D., Allibert, M., Ghetta, V. and Le Brun, C. (2008) "Introduction to the Physics of Molten Salt Reactor", Materials Issues for Generation IV Systems, NATO Science for Peace and Security Series - B, Editions Springer, p. 501-521.

[10] Mourogov, A. and Bokov, P.M. (2006) "Potentialities of the fast spectrum molten salt reactor concept: REBUS-3700", *Energy Conversion and Management*, vol. 47, p. 2761-2771.

[11] Bettis, E.S., Bettis, Schroeder, R.W., Cristy, G.A., Savage, H.W., Affel, R.G. and Hemphill, L.F. (1957) "The Aircraft Reactor Experiment", *Nuclear Science and Engineering*, vol. 2, p. 804-825.

[12] Haubenreich, P.N. and Engel, J. R. (1970) "Experience with the Molten-Salt Reactor Experiment", *Nuclear Applications and Technology,* vol. 8, p. 118-136.

[13] Bettis, E. S. and Robertson, R. C. (1970) "The design and performance features of a single-fluid Molten Salt Breeder Reactor", *Nuclear Applications and Technology*, vol. 8 , p. 190-207.

[14] Robertson, R.C. (1971) "Conceptual design study of single-fluid molten-salt breeder reactor", Technical Report ORNL-4541.

[15] Beneš, O. and Konings, R. J. M. (2009) "Thermodynamic properties and phase diagrams of fluoride salts for nuclear applications", *Journal of Fluorine Chemistry*, vol. 130, p. 22-29.

[16] Williams, D.F. (2006) "Assessment of candidate molten salt coolants for the NGNP/NHI heat-transfer loop", Technical Memoranda ORNL-TM-2006/59.

[17] Williams, D. F., Toth, L. M. and Clarno, K. T. (2006) "Assessment of Candidate Molten Salt Coolants for the Advanced High-Temperature Reactor (AHTR)", Technical Memoranda ORNL-TM-2006/12.

[18] Moriyama, H., Sagara, A., Tanaka, S., Moir, R. W. and Sze, D.K. (1998) "Molten salts in fusion nuclear technology", *Fusion Engineering and Design*, vol. 39-40, p. 627-634.

[19] Grimes, W. R. and Cantor, S. (1972) "Molten salts as blanket fluids in controlled fusion reactors", Technical Memoranda ORNL-TM-4047.

[20] Robertson, R. C. (1965) "MSRE design and operations", Technical Memoranda ORNL-TM-728.

[21] "Status of small reactor designs without on-site refuelling" (2007), Technical report IAEA-TECDOC-1536.

[22] Delpech, S., Merle-Lucotte, E., Heuer, D., Allibert, M., Ghetta, V., Le-Brun, C., Doligez, X. and Picard, G. (2009) "Reactor physics and reprocessing scheme for innovative molten salt reactor system", *Journal of Fluorine Chemistry*, vol. 130, p. 11-17.

[23] Zherebtsov, A. L. and Ignatius, V. V. (2006) "Experimental Mock-Up of Accelerator-Based Facility for Transmutation of Radioactive Waste and Conversion of Military Plutonium", Technical Report Nr. 1606, Annual Report.

[24] Malcolm W. Chase, Jr. (1998) "NIST-JANAF Thermochemical tables 4^{th} edition", *Journal of Physical and Chemical Reference Data*, Monograph 9.

[25] Kaufman, L. and Bernstein, H. (1970) "Computer Calculation of Phase Diagrams", Academic press, New York.

[26] Wani, R.N., Patwe, S.J., Rao, U.R.K. and Venkateswarlu, K.S. (1989) "Fluorination of oxides of uranium and thorium by ammonium hydrogen fluoride", *Journal of Fluorine Chemistry*, vol. 44.

[27] Afonichkin, V., Bovet, A. and Shishkin, V. "Salts purification and redox potential measurement for the molten LiF-ThF_4-UF_4 mixture" Proceedings of the First ACSEPT International Workshop, Portugal, 2010.

[28] Konings, R.J.M., van der Meer, J.P.M. and Walle, E. (2005) "Chemical Aspects of Molten Salt Reactor Fuel", Technical Report ITU-TN 2005/25.

[29] Beneš, O., Konings, R.J.M., Wurzer, S., Sierig, M., and Dockendorf, A. (2010) "A DSC study of the $NaNO_3$–KNO_3 system using an innovative encapsulation technique", *Thermochimica Acta* , vol. 509 p. 62–66.

[30] Beneš, O., Konings, R.J.M., Kuenzel, C., Sierig, M., Dockendorf, A., Vlahovic, L. (2009) "The high-temperature heat capacity of the (Li,Na)F liquid solution" , *Journal of Chemical Thermodynamics*, vol. 41 p. 899–903.

[31] Archer, D. G. (1993) "Thermodynamic properties of synthetic sapphire (α-Al_2O_3), standard reference material 720 and the effect of temperature-scale differences on thermodynamic properties", *Journal of Physical and Chemical Reference Data,* vol. 22, No. 6, p. 1441-1453.

[32] Arblaster, J.W. (1994) "Thermodynamic properties of platinum in ITS-90", *Platinum Metal Review*, vol. 38, No. 3, p. 119-125.

[33] Desai, P.D. (1987) "Thermodynamic properties of nickel", *International Journal of Thermophysics*, vol. 8, No. 6, p. 763-780.

[34] Bergmann, A. G. and Dergunov, E. P. (1949) "Fusion diagram of LiF-KF-NaF", *Comptes Rendus de l'Acadèmie des Sciences de l´URSS*, p. 753-754.

[35] Aukrust, E., Björge, B., Flood, H., Førland, T. (1960) "Activities in molten salt mixtures of potassium-lithium-halide mixtures: a preliminary report", *Annals of the New York Academy of Sciences*, vol. 79, p. 830-837.

[36] Gilbert, R. A. (1962) "Molar enthalpies of mixing in the molten lithium fluoride-potassium fluoride system", *Journal of Physical Chemistry*, vol. 67, p. 1143-1145.

[37] Holm, J. L. and Kleppa, O. J. (1968) "Enthalpies of mixing in binary liquid alkali fluoride mixtures", *Journal of Chemical Physics*, vol. 49 p. 2425-2430.

[38] Hong, K. C. and Kleppa, O. J. (1976) "Enthalpies of mixing in some binary liquid alkali fluoride mixtures", *Journal of Chemical Thermodynamics*, vol. 8, p. 31-36.

[39] Beneš, O. and Konings, R. J. M. (2008) "Thermodynamic evaluation of the MF-LaF_3(M=Li, Na, K, Rb, Cs) systems", *CALPHAD*, vol. 32, p. 121-128.

[40] Thoma R. E., Insley, H., Landau, B.S., Friedman, H. A. and Grimes, W.R. (1959) "Phase equilibria in the fused salt systems LiF-ThF_4 and NaF-ThF_4", *Journal of Physical Chemistry,* vol. 63, p. 1266-1274.

[41] Harris, L. A. and White, G. D. (1959) "X-ray analyses of the solid pheases in the system LiF-ThF_4", *Journal of Physical Chemistry,* vol. 63, p. 1974-1975.

[42] Beneš, O., Beilmann, M. and Konings, R. J. M. (2010) "Thermodynamic assessment of the LiF-NaF-ThF_4-UF_4 system", *Journal of Nuclear Materials*, vol. 405, p. 186-198.

[43] Thoma, R. E. (1975) "Phase diagrams of binary and ternary fluoride systems" in: Advances in molten Salt Chemistry vol. 3, Plenum, New York.

[44] Brunton, G.D. (1965) "The crystal structure of $LiUF_5$", Annual Progress Report ORNL-3913, p. 10-12.

[45] Van der Meer, J. P. M., Konings, R. J. M., Jacobs, M. H. G. and Oonk, H. A. J. (2005) "A miscibility gap in LiF-BeF_2 and LiF-BeF_2-ThF_4", *Journal of Nuclear Materials,* vol. 344, p. 94-99.

[46] Gilbert, R.A. (1962) "Heat of fusion of 3LiF ThF_4", *Journal of chemical and Engineering data*, vol. 7, p. 388-389.

[47] Laligant, Y., Le Bail, A., Avignant, D., Cousseins, J.C. and Ferey, G. (1989) "Crystal structure of Li_3ThF_7 solved by X-ray and neutron diffraction", *Journal of Solid Chemistry*, vol. 80, p. 206-212.

[48] Macleod, A.C. (1973) "High-temperature thermodynamics properties of the alkali-metal fluorides", *Journal of the Chemical Society*, vol. 69, p. 2026-2035.

[49] Wagman, D. D., Schumm, R. H. and Parker, V. B. (1977) "A computer-assisted evaluation of the thermochemical data of the compounds of thorium, US National Bureau of Standards, Report NBSIR 77- 1300.

[50] Dworkin, A.S. (1972) "Enthalpy of uranium tetrafluoride from 298-1400K: enthalpy and entropy of fusion", *Journal of inorganic nuclear chemistry*, vol. 34, p. 135-138.

[51] Shannon, R.D. (1976) "Revise effective ionic radii and systematic studies of interatomic distances in halides and chalcogenides", *Acta Crystallographica*, A32, p. 751-767.

Acknowledgments

I acknowledge Prof. Dr. T. Fanghänel, the Director of the Institute for Transuranium Elements (ITU), for the training provided through his institute and Prof. Dr. R. J. M. Konings for his interest and his advices supervising the entire project. I also acknowledge the European Commission for support given in the frame of the program 'Training and Mobility of Researchers'.

The work presented in this thesis would not have been possible without my close collaboration with many people.

I want to thank Dr. O. Beneš, who has supervised my work, helping and encouraging me in every single step while working on this thesis. I am deeply grateful to him for his time, his constant support and his precious advices.

I acknowledge Prof. Dr. L. Luzzi for his confidence and his suggestions. This work would not be possible without the opportunity he has given to me.

I would like to thank to M. Beilmann, his friendship and professional collaboration meant a great deal to me.

In addition, it was a great pleasure to get to know and to collaborate with many great people. I would like to express a special thank to Andrea, Fidelma, Luca and Valentina for their friendship and their support during this experience.

Last, but not least I would like to express my heartfelt thanks to my parents and my brother, the support and the continuous encouragement along the way were of inestimable value to achieve my goals.